FAST NO_x PREDICTION METHODOLOGY VIA 1D THERMODYNAMICAL TOOLS

by

Emre Özgül

B.S., Mechanical Engineering, İstanbul Teknik University, 2005

M.S., Mechanical Engineering, Boğaziçi University, 2008

Submitted to the Institute for Graduate Studies in
Science and Engineering in partial fulfillment of
the requirements for the degree of
Doctor of Philosophy

Graduate Program in Mechanical Engineering

Boğaziçi University

2019

FAST NO_x PREDICTION METHODOLOGY VIA 1D THERMODYNAMICAL TOOLS

APPROVED BY:

Assoc. Prof. Hasan Bedir (Thesis Supervisor)	.....
Prof. Ahmet Erhan Aksoylu	.....
Prof. Hakan Ertürk	.....
Assist. Prof. Osman Akın Kutlar	.....
Assist. Prof. Hikmet Aslan	.....

DATE OF APPROVAL: 22.05.2019

ACKNOWLEDGEMENTS

Firstly, I would like to express my sincere gratitude to my advisor Assoc. Prof. Hasan Bedir for his continuous support during my PhD study and his patience, motivation, and immense knowledge. His kind guidance helped me in all the time of the study and writing of this thesis. I could not have imagined that I can accomplish this PhD study without his leadership.

Besides my advisor, I would like to thank the rest of my thesis committee: Prof. Ersoylu, Prof. Ertürk, Assist. Prof. Kutlar and Assist. Prof. Aslan for their kindness, insightful comments and encouragement.

I want to thank my parents Semra and Muhammet, to my brothers Evrim and Anıl; for encouraging me to go further.

Finally, I must express my very profound gratitude to my lovely wife Fatma for providing me with unfailing support and continuous encouragement throughout my years of study and through the process of researching and writing this thesis. This accomplishment would not have been possible without her and our lovely daughter Mira's support.

This thesis is dedicated to memories of my beloved grandmother and grandfather: Şerife and Hüseyin Okgerman.

ABSTRACT

FAST NO_x PREDICTION METHODOLOGY VIA 1D THERMODYNAMICAL TOOLS

Accurate modelling of Nitrogen Oxide, soot, CO and UHC emissions from diesel engines plays a crucial role during the development phases of powertrain systems due to increasingly more strict emission legislation. Undoubtedly, generating accurate and robust methods of emission prediction will serve to global optimization of engine systems at very early stages of engine development. Engine component selection, accurate prediction of specific fuel consumption and defining the correct EGR strategy (low and mid-high) can only be achieved via reliable and fast NO_x emission prediction. There are many possible ways of emission prediction in literature such as 3D, stochastic reactor, semi-empirical, phenomenological models and neural networks. However, these prediction methods either need excessive test data or simulation duration.

On the other hand, using 1D simulation tools is a faster way of emission prediction but has low accuracy. In this study, it is aimed to improve a fast and accurate NO_x emission prediction methodology by utilizing 1D Models generated in GT-Suite© software. Two different heavy-duty diesel engines with two different combustion models are modelled and correlated to test data. A NO_x emission prediction methodology is developed in 9L heavy-duty diesel engine model and experimented with the 12.7 L heavy-duty diesel engine model. In both studies, extended Zeldovich mechanism outputs included in the software is tuned via embedding calibration multiplier maps, depending on different engine operating parameters. Comparison of simulation results with the use of varying NO_x calibration multiplier maps against test data, shows that the developed methodology can be used to predict NO_x values with high speed and accuracy.

ÖZET

BİR BOYUTLU TERMODİNAMİK MODELLEME İLE NO_x EMİSYON TAHMİNİ METODOLOJİSİNİN GELİŞTİRİLMESİ

Dizel motorlarda Nitrojen Oksit, kurum, CO ve UHC emisyonlarının doğru modellenmesi güç aktarım sistemlerinin geliştirme süreçlerinde günden güne sıkılaşan emisyon regülasyonları sebebiyle büyük önem arzetmektedir. Hiç kuşkusuz, yüksek doğrulukta ve gürbüz emisyon tahmini metotlarının geliştirilmesi çok erken geliştirme safhalarında motor sistemlerinin global optimizasyonunun önünü açacaktır. Motor komponentlerinin doğru seçimi, özgül yakıt tüketimi hesabı ve doğru EGR stratejisinin belirlenmesi (düşük ve orta-yüksek) ancak NO_x emisyonlarının doğru ve hızlı tahmini ile gerçekleşebilir. Literatürde 3D, stokastik reaktör, yarı empirik, fenomenolojik modeller ve sinir ağları gibi birçok emisyon tahmin metodolojisi bulunmaktadır. Fakat, bu yöntemler ya çok fazla data gerektirir ya da simülasyon süreleri oldukça yüksektir.

Diğer bir taraftan, 1D simülasyon programları emisyon tahmini için hızlı fakat doğruluğu düşük bir alternatiftir. Bu çalışma kapsamında, hızlı ve doğru NO_x emisyon tahmini metodolojisinin GT-Suite© programında hazırlanan 1D Modeller yardımı ile geliştirilmesi hedeflenmiştir. İki farklı yanma modeline sahip iki farklı ağır yük ticari araç dizel motoru modellenmiş ve test datasına korale edilmiştir. NO_x emisyon tahmin metodolojisi öncelikle 9L ağır yük dizel motorda geliştirilmiş, akabinde 12.7L ağır yük dizel motor üzerinde de denenmiştir. Her iki çalışmada da; extended Zeldovich denklem çıktıları, farklı performans parametrelerine bağlı kalibrasyon çarpan haritaları ile ayarlanmıştır. Bu şekilde elde edilen simülasyon sonuçlarının test dataları ile karşılaştırılması; geliştirilen metodolojinin NO_x emisyonlarının yüksek hız ve doğrulukta tahmini için kullanılabileceğini göstermektedir.

TABLE OF CONTENTS

LIST OF FIGURES

LIST OF TABLES

LIST OF SYMBOLS

A	Heat transfer surface area
A_{eff}	Effective flow area
A_f	Constant (First-order reaction) representing the agreement between soot model and test data
A_o	Constant (Second-order reaction) representing the agreement between soot model and test data
A_R	Reference flow area
A_s	Heat transfer surface area
C	Constant part of FMEP
C_D	Discharge coefficient
C_f	Friction coefficient of smooth pipe
$C_{f,rough}$	Friction coefficient of rough pipe
C_p	Specific Heat
D	Cylinder Diameter
dx	Length of mass element in the flow direction
dp	Pressure differential acting across dx
d_s	Soot diameter
e	Total internal energy (internal energy plus kinetic energy) per unit mass
E_{sf}	Reaction rate of soot formation
E_{so}	Reaction rate of soot oxidation
f	Friction Factor
h	Heat transfer coefficient
H	Total Enthalpy
h_g	Heat transfer coefficient
$h_{g,rough}$	Heat transfer coefficient of rough pipe
h_{in}	Inlet enthalpy (known from the upstream state conditions),
h_{out}	Outlet enthalpy (predicted from the upstream state conditions and the efficiency)
k_A	Rate constant for NSC soot oxidation model

k_B	Rate constant for NSC soot oxidation model
k_P	Pressure Loss Coefficient
k_T	Rate constant for NSC soot oxidation model
k_Z	Rate constant for NSC soot oxidation model
L	Length
$\dot{m}$	Mass flow rate
M_C	Carbon Molecular Weight
m_{fg}	First-order reaction of vaporized fuel
m_s	Soot Mass
m_{sf}	Soot Mass Formation
m_{so}	Second order reaction of soot and oxygen
P	Power
P_c	Cylinder inside pressure
P_f	Peak cylinder pressure factor
P_r	Absolute pressure ratio (static outlet pressure / total inlet pressure)
Pr	Prandtl number
p1	Total pressure at pipe outlet
p2	Total pressure at pipe inlet
Q_M	Heat Transfer to Heat Exchanger
Q_S	Heat Transfer to Fluid
R	Reference Gas Constant
Re_D	Reynolds number based on pipe diameter
S	Stroke
s	Soot Emitted
s_f	Soot Formed
s_o	Soot Oxidized
R^2	Coefficient of Determination
T_0	Upstream stagnation temperature
T_c	Cylinder inside gas temperature
T_{fluid}	Fluid temperature

T_{in}	Inlet Temperature
$T_{surface}$	Surface temperature
$T_{tot,in}$	Inlet Total Temperature
T_{wall}	Wall temperature
U	Mean Axial Velocity
U_{eff}	Effective velocity outside boundary layer
U_{in}	Inlet Velocity
U_{is}	Isentropic velocity at the throat
U_{piston}	Mean velocity of piston
V	Volume
V_1	Inlet Velocity
V_C	Cylinder volume
V_{UDP}	Cylinder volume when the piston is upper dead point
x	Proportion factor in soot equations
w	Reaction rate
γ	Specific Heat Ratio
Δh_s	Isentropic enthalpy change
ΔT	Temperature difference between the fluid and wall,
ρ	Density
ρ_{is}	Density at the throat
ρ_o	Upstream stagnation density
ρ_{ox}	Oxygen partial pressure
ρ_s	Soot density

LIST OF ACRONYMS/ABBREVIATIONS

1D	One Dimensional
2D	Two Dimensional
3D	Three Dimensional
AFR	Air to Fuel Ratio
ANN	Artificial Neural Network
AP	Adblue Price
ASM	Active Shape Model
ATS	Aftertreatment System
AWI	Calculated time of crank angle for %10 and %90 burned of fuel by combustion model
BDUR	Entered time of crank angle for %10 and %90 burned of fuel by user
BMEP	Brake Mean Effective Pressure
BSFC	Brake Specific Fuel Consumption
CA	Crank Angle
CAD	Computational Aided Design
CAE	Computational Aided Engineering
CA50	Crank Angle in which 50% of Injected Fuel is burnt
CF	Conversion Factor
CFD	Computational Fluid Dynamics
CI	Compression Ignition
CNG	Compressed Natural Gas
CO	Carbon Monoxide
CO_2	Carbon Dioxide
CPU	Central Processing Unit
CRDI	Common Rail Diesel Injection
DOC	Diesel Oxidation Catalyst
DOE	Design of Experiment
DI	Direct Injection

DPF	Diesel Particule Filter
EGR	Exhaust Gas Recirculation
EU	European Union
EVO	Exhaust Valve Opening
F/A	Fuel Air Ratio
FMEP	Friction Mean Effective Pressure
FP	Fuel Price
FTP	Federal Test Procedure
GMEP	Gross Mean Effective Pressure
HCCI	Homogeneous Charge Compression Ignition
HD	Heavy-Duty
HDV	Heavy-Duty Vehicle
HIL	Hardware in the Loop
IMEP	Indicative Mean Effective Pressure
IVC	Intake Valve Closing
LNG	Liquified Natural Gas
MAF	Mass Air Flow
MEP	Mean Effective Pressure
MFB	Mass Fuel Burn
MFB50	Crank Angle for 50% of Total Mass Fuel Burn
MPS	Mean Piston Speed
MPSF	Mean Piston Speed Factor
MPSSF	Mean Piston Speed Squared Factor
NO_x	Oxides of Nitrogen
NSC	Nagle and Strickland Model
nRMSE	Non-dimensional
NSGA	Non-dominated Sorting Genetic Algorithm
OEM	Original Equipment Manufacture
PAH	Poly-aromatic Hydrocarbon
PCCI	Premixed Charge Compression Ignition
PCOMPO	Compressor Outlet Pressure

PDF	Probability Density Function
PF	Peak Cylinder Pressure Factor
PFP	Peak Firing Pressure
PID	Proportional Integral Derivative
PMAX	Maximum In-cylinder Pressure
PMEP	Pumping Mean Effective Pressure
PPM	Part per Million
PR	Pressure Ratio
PTURI	Turbine Inlet Pressure
RMSE	Root Mean Square Error
RPM	Revolution per Minute
RTE	Radiative Heat Transfer
SCR	Selective Catalytic Reduction
SI	Spark Ignition
SOI	Start of Injection
SPEEDMP	Mean Piston Speed (n/min)
SRM	Stochastic Reactor Model
SVM	Support Vector Machine
TBOOST	Boost Temperature
TCOMPO	Compressor Outlet Temperature
TMAX	Maximum In-cylinder Temperature
TOC	Total Operating Cost
TTURI	Turbine Inlet Temperature
UHC	Unburned Hydrocarbons
UP	Urea Price
VECTO	Vehicle Energy Consumption Calculation Tool
W	Total combustion mass
WEXP	Entered Wiebe curve grade by user.

1. INTRODUCTION

Progressively more stringent legislative measures aiming to reduce the levels of many emissions such as unburned hydrocarbons, soot, and oxides of nitrogen (NO_x) generates increasing attention to the environmental impact of long haul trucks. Furthermore, carbon dioxide (CO_2) emissions have come into focus due to concerns about their relationship with global warming. Figure 1.1 shows the contribution of CO_2 emissions originated from heavy-duty vehicles (HDVs).

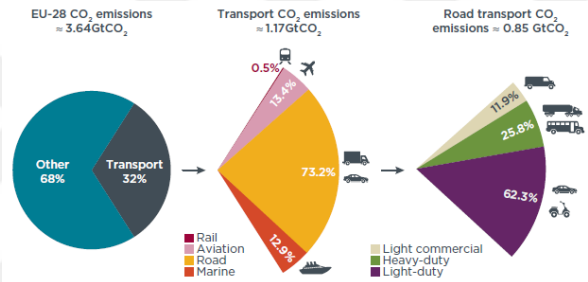

Figure 1.1. Distribution of total direct CO_2 emissions in the EU for 2015 [1]

On May 17, 2018, the European Union (EU) declared a regulatory proposal regarding CO_2 emissions reduction. Figure 1.2 shows the EU proposal. The plan which is valid for new HDVs sold in the European Union aims 15% reduction in CO_2 emission by 2025 and 30% reduction by 2030; from 2019 baseline [1]. An open-source, C based, multipurpose, publicly available object-oriented computer code, Vehicle Energy Consumption Calculation Tool (VECTO) is developed to follow the reduction process. According to the scheme, OEMs will report their fleet average CO_2 emissions in 2019 via VECTO. In 2025 and 2030; Original Equipment Manufacturers (OEM) will report their fleet average CO_2 emissions again [6]. Failing to reduce the emissions by the targeted amount, OEMs will have to pay severe penalties for each 1% difference from the reduction target.

Besides; it is expected to that Euro7 emission regulations will be in effect starting from 2024. Forecasts on Euro7 emission regulations are showing that NO_x emission

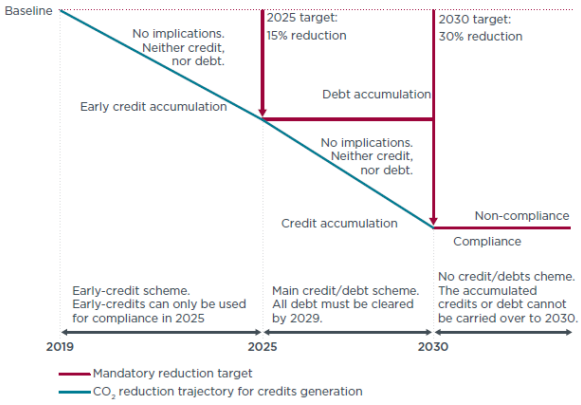

Figure 1.2. Illustration of EU Commission proposal- March 2018 [2]

targets will be decreasing by approximately 30%. These two facts are making OEMs focus on emission reduction techniques.

Higher efficiency is the reason why diesel engines have lower CO_2 emissions compared to gasoline engines. However, diesel engines suffer from higher NO_x emissions due to their higher compression ratio and consequently higher in-cylinder temperatures, which is resulting as higher NO_x production.

Reducing diesel engine emissions is challenging due to the inherent trade-off between lowering NO_x output and improving fuel economy. Conditions which help ensure good fuel economy and complete combustion will typically lead to higher in-cylinder temperatures, which, unfortunately, creates better conditions for the oxidation of nitrogen, thus increasing NO_x output. Exhaust gas recirculation (EGR) and engine cooling may reduce the rate of NO_x formation, while but in return, carbon monoxide (CO) production may increase. Retarding the injection timing is also a common strategy [7].

Global optimization is one of the critical topics that OEMs are currently working on. The primary target of global optimization is ensuring engine operation at optimum specific fuel consumption and NO_x trade-off. Also, patterns of emissions caused by fluctuations in the temperature of the combustion chamber, changes in the air-fuel ratio, and fuel injection rate are receiving increasing attention.

Determination of global optimum conditions via tests is a very costly process (sensors, fuel, engineer/room allocation costs, etc.). Also, to reduce the probability of mechanical failures of an engine during a test, tests are generally performed within mechanical/calibration limits or already investigated calibration set point boundaries.

On the other hand, it is possible to perform computer simulations covering full range of engine operating conditions. Simulation tools make it easier to examine the global optimum conditions without encountering any physical test problems, and some of these tools have a significantly lower cost.

Detailed chemistry calculations via three dimensional computational fluid dynamics (3D CFD) simulations, 1D-stochastic reactor models or use of full data-driven methods (such as neural networks) are the most apparent ways of NO_x emission prediction. However, these solutions either need excessive data or very long simulation duration.

One dimensional (1D) thermodynamic models can also be used for NO_x emission prediction. In 1D thermodynamic simulations, it is possible to model an engine with all accessories such as EGR cooler, inter-cooler, turbine, compressor, air-box, etc. [3], [8]. Simulation duration is significantly lower than the other options since Navier-Stokes and energy equations are simplified to a sigle dimension. Although these tools are handy to perform torque and power predictions for both full load and part load conditions, they cannot provide accurate predictions for NO_x emissions at different operating points. This is primarily due to the lack of examination of detailed chemical kinetics in 1D engine models. In this study, an investigation of a new methodology for fast NO_x emission prediction via the use of 1D Engine Models is performed.

2. LITERATURE SURVEY

Diesel emission prediction is one of the most significant problems of automotive scientists. Detailed chemistry calculations via 3D CFD models, 1D-stochastic reactor model couplings and artificial neural network (ANN) based models are the most obvious ways of diesel emission prediction. Some of the studies in the literature are mentioned below.

2.1. 3D CFD Simulations

Shi *et al.* [9] worked on a 3D CFD simulation of a direct-injection diesel engine and used Hiroyasu-Kadota averaged-reaction-rate soot model for soot emission calculations. Via model calculations, they have shown that post-injection of fuel reduces soot production.

The objective of the study conducted by Almeida *et al.* [10] was to create a model which predict of the NO_x and soot and to improve the engine design on combustion aspects. A 1D-3D CFD coupled analysis was generated and calibrated with data from engine dynamometer tests. The 1D analysis provided the boundary conditions of the CFD model. They have shown that both NO_x and soot calculations of the model are in good correlation with the test data gathered from 3.2 L compression ignition (CI) turbocharged engine and that the coupling could successfully predict the emission trends in 93% of the cases.

Kim *et al.* [11] studied combustion and emission characteristics of a direct-injection (DI) engine under various operating conditions. For NO_x emission prediction, they used the extended Zeldovich mechanism. They have shown that NO_x emission increases with the increase in injected fuel mass. They have also demonstrated that it is possible to decrease NO_x emission via low-temperature combustion and retarded injection timing.

2.2. Stochastic Reactor Models

Apart from 3D CFD based emission prediction methodologies, there are studies in the literature which include the use of 1D engine modelling tools and stochastic reactor models. Amit Bhave *et al.* [12] studied combustion in a six-cylinder 16 L truck engine, operating in homogeneous charge compression ignition (HCCI) conditions. They used a stochastic reactor model (SRM) to take chemistry of combustion process into account in between intake valve close, IVC to exhaust valve open, EVO times. Equi-weighted Monte Carlo particle method was used to solve probability density function (PDF) based transport equation. The 1D model passed the in-cylinder pressure, temperature and internal EGR rate values to SRM as initial values. SRM then was used to simulate the combustion in engine cylinder from IVC to EVO. It was shown that the model in-cylinder pressure curves were in good correlation with dynamometer data and there was an excellent agreement between model predictions and measurements of CO, HC, and NO_x emissions.

Andrew Smallbone *et al.* [13] worked on modelling a DI diesel engine. They coupled 1D model and SRM and focused on virtual engine optimization and intelligent design of experiments. They correlated the engine model against 46 steady state operating points by taking the in-cylinder pressure and emission outputs into account. EGR rate, boost pressure, and injection timing were the primary reference parameters. By using the correlated model, they performed 968 simulations to examine the local in-cylinder temperature, equivalence ratio, and exhaust emissions. They identified optimum operational conditions by taking limitations on regulated emissions into consideration.

Maurya *et al.* [14] performed a detailed study to generate an approach for examination of combustion and emission characteristics of a 7.8 L diesel engine. They utilized SRM and 3D CFD software (STAR-CD). Experimental data were used to validate the SRM model, and parametric analysis of dual fuel engine was performed for different engine speed, EGR rate and the premixing ratio of the fuels. The results showed that the simulation and experimental data were in good agreement.

Jochim *et al.* [15] worked on multi-zone modelling to capture premixed charge compression ignition (PCCI) diesel engine combustion characteristics. They firstly made a comparison of the multi-zone model with 3D CFD simulation outputs; then they performed another comparison with test data. Calculations showed that the simulation duration of multi-zone models is significantly smaller than 3D CFD. In the experiments, they collected test data at 105 different operating conditions including variations of the start of injection, injected fuel mass and EGR rate in a four-cylinder diesel engine. They have illustrated that NO and unburned hydrocarbons (UHC) prediction of CFD simulations ware in good correlation with the test data and the multi-zone model trends are the same with test data.

Wang *et al.* [16] utilized reduced chemical reaction mechanisms to model combustion and emission characteristics of hydrocarbon fuels. They generated an n-heptane mechanism in which a detailed poly-aromatic hydrocarbon (PAH) mechanism is embedded. The final version of the mechanism included 349 reactions and 76 species. Shock tube experiments and test-bed engine data were used to validate the mechanism. They calculated combustion characteristics and soot emissions of n-butanol, n-heptane and diesel fuel. Soot emission trend was well captured, and the predicted NO_x emissions were in good agreement with experimental data.

Paul *et al.* [17] explored the radiative heat transfer effects on NO_x and soot emissions, energy distribution in the combustion chamber and heat losses in a heavy-duty diesel engine with CFD. Different combinations of turbulent combustion models, spectral radiation property models and radiative heat transfer (RTE) equation solvers were examined. Engine operating conditions were varied by load and EGR rate percentages. Combustion chamber mean temperature values change in 50-100 K range with the consideration of radiation, but with a minimal effect on engine emissions. It was mentioned that radiative effects would be more dominant in bigger scale engines such as ones for a locomotive or marine applications.

Aubagnac-Karkar *et al.* [18] focused on the development of a soot emission prediction capability.

They coupled a sectional soot model and IFP-C3D RANS CFD code. Soot and combustion model outputs were compared with test data including two different operating points (2200 and 4000 rpm) with different EGR rate, injection pressure and injection duration values. They concluded that the proposed model predicts the soot volume fraction and distribution with reasonable accuracy.

Duvvuri *et al.* [19] studied on soot particle size prediction in both heavy-duty (Scania 12.7 L) and light-duty (GM 1.9 L) diesel engines. They used a sectional Converge model (45 degrees for heavy-duty and 60 degrees for light-duty diesel engine). SAGE detailed kinetics model with a multizone approach was preferred for the simulations. Qualitative trends of soot particle number density predicted showed a good match with the experimental results for both types of engines.

2.3. Phenomenological Models

Phenomenological and semi-empirical models are other alternative emission prediction methods. Rajkumar *et al.* [20] investigated the use of phenomenological models to predict NO_x and soot emissions of Ford DV3 common rail diesel injection (CRDI) engine at different engine speed and load conditions. Their multizone model included modules such as spray growth, fuel-air mixing, evaporation, ignition, combustion, and emissions (NO_x and soot). NO_x predictions were based on the Zeldovich mechanism. Soot predictions were performed via Fusco (for soot formation) and Nagle and Strickland-Constable (for soot oxidation) models. Results showed that the maximum deviation of predicted NO_x emission values from measurements was 10%.

Rakopoulos *et al.* [21] studied the effect of EGR on combustion and emissions in a diesel engine. They performed tests on a single-cylinder engine at different engine speed, load and EGR rates. They also developed a two-zone phenomenological combustion model. No root mean square error, RMSE, values were given in the study, but the crank angle based comparison of model results and test data at the different start of injection times showed that the model outputs were in good correlation with the test data.

Provataris *et al.* [22] worked on a semi-empirical, two-zone model to generate a methodology for NO_x prediction. The developed model used geometrical data of cylinder and experimentally measured combustion rate for the calculation of tailpipe NO_x emissions. The extended Zeldovich mechanism was employed. Provataris *et al.* used the model for two different engines: 6.37 L heavy-duty diesel engine and 2.15 L passenger car engine. The calculations were made for an engine speed range of 1400-2200 rpm and a load range of 20% to 100%. Heavy-duty diesel engine NO_x emission prediction mean relative error was 18%. They reported that the calculation time of the model was lower in comparison to other phenomenological models [23].

Finesso *et al.* [24] focused on prediction of NO_x emission in a light-duty diesel engine. They performed experiments at 123 different engine speeds and loads, and also completed an EGR rate sweep in the test environment. They created a predictive combustion model which includes six different sub-models for calculating: chemical energy release, in-cylinder pressure, friction loss, pumping loss, in-cylinder temperature and NO_x emission. The NO_x emission model was a semi-empirical correlation which was a function of total injected fuel quantity, engine speed, intake oxygen concentration, injection pressure, crank angle for 50% of fuel mass is burnt (MFB50), and burned gas temperature evaluated at MFB50. MFB50 was calculated via the heat release model. They reported that when compared to experimental data engine out steady state NO_x emission R^2 value was 0.96.

Finesso *et al.* [25] performed another study and predicted NO_x emission via a semi-empirical model in diesel engines. They assumed that NO_x molar formation rate is an exponential function of the burned gas temperature. They reported that the NO mass per cycle mainly depends on the mass of nitrogen and oxygen available in the diffusion flame region. They investigated the effect of maximum in-cylinder temperature, especially after the main injection and showed the correlation between maximum in-cylinder temperature with NO_x formation. They used maximum in-cylinder temperature, injected fuel quantity, equivalence ratio, engine speed and injection pressure as parameters of NO_x emission modelling.

2.4. Artificial Neural Networks (ANN)

Use of ANN employing engine performance parameters is another way of predicting emissions. Pennycott *et al.* [26] utilized an ANN model to predict CO_2 emission of a 2.4 L, four-cylinder diesel engine. They employed engine speed, engine torque, start time of injection, air mass flow rate, rail pressure and oil temperature values as the ANN parameters. They showed that it is possible to use ANN for accurate emission prediction. Although this study was not focusing on NO_x prediction, it is a successful example of emission prediction.

Traver *et al.* [27] explored the feasibility of using variables such as brake mean effective pressure (BMEP), gross mean effective pressure (GMEP) to predict emission values of a diesel engine. They performed instrumentation on a 7.3 L V8 diesel engine to measure and record engine speed, fuel injection pulse width, injection timing, manifold air pressure values. They calculated BMEP, GMEP at steady state conditions over full speed and load test matrix. They performed model correlations on the data gathered at 64 different operating points. They tested the generated ANN over FTP (Federal Test Procedure) cycle data. Results showed that there was a considerable success in NO_x and CO_2 predictions. Traver *et al.* also showed that ANN prepared with steady-state data would be sufficient to perform emission prediction at transient conditions.

Brahma *et al.* [28] worked on empirical regression based ANN model to predict transient NO_x to develop the capability of transient optimization. They used unsteady data for the model generation. They argued that transient emissions and some independent engine parameters (such as fuel flow rate) differ from their corresponding steady-state values. They showed the effect of sensor lags and transport delays on unsteady test data usage. They obtained proper matching between experimental data and predictions.

Liu *et al.* [29] studied ANN to predict emissions of a compressed natural gas (CN)G/diesel dual fuel engine. They used 100 points gathered at different operating conditions for model generation and 20 points for verification. Generated neural net-

work maps mainly based on the quantity of main and pilot injections and injection timing parameters. They stated that the simulated results are in good agreement with the test data. They showed that increasing the amount of fuel injection leads to a reduction in CO emission and an increase in NO_x emission due to higher in-cylinder temperature values.

Zhang *et al.* [30] generated an ANN model which uses torque, speed, oil temperature, the start of injection (SOI), EGR rate and rail pressure. They collected emission data from a 2L, four-cylinder diesel engine. They used both hot and cold drive cycles to generate neural networks and assess them. Model outputs were within ± 20% error margin of dynamometer test data.

Shailaja *et al.* [31] developed an ANN to predict diesel engine NO_x, CO, and HC emissions. They practised a feedforward network and Levenberg-Marquardt algorithm. They collected the experimental data in a single cylinder, four stroke and variable compression ratio diesel engine at different operating conditions by adjusting compression ratio, injection time, injection pressure and load. They conducted 320 experiments. Out of these 320 data sets, 85% is used for model training, and 15% is employed for testing. A strong correlation (R^2 is 0.99) to experimental data was reported.

Saez *et al.* [32] studied emission prediction of a diesel engine fueled with animal fat using ANN. They conducted the study with a 2.0L 140 hp, Euro 4, turbocharged diesel engine. Main input variables of the neural network were vehicle speed, acceleration, engine speed and torque, air inlet temperature, boost pressure, mass air flow and fuel consumption. They reported that when compared to the testing data set; model NO_x and CO_2 emission prediction R^2 value is 0.78.

Niu *et al.* [33] focused on the performance comparison of ANN and support vector machine (SVM) in a marine diesel engine application. They created two different models with the same sampling data which includes 25 different operating points. Rail pressure, injection timing, charge pressure and charge temperature parameters are selected as the primary input variable in ANN generation. Besides, a nonlinear

regression function was created for SVM. Via these models, they have performed model vs test data comparison for brake specific fuel consumption (BSFC), NO_x and soot emission values. They showed that, although SVM model can find the global optimum, the ANN model can only detect local minima in some cases. Soot and NO_x emission predictions of the models were in good correlation to test data.

Bhowmik *et al.* [34] investigated the usage of an ANN model for performance and emission prediction of a diesel engine in which adulterated diesel fuel is used. They used 70% of the test data to train the model, 30% of the test data for validation and test. Brake thermal efficiency, brake specific fuel consumption, NO_x, UHC and CO emissions were the main outputs of the ANN model. They showed that the model could be developed with minimal data requirement and it is useful in the prediction of main engine performance outputs.

Nikzadfara *et al.* [35] worked on a model based calibration methodology. A coupled thermodynamical and ANN model was developed. In the ANN model, inlet air pressure, inlet air temperature, engine speed, rail pressure, the mass of injected fuel, the mass of pilot injection, CA at main injection, pilot retard, EGR rate and exhaust pressure parameters were used as the primary inputs. Aspirated air, torque, exhaust temperature, maximum combustion temperature, maximum combustion pressure, soot and NO_x emission values were the main outputs. They utilized from a genetic algorithm which was optimizing a cost function including the effect of BSFC, brake torque, NO_x and soot emissions. The genetic algorithm runs included 500 generations with a population size of 50. Torque, NO_x and soot emissions and BSFC comparisons of coupled model and the test data were in good agreement. They stated that the developed methodology lowers required time, cost and overall complexity that may be encountered in calibration development.

Lotfan *et al.* [36] focused on the coupling of an ANN model and non-dominated sorting genetic algorithm II (NSGA-II). They aimed to predict both CO and NO_x emissions. They selected engine speed, power, intake temperature, fuel flow rate and air mass flow parameter as the main controllable. The black box engine model was

created by using 400 sets of experimental data. Then, model outputs were compared with test data. It was shown that correlation factors for CO and NO_x emissions are 0.9963 and 0.9953, respectively.

Burke *et al.* [37] worked on modelling of diesel NO_x, CO_2, CO, UHC emissions using the parametric Volterra series of a 2.0 L diesel engine. Results showed that RMSE values of NO_x emissions and CO_2 emissions are 6.8% and 6.6% respectively.

As can be seen from the studies mentioned above, 3D CFD, semi-empirical, phenomenological, reaction kinetics, and artificial neural networks are preferred for NO_x emission prediction. The models mentioned can be ordered with their computational time requirement as thermodynamical models, phenomenological models, reaction kinetics based models and 3D CFD models. The thermodynamical models have the lowest computational time required for calculation [14], [38] and 3D CFD models have the highest. For example, with 1D based models; the duration required for collecting data at ten different engine speed and 20 different load points is approximately a couple of hours on a desktop workstation. On the other hand, via 3D CFD or SRM models; the duration needed for the same operation may be a week or even higher. Besides the complexity level of these methods increase in the same order. 1D thermodynamical models have the lowest complexity [14], [38]. Using a single cylinder thermodynamical model rather than a detailed model (six-cylinders) can even further reduce both complexity and computational costs.

Furthermore, the minimum data requirement for thermodynamical model generation and correlation is lower in comparison to other models. For example; the artificial neural network based emission prediction methods are generally highly dependant on test data for creating the maps that are used for emission prediction. This condition makes artificial neural network model use at early stages of engine development infeasible.

However, thermodynamical models are physical-based models. It is possible to generate the thermodynamical models at early stages of engine development and cor-

relate with single cylinder test or 3D CFD data collected at a few operating points. Then, it is possible to predict the engine performance outputs for full engine speed and load range.

Thermodynamical models can be used for various engine operation modes such as HCCI, PCCI, engine types CI, SI, and fuels such as liquified natural gas (LNG), biodiesel, etc. with high accuracy. Although 1D-Stochastic reactor model coupling studies offer promising accuracy at different operating points; this accuracy range is generally restricted with HCCI or SI operation modes.

If a robust and accurate method is developed for emission prediction via 1D thermodynamical model, generic engine models can be modified and used at early development stages as well. In this thesis, the focus is on an alternative way of emission prediction via thermodynamical models. Emission prediction capability of correlated 1D engine models is investigated to develop a fast and accurate methodology of emission prediction.

In this thesis; a new methodology is developed in order to enable fast and accurate NO_x emission prediction via an alternative way: 1D Thermodynamical Models. The methodology developed within the scope of this thesis is proven that;

- Engine performance parameters that cannot be measured in actual tests can be used to increase prediction accuracy.
- The methodology is effective even at very early stages of engine development.
- The methodology does not require excessive test data.
- Accuracy is very high.
- The methodology is independent from engine volume, power or combustion characteristics.

3. THEORETICAL BACKGROUND

Available 1D engine simulation tools offer an advanced understanding of internal combustion engines. That's why 1D engine simulation software programs are increasing their popularity in many studies on engine performance, cooling system, lubrication system, acoustics and electrification since they reduce the size of optimization space in these problems via providing fast and accurate simulation results. AVL Boost, Ricardo Wave and GT-Suite of Gamma Technologies are some examples of today's most popular thermodynamical analyses tools.

In this thesis, GT-Suite tools such as GT-Power and Gem-3D are used. GT-Power is mainly used for engine performance model generation and simulations. This tool solves unsteady conservation equations in one dimension. On the other hand, Gem-3D tool is used for converting three dimensional CAD geometries into one-dimensional models.

There are many significant advantages of 1D thermodynamical models such as:

- It is a cost-effective solution since the simulation duration of thermodynamic tools are significantly lower in comparison with 3D simulations, stochastic reactor model or phenomenological models.
- It is possible to use these models for multi-purposes such as engine performance development studies, thermal management based projects, acoustics or electrification studies.
- It is possible to lower actual dynamometer tests via correlated engine performance models.
- These models are able to run real-time. Hence, it is poosible to couple them with Hardware in the Loop (HIL) systems.

Many OEMs are preferring these codes to perform engine performance simulations to cover some critical studies such as:

- Engine performance target setting
- Fuel consumption and emission analyzes
- Valve timing analyzes
- EGR capability
- High altitude simulations
- Component selection
- Intake or exhaust system geometrical design
- Engine brake simulations
- Technology evaluation at the early stages of engine development

3.1. Theory of 1D Simulations

1D simulations are mainly based on the assumption that the axial velocity component is much larger than the velocity components in the cross-sectional plane. The governing equations for 1D simulation are continuity, momentum and energy equations.

3.1.1. Governing Equations

In GT-Suite, the whole system is discretized to small volume elements by dividing each flow split or pipe elements to different subsections. It connects these volumes via creating boundaries. Then; simplified continuity, momentum and energy equations are solved simultaneously. Total internal energy, density and mass flow are the critical outputs. In these calculations, all quantities are calculated via averaging through the flow direction. Calculations are mainly based on staggered grid configuration, shown in 3.1. In this configuration, scalar variables such as pressure, total enthalpy, temperature, density, total internal energy and species concentrations are calculated at the centre of the volume. On the other hand velocity, mass flux are computed at each boundary. The conservation equations for each control volume are shown in Equations 3.1, 3.2 and 3.3.

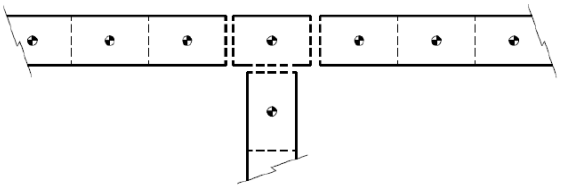

Figure 3.1. The volume elements evaluation points [3]

3.1.1.1. Continuity.

$$\frac{dm}{dt} = \sum_{boundaries} \dot{m} \tag{3.1}$$

3.1.1.2. Momentum.

$$\frac{d\dot{m}}{dt} = \frac{dpA + \sum_{boundaries} (\dot{m}u) - 4C_f \frac{1}{2}\rho u|u| \frac{dxA}{D} - K_p \left(\frac{1}{2}\rho u|u|\right) A}{dx} \tag{3.2}$$

3.1.1.3. Energy.

$$\frac{d(me)}{dt} = p\frac{dV}{dt} + \sum_{boundaries} (\dot{m}H) - hA_s(T_{fluid} - T_{wall}) \tag{3.3}$$

3.1.2. Time Step Calculation

The flow solution is carried out by integration of the conservation equations in both space and time. This integration is either implicit or explicit [3].

3.1.3. Explicit Method

The initial solution variables in the explicit method are internal energy, mass flow rate and density. The values of mass flow, density and internal energy at each new

time step are calculated based on the conservation equations.

In the explicit method, values from the previous time step are used for computing the right-hand side of the equations. This allows the value at the new time to be calculated by integration of that derivative over the time step by yielding the derivative of the primary variables. The time step must be limited to fulfill the Courant condition to guarantee numerical stability.

This method is not generally preferred for relatively long simulations since small time steps are required. But capturing the extremes of the flow characteristics especially for highly unsteady flow would be the most suitable case for explicit method. To obtain more accurate predictions of pressure pulsations encountered in fuel injection systems or engine air flow is smooth with this method. Some system analyses such as lubrication, injection, or hydraulic system simulations work well with the explicit method. For example, cooling analyses do not require a detailed calculation of pressure pulsations. So cooling system simulations are generally accomplished with the implicit flow solver.

At each time step, the pressure and temperature are calculated in the following way [3]:

- Mass and energy in the volume are calculated via continuity and energy equations
- The density is calculated by using the calculated volume and mass.
- To define density and energy as a function of pressure and temperature, the equations of state is defined for each species. Iterations on pressure and temperature are initiated and proceeded until they satisfy the density and energy already calculated for this time step.

3.1.4. Implicit Method

Mass flow, pressure, and total enthalpy are the primary solution variables in the implicit method. The energy equation is written in terms of enthalpy. This method

calculates the values of all sub-volumes at the new time step concurrently, by iteratively determining a non-linear system of algebraic equations. Implicit method is beneficial for fluid systems in which high-frequency pressure fluctuations are not of interest (i.e. cooling systems). Besides, this approach is useful if simulation durations are significant since it enables proceeding with large time steps. It is critical to note that using relatively large steps with a stable solution exceeds the CPU cost of an iterative solution for each step. Since implicit method provides a significant advantage in terms of speed; it may be preferred only in simulations that satisfy both of the following criteria [3]:

- Insignificant wave dynamics exist in the system, or accurate calculation of wave dynamics is unnecessary.
- The highest Mach number in the system is smaller than 0.3.

3.1.5. Discretization

Discretization is performed to split the large parts into smaller sections. Discretization aims to enhance the accuracy of the calculations.

3.2. Pipes

To model pipe objects, CAD data of these components are needed. Via using Gem-3D tool embedded in GT-Suite, it is possible to discretize the pipes into small tubes. Pipe templates varying with respect to geometrical features are available in GT-Suite library. It is essential to correctly set the friction multiplier, heat-transfer multiplier, and the pressure loss coefficients for effects of other geometry. These data are generally gathered from suppliers. The length and cross-sectional area of the pipe should be conserved [3].

Generally encountered flow related losses can be listed as below:

- Expansion losses
- Narrowing losses

- Pipe surface friction losses
- Geometrical losses
- System elements losses

3.2.1. Friction Losses

By using the surface roughness of the walls and Reynolds number, it is possible to calculate the flow losses due to friction. The friction factor of smooth walls is given by:

$$C_f = \frac{16}{Re_D} \text{in laminar region}, Re_D < 2000 \tag{3.4}$$

$$C_f = \frac{0.08}{Re_D^{0.25}} \text{in turbulent region}, Re_D > 4000 \tag{3.5}$$

with a transitional region in between. When the wall surface is rough, and the flow is not laminar, the value of the friction coefficient is the larger coefficient calculated via equations 3.4 and and can be represented with Nikuradse's formula below:

$$C_{f,rough} = \frac{0.25}{((2\log_{10}(\frac{1}{2}\frac{D}{h})) + 1.74)^2} \tag{3.6}$$

3.2.2. Pressure Losses

Bends or irregular cross-sections can result in pressure losses throughout the pipe. In pipe objects, there are pressure loss coefficients that can be used as forward or reverse pressure loss coefficients of pipe object. The pressure loss coefficient K_p is defined as:

$$K_p = \frac{p_1 - p_2}{\frac{1}{2}\rho V_1^2} \tag{3.7}$$

3.2.3. Heat Transfer

Heat transfer coefficients can be used to model the heat transfer from fluids inside of pipes and flow split to their walls. The heat transfer coefficient is estimated at every time step by using the wall surface roughness, the velocity of the fluid and the thermophysical properties. The heat transfer coefficient of smooth pipes is computed by using the Colburn analogy.

$$h_g = \frac{C_f}{2}\rho U_{eff} C_p Pr^{-(\frac{2}{3})} \tag{3.8}$$

Surface roughness is one of the critical parameters on heat transfer coefficient. For rough pipes, the heat transfer coefficient is calculated by using the equations and [3].

$$h_{g,rough} = h_g\Big(\frac{C_{f,rough}}{C_f}\Big)^n \tag{3.9}$$

$$n = 0.68Pr^{0.215} \tag{3.10}$$

Internal heat transfer coefficient, the predicted fluid temperature, and the inner wall temperature values are used to perform total heat transfer calculation. Wall temperature is the critical part of heat transfer calculation. It is both possible to use an already defined value to fix the wall temperature or make the model perform the calculations automatically [3].

3.3. Wall Thermal Solution

Pipe and flowsplit wall temperatures will be calculated for the case that the "Calculated Wall Temperature option" is chosen. The internal heat transfer, the external heat transfer, the thermal capacitance of the walls, and the initial wall temperature

entered by the user are the main parameters that are used for pipe and flow split wall temperature calculations. Besides, by entering the required data in the 'WallThermalBoundary' and 'WallThermalProperty' reference object describing forced convection, free convection, and radiation; it is possible to calculate the external heat transfer which occurs from outside of the pipe walls to the environment. Typical values for the external convection heat transfer coefficient are 5-20 W/m^2K (for free convection of air) [3].

3.4. Flow Connections

Links between different components are obtained via connection objects. These connections are planes at which the momentum equation is solved to estimate the mass flow and velocity.

Flow discharge coefficients must be entered in both directions for orifices, valves, throttles and ball valves. These discharge coefficients are mainly originated from the isentropic relations. For gases, discharge coefficients may be calculated by using following equations:

$$\dot{m} = A_{eff}\rho_{is}U_{is} = C_D A_R \rho_{is} U_{is} \tag{3.11}$$

$$\rho_{is} = \rho_0 (P_r)^{\frac{1}{\gamma}} \tag{3.12}$$

$$U_{is} = \sqrt{RT_0}\{\frac{2\gamma}{\gamma - 1}[1 - P_r^{\frac{\gamma-1}{\gamma}}]\}^{\frac{1}{2}} \tag{3.13}$$

$$C_f = \frac{4A_{eff}}{\pi D^2} \tag{3.14}$$

$$C_D = \frac{A_{eff}}{\pi DL} \tag{3.15}$$

3.5. Heat Transfer In Cylinder

Following equation is mainly used for calculating the heat transfer between combustion chamber surfaces in the cylinder and the gas.

$$Q = hA(T_{fluid} - T_{surface}) \tag{3.16}$$

Heat transfer is calculated between each fluid and heat exchanger structure by taking the effects of the wall thermal capacitance into consideration.

$$\frac{dT_{wall}}{dt} = \frac{Q_{M+}Q_S}{\rho V C_p} = \frac{(hA\Delta T)_M + (hA\Delta T)_S}{\rho V C_p} \tag{3.17}$$

Equation 3.17 is used to calculate the temperature of the structure from a balance of the heat transfer rates between the structure and two fluids [3].

Heat transfer coefficient is calculated from Woschni formulation as below [3]:

$$h = D^{-0.2} P_c^{0.8} T_c^{-0.53} (C_1 U_{piston} \Big[1 + 2\Big(\frac{V_{UDP}}{V_C}\Big)^2 IMEP^{-0.2}\Big]^{0.8} \tag{3.18}$$

where C_1 is the calculated value from piston mean velocity and gas velocity with the following equation:

$$C_1 = 2.28 + 0.308\frac{C_u}{U_{piston}} \tag{3.19}$$

Hence; it is possible to calculate the heat transfer between piston, engine block and liner structures. In order to perform a proper computations below parameters

need to be entered to the model [39].

- Heat capacity of the materials
- Surface thickness
- Surface area for heat transfer
- Engine oil temperature
- Cooling water temperature

3.6. Combustion and Emissions

3.6.1. Combustion

Combustion is simply the fast chemical combination of a substance with oxygen, resulting as the generation of heat and light. It occurs via the transfer of a determined amount of unburned fuel mass and air along with the affiliated enthalpy from an unburned zone to a burned zone in the cylinder. The main result is the release of the chemical energy in the fuel-air mixture. Combustion model simulates the amount of energy generated during combustion [4].

3.6.2. Burn Rate

During the combustion process, fuel and air molecules are transferred to the burned zone from the unburned zone and begin to engage in the chemical reactions. Burned rate represents the rate of the process. In other words, it is the instantaneous rate of fuel consumption within the cylinder combustion process. The combustion rate is controlled by the burn rate [4].

3.6.3. Heat Release Rate

During the combustion, the energy stored in the fuel molecules is released in the cylinder as thermal energy. The instantaneous rate of this process is the so-called heat release rate. This quantity deviates from the burn rate since the fuel-air mixture

entering the equilibrium equations does not break down spontaneously into its final products of combustion [3], [39].

3.6.4. Combustion Models

In 1D models, it is possible to model diesel combustion in various ways. These can be listed as :

3.6.4.1. Imposed Heat Release Rate. By using the measured in-cylinder pressure curves, it is possible to generate heat release rates. One can prefer embedding these heat release rates directly to the engine model. The main drawback of this methodology is; the integrated heat release rates will only represent one operating mode with one set of calibration set points. For the case that user needs to work with different calibration set points, the embedded heat release rate values will differ from reality.

3.6.4.2. Diesel Wiebe Model Generation. Alternatively it may be preferred to generate a semi-predictive combustion model by utilizing from Wiebe function concept.

$$W = 1 - exp\Big(- AWI\Big(\frac{\theta}{BDUR}\Big)^{(WEXP+1)}\Big) \tag{3.20}$$

Equation 3.20 represents the main diesel Wiebe formula [3] which consists of three main parts. The first parameter is the crank angle for %50 fuel burned, the second one is the calculated duration between the crank angles valid for %10 and %90 burned of fuel, and the third one is the exponential value of Wiebe curve. In GT-Suite this combustion model is represented by nine different parameters to increase the accuracy. These parameters are ignition delay, premixed fraction, tail fraction, premixed duration, main duration, tail duration, premixed exponent, main exponent and tail exponent. A set of parameters which provides results in good agreement with tests is needed.

3.6.4.3. DI-Pulse Model Generation. As final alternative DI-Pulse models can be utilized. DI-Pulse is a predictive combustion model generated for modelling different in-

jection strategies. DI-Pulse predictive combustion model mainly represents the diesel combustion phases. These phases are ignition delay (the difference between the start of injection and the start of combustion), premixed combustion (rapid combustion period), diffusion controlled combustion and late combustion (combustion of poorly distributed fuel particles). DI-Pulse mainly calculates these four critical regions of combustion. To perform the evaluation, DI-Pulse models need energising time, rail pressure and injected quantity maps for the injector. These maps are generally gathered from suppliers. Details of this model are in Section 5.1.

3.7. Engine Friction and Auxiliary Loads

In 1D Models, an empirically derived model which states that total engine friction is a function of peak cylinder pressure, mean piston speed, and mean piston speed squared, is in use. Equations 3.21 and 3.22 are showing the formulas used for engine friction calculation.

$$\text{FMEP} = C + (\text{PF PFP}) + (\text{MPSF} \quad \text{MPS}) + (\text{MPSFF MPS}^2) \tag{3.21}$$

$$\text{Piston Speed} = 2*\text{S}*\text{RPM}/60 \tag{3.22}$$

3.8. Indicated, Gross and Pumping Mean Effective Pressure Calculations

The mean effective pressure (MEP) is a valuable comparative engine performance measure and is achieved by dividing the work done per cycle by the cylinder(s) total displaced volume per cycle. It is the assumed pressure, which is considered to be acting on the piston during the power stroke. There are other critical engine performance related terms such as Gross Mean Effective Pressure (GMEP), Pumping Mean Effective Pressure (PMEP), Indicated Mean Effective Pressure (IMEP), Brake Mean Effective Pressure (BMEP) and Friction Mean Effective Pressure (FMEP); which are derived by the use of MEP definition.

Gross mean effective pressure (GMEP) and pumping mean effective pressure (PMEP) values represent positive and negative work of PV diagram; respectively. Indicated mean effective pressure (IMEP) is the net work of cylinder. Friction mean effective pressure (FMEP) is the theoretical mean effective pressure needed to overcome engine friction. It can be also considered as mean effective pressure lost due to friction. As a last parameter, brake mean effective pressure (BMEP) is the mean effective pressure computed from the dynamometer power (torque). The relation between these parameters are:

$$\text{GMEP} + \text{PMEP} = \text{IMEP} \tag{3.23}$$

$$\text{IMEP - FMEP} = \text{BMEP} \tag{3.24}$$

3.9. Turbines and Compressors

It is possible to model turbine and compressor performance by utilizing from supplier based performance maps. These maps mainly consist of a series of performance data points, each of which describes the operating condition by speed, pressure ratio, mass flow rate, and thermodynamic efficiency. For the case that the speed and either the mass flow or pressure ratio are known, the efficiency, pressure ratio and the mass flow rate can be calculated via these maps. A representative turbocharger map is shown in Figure 3.2. The pressure ratio (PR) and the turbocharger speed are calculated at each time step. The mass flow rate and efficiency are then looked up in the table and imposed in the solution. The mass flow rate from the map lookup is then forced as a flow boundary on the volumes near to the turbine/compressor. By using the change in enthalpy across the turbine and compressor, the imposed outlet temperature value is calculated. The enthalpy difference, and consequently the power produced/consumed by turbines/compressors, are derived from the efficiency as follows [3]:

Compressor :

$$h_{out} = h_{in} + \Delta h_s \frac{1}{\eta_s} \tag{3.25}$$

$$P = \dot{m}(h_{in} - h_{out}) \tag{3.26}$$

$$\Delta h_s = c_p T_{tot,in}(PR^{\frac{\gamma-1}{\gamma}} - 1) \tag{3.27}$$

Turbine :

$$h_{out} = h_{in} - \Delta h_s \eta_s \tag{3.28}$$

$$P = \dot{m}(h_{in} - h_{out}) \tag{3.29}$$

$$\Delta h_s = c_p T_{tot,in}(1 - PR^{\frac{1-\gamma}{\gamma}}) \tag{3.30}$$

Total temperature is:

$$T_{tot,in} = T_{in} + \frac{u_{in}^2}{2c_p} \tag{3.31}$$

The fluctuation of the mass flow rates can be encountered in compressors. This is mainly originated from the briefly crossed stall or surge line or because of the flat speed lines. This condition results as significant changes in mass flow rate even though only

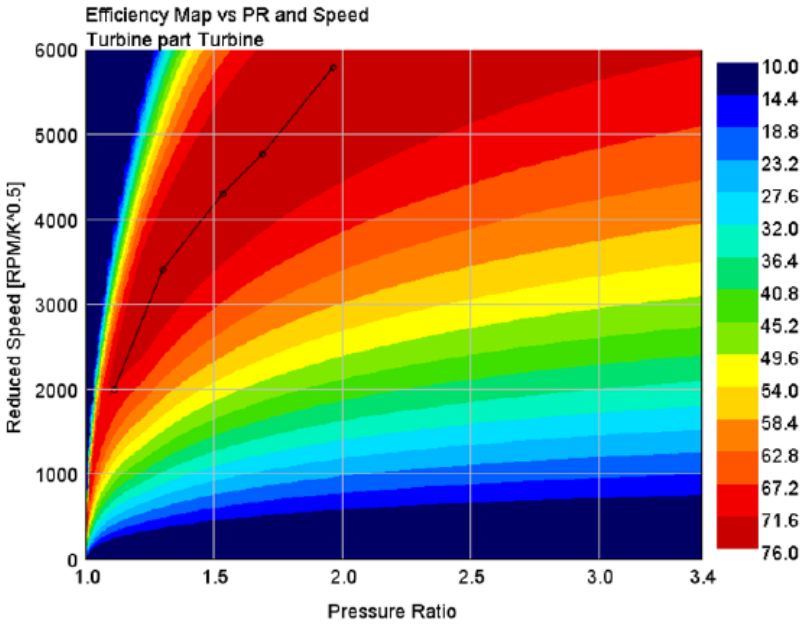

Figure 3.2. Example turbocharger map: efficiency map vs PR and speed [3]

small changes in pressure ratio is encountered. To reduce the magnitude of any extreme fluctuations in the compressor mass flow rate, the code has a damping mechanism (representing the physical damping nature of the air mass and momentum inside the compressor).

3.10. 1D Model Generation

In this section, geometrical properties of a 1D engine model, dynamometer correlation parameters, and general correlation steps will be mentioned.

3.10.1. Geometrical Composition of 1D Model

All 1D Model generation studies must be initiated with CAD data evaluation. Model geometry needs to be transferred from 3D Geometry. To do this, Gem3D tool embedded in Gt-Suite can be used. This tool can open CAD files and enables slicing, meshing, and discretization of any components such as pipes, flow splits, junctions, manifolds, etc. Selection of the cutting planes is critical since they represent the dis-

cretization of the components. Figure 3.3 is a representative illustration of the process.

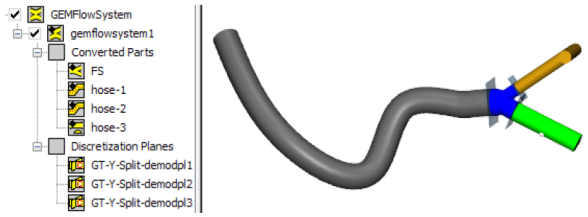

Figure 3.3. Discreatization of 3D geometry to 1D model [3]

3.10.2. Main Modeling inputs

There are many critical data that must be gathered before engine performance model generation. These data will be used as the main inputs of the model. Most crucial ones are listed as below:

- Engine type as SI or DI
- Cylinder unit
- Stroke number for one cycle
- Ignition sequence
- Friction (Chenn-Flyn) parameters
- Valve radius
- Valve Opening
- Valve Timing and Flow Coefficients
- Cylinder stroke, radius, and compression ratio
- Reference conditions of engine simulation
- Length and radius of pipes
- Surface roughness
- Heat transfer parameters
- Heat transfer and friction coefficients
- Wall temperature
- Discretization length
- Initial conditions

- Pressure loss coefficient

1D Engine performance models include all systems such as;

- Low pressure intake system: pipes, air filter
- Compressor
- High pressure intake system: pipes, charge air cooler geometry and throttle
- Intake Manifold
- Cylinders, cranktrain
- Exhaust Manifold
- Turbine
- Aftertreatment System (ATS)

3.10.3. Dynamometer Data

After creating the model, the very first step is to perform the correlation of the model to test data. To accomplish this goal, dynamometer tests must be completed. In these tests, below-listed channels must be gathered via proper sensors.

- Engine rpm
- Engine power
- In-cylinder pressure curve
- Specific fuel consumption
- Air mass flow
- Fuel mass flow
- Pressure and temperature of inlet and exhaust manifolds
- Cooling water and oil temperature
- Compressor and turbine inlet and outlet pressure and temperature
- Turbocharger shaftspeed
- Charge air cooler inlet and outlet pressure and temperature
- Throttle inlet and outlet pressure and temperature

- EGR cooler inlet and outlet pressure and temperature
- Peak firing pressure (PFP)
- NO_x, soot emissions
- Main, plot, post start of injection timings and quantities.
- Rail Pressure
- EGR Rate calculation

The examination of dynamometer data is crucial since in many cases some problems such as leakages, automatization failures, sensor failures and engineer based errors exist. To eliminate issues mentioned above, test data may be compared with previous calibration data or with another similar engine's test data.

After completing the initial diagnostics of the test data, the model correlation step can be initiated. To proceed in model correlation, 1D engine performance model simulations must use the dynamometer calibration set points. Then the comparison of previously mentioned channels needs to be performed. If the model results are in good agreement with error bands derived from dynamometer data; model correlation process is successfully accomplished. In this thesis, two different heavy-duty diesel engine models are generated. Correlations both engine models are performed to dynamometer test data. Error band has been defined for pressure measurements as ± 3%, mass flow measurements as ± 3%, and power as ± 3%. Mean effective pressure values are defined as ± 3%.

3.10.4. 1D Engine Model Correlation

After generating a 1D engine performance model, correlation studies can be initiated via tracing five main correlation steps. These steps can be summarized as air inlet, charge air system, exhaust system, base engine model and full model correlation.

3.10.4.1. Air Inlet System Correlation. Low-pressure air inlet system correlation is critical since it derives the compressor inlet boundary conditions. In the correlation of

the system, the main goal is to correlate the pressure drop at the desired air mass flow rate. Target values are generally calculated with the data obtained from suppliers or 3D CFD analyses. Once the target pressure drop is set for a constant air mass flow; then the first correlation step can be initiated. Sub-model starting with air inlet to compressor inlet is generated. Inlet boundary conditions for this sub-model is ambient pressure and temperature. Outlet boundary conditions are compressor inlet temperature and air mass flow. By arranging the diameter of one of the selected nozzles, the pressure drop across the system is correlated to pre-defined targets.

3.10.4.2. Charge Air Cooler System Correlation. Charge temperature increases after the compression process in compressor. However, to increase the amount of fresh air charge within the cylinders, lower charge temperature values are needed. Charge air cooler or intercooler systems are in-use to fulfill that purpose. As it was mentioned in the Section 3.10.4.1, the main goal is to correlate the pressure drop at the desired air mass flow rate. The target value for the correlation is calculated by using both charge air cooler supplier data and 3D CFD pressure loss analyses for the surrounding pipes and junctions. Once the target is set for the whole system, a sub-model must be created for the correlation. Inlet boundary conditions for this sub-model is compressor outlet pressure and air mass flow. Outlet boundary conditions are charge air cooler outlet pressure and temperature. By tuning the diameter of one of the selected nozzles, the pressure drop across the system is correlated to pre-defined targets.

3.10.4.3. Exhaust System Correlation. Exhaust system modelling is the other correlation step of engine model. Exhaust systems pressure drop vs exhaust mass flow target point is generally created by adding the pressure drop values of the aftertreatment system components such as diesel oxidation catalyst (DOC), selective catalytic reduction (SCR) and diesel particulate filter (DPF) systems. These pressure drop values are generally gathered from suppliers, separately. Once the target pressure drop value is set, the sub-model generation is performed. Inlet boundary conditions for this sub-model is turbine outlet temperature and exhaust mass flow. Outlet boundary conditions are ambient temperature and pressure. By tuning the diameter value of a selected nozzle,

the pressure drop correlation of the whole system can be accomplished. In exhaust system submodels, modelling the main system components such as DOC, SCR and DPF is not an obligation. It is possible to proceed by only tuning the pressure drop effects of these systems to reduce the model complexity and simulation durations.

3.10.4.4. Base Engine Correlation. As it is mentioned above, the sub-section model correlation studies are mainly for tuning the pressure drop of these systems to the pre-defined targets. However, the base engine correlation primarily focuses on both combustion and air mass flow correlation. To accomplish this goal, a base engine sub-model must be generated. Inlet boundary conditions for this sub-model is intercooler outlet pressure and temperature. Outlet boundary conditions are turbine inlet pressure and temperature. In the correlation of the base engine sub-model, main combustion parameters can be tuned to obtain targeted brake torque and exhaust manifold temperature values. Besides; if the valve timing, model geometry and the used set points (such as intercooler outlet pressure and temperature) are correctly set, then it is expected to obtain the air mass flow in good agreement with test data.

3.10.4.5. Full Engine Correlation. After performing the correlation of models mentioned above, it is possible to integrate them all to create the full engine performance model. In the entire engine model generation, turbine and compressor objects are also integrated with the subsystems mentioned above. The full model must be run with the dynamometer set points such as boost pressure target, air mass flow target, injected fuel quantity and timings. Then, the final comparison of the full model outputs with the dynamometer test data must be done.

It is important to emphasize that, in many cases, users may select to proceed with full engine model correlation only. It is also possible to generate the full model and perform all of the correlation steps mentioned above on the full model rather than different sub-models. After creating the full engine performance model, it is possible to fulfill the pressure drop targets by the aid of different PID control mechanisms providing the correct nozzle diameters. Hence, the correlation of the model can be

performed with less effort. The only complexity is to find out the correct P and I gains for PID control mechanisms.

4. 9L HEAVY-DUTY DIESEL ENGINE STUDIES

4.1. 1D Engine Model and Calibration

Thermodynamical engine model of a 9L heavy-duty diesel engine is generated in GT-Suite software by using CAD geometries valid for intake and exhaust manifolds, intake and exhaust system piping, and also critical inputs such as valve timings, firing order, turbocharger, charge air cooler, and EGR cooler performance data. All of the required data was mentioned in Subsections 3.10.2 and 3.10.3. Table 4.1 shows the specifications of the heavy-duty diesel engine used for methodology development.

Table 4.1. 9L HD diesel engine specifications

Parameter	**Value**
Volume	9L
Max Power	330 PS
Compression ratio	16.5:1
Bore	130 mm
Stroke	160 mm
Number of Cylinders	6
Injection System	Common Rail
Injection System Pressure	1800 bar

Direct Injection Diesel Wiebe Model (EngCylCombDIWiebe) is used for combustion modelling [40]. This function imposes the burn rate for direct injection diesel engines using nine parameter Wiebe function. These parameters are ignition delay, premixed fraction, tail fraction, premixed duration, main duration, tail duration, premixed exponent, main exponent and tail exponent. To ensure that these parameters are correctly set for different operation conditions critical engine performance output values such as; peak firing pressure values, turbine inlet temperature and brake torque values should be thoroughly compared with test data. Besides, the comparison of in-

cylinder pressure curves between model and test data is a necessity. Correlation of above-listed performance outputs should be within accepted margins to use a thermodynamical model for further studies.

Diesel Wiebe combustion model is valid for direct injection engines. This model typically uses a single injection time corresponding to the main injection and does not consider pilot and post-injection processes. However, the amount of fuel delivered is the total quantity of fuel in all of the injections. The experimentally measured start of injection (SOI) values hence cannot be used in 1D engine model directly. It is essential to find out the engine model representative start of injection values by correlating the thermodynamical model to test data.

The primary inputs of the thermodynamical model are air mass flow target (to define EGR rate), boost pressure and temperature, injected total fuel quantity, engine speed and maximum in-cylinder pressure. Air mass flow rate values are targeted in the model via using a PID controller which adjusts EGR valve position. To secure that the correct EGR rate is achieved in the model; boost and turbine inlet pressure, and temperature values should have a good correlation with test data.

Fuel loop is a naming convention used in dynamometer testing. A fuel loop test requires data collection at engine speed and load values spanning the full operation range (0% to 100%). In this section of the study, three different fuel loop data are gathered in dynamometer tests.

The primary goal is to collect sufficient data covering different feedgas (engine out) NO_x levels for methodology generation and validation. It is aimed to investigate the accuracy of the methodology with the same hardware and at same engine speed and torque values but at different operating conditions such as air flow, boost pressure, turbine inlet temperature, and hence different emission outputs. Collecting the fuel loop data at different boost temperature values served explicitly to this purpose. Table 4.2 shows the boost temperature values of the three different fuel loop data sets measured in the dynamometer tests. In each of these three experiments, data are collected

at 140 different operating points corresponding to 10% intervals of engine load at different speeds. Figure 4.1 shows the operating locations used in the measurements of fuel loops. Same operating points are used for all three fuel loop. The y-axis represents the brake torque values non-dimensionalized with maximum brake torque value.

Table 4.2. Fuel loop data sets

Test Data:	**Boost Temperature**	**Number of Points**
Fuel Loop 1	30 ^{o}C	140
Fuel Loop 2	40 ^{o}C	140
Fuel Loop 3	50 ^{o}C	140

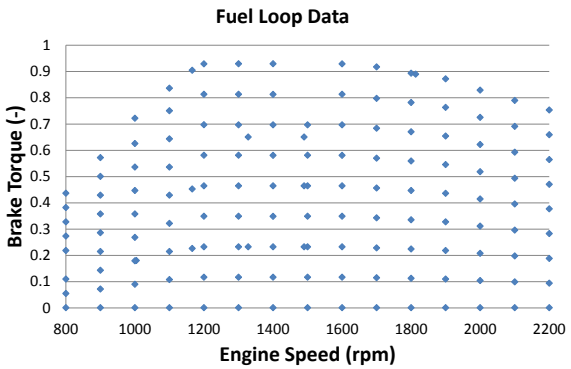

Figure 4.1. Fuel loop points

Fuel loop 1 is used for model correlation. Figures 4.2-4.11 show the comparison between model predictions and the test measurements under full load conditions.

Figures 4.2,4.3, 4.4, 4.5 and 4.6 show that non-dimensional IMEP, GMEP, BMEP, PMEP and FMEP are mostly within ± 3% accuracy band indicating that accuracy of combustion and friction models is quite good. The main contribution of PMEP is the difference between turbine inlet pressure and boost pressure. Increase in this difference results as an increase in pumping losses. In this study, the fuel loop correlation was performed with high accuracy in both turbine inlet pressure and boost pressure. Hence, for any operating condition, the thermodynamic model calculates the pumping losses

accurately.

Generally, thermodynamical models need some efficiency or mass flow multipliers to ensure a good correlation of compressor outlet temperature and turbine inlet pressure values. This condition is mainly a result of miscalculated heat transfer or ignored friction values during turbocharger map generation in a turbocharger test bench. To keep the model outputs in alignment with dynamometer test bench data, efficiency multipliers (located in the thermodynamic model's turbocharger objects) can be used. Figure 4.7 and 4.8 show that compressor outlet pressure and compressor outlet temperature values lay within the acceptable ± 3% and ± 10 ^{o}C accuracy bands respectively. Figure 4.9 and 4.10 show that turbine inlet pressure and turbine inlet temperature values are also within the acceptable ± 3% and ± 50 ^{o}C accuracy bands respectively. In this study use of such efficiency multipliers are not needed and compressor and turbine maps successfully cover the real test conditions, including heat transfer, friction, etc.

Figure 4.11 shows that model in-cylinder pressure values are also in good correlation with test data. The peak firing pressure outputs of the model are mostly within ±2.5 bar difference range.

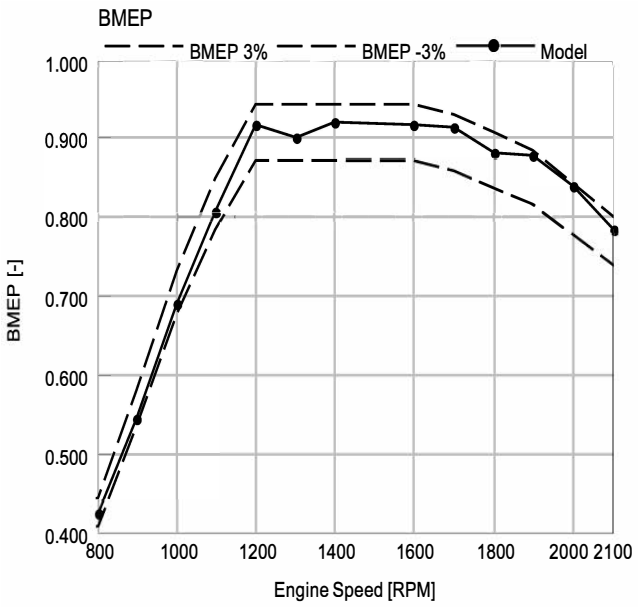

Figure 4.2. Full load correlation comparison: BMEP

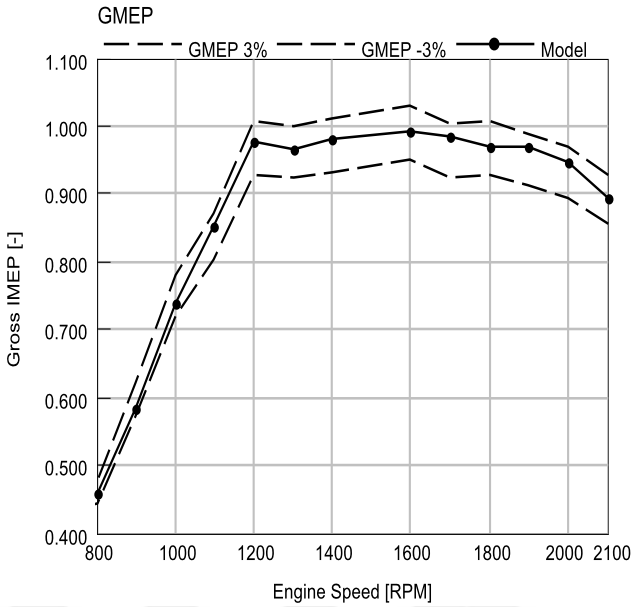

Figure 4.3. Full load correlation comparison: GMEP

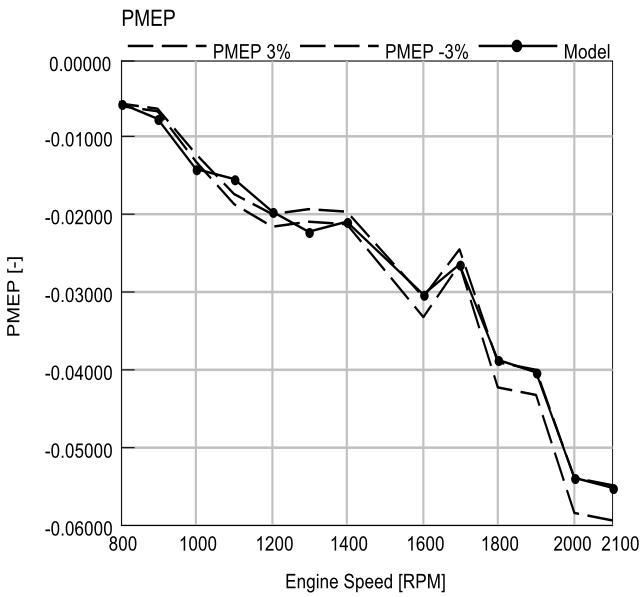

Figure 4.4. Full load correlation comparison: PMEP

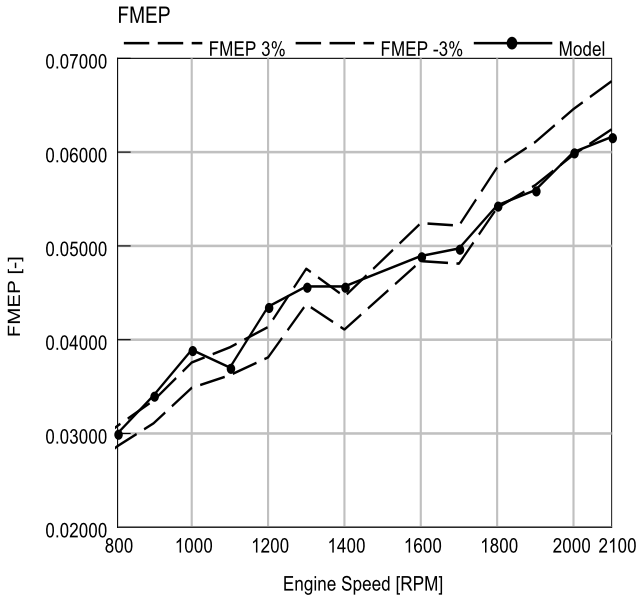

Figure 4.5. Full load correlation comparison: FMEP

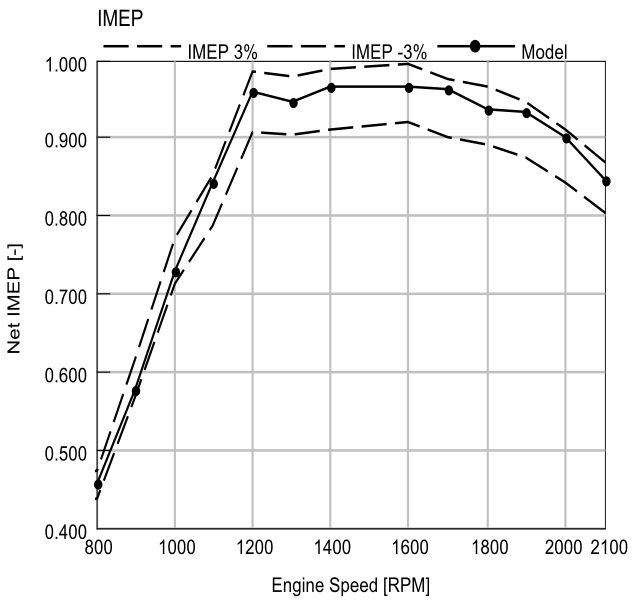

Figure 4.6. Full load correlation comparison: IMEP

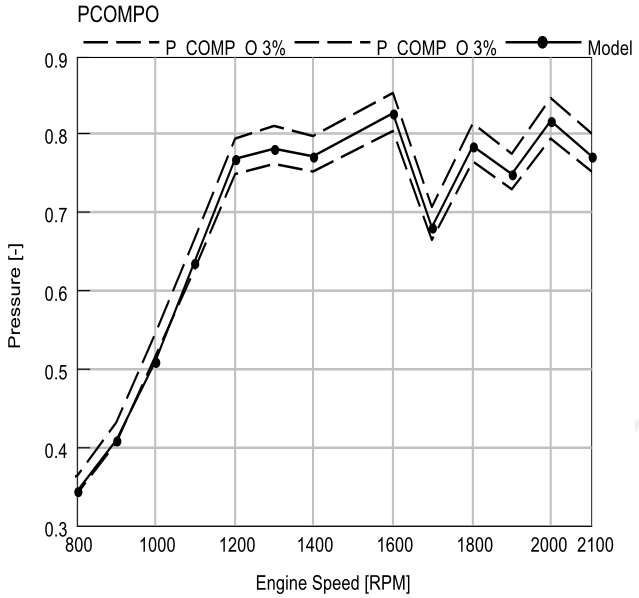

Figure 4.7. Full load correlation comparison: compressor outlet pressure

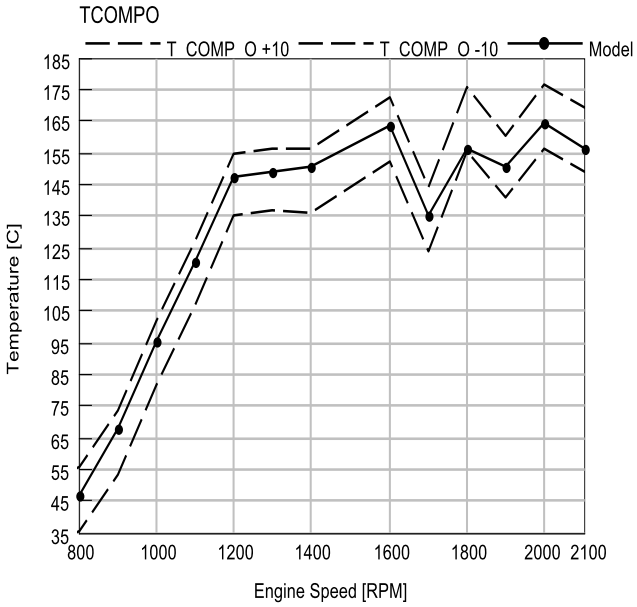

Figure 4.8. Full load correlation comparison: compressor outlet temperature

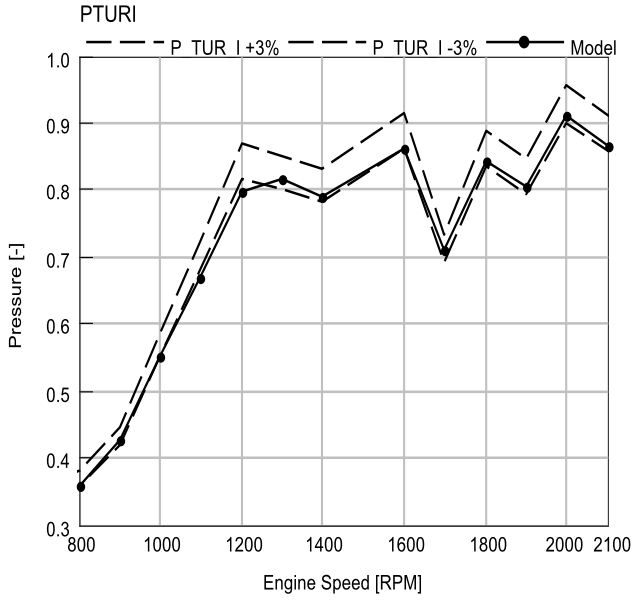

Figure 4.9. Full load correlation comparison: turbine inlet pressure

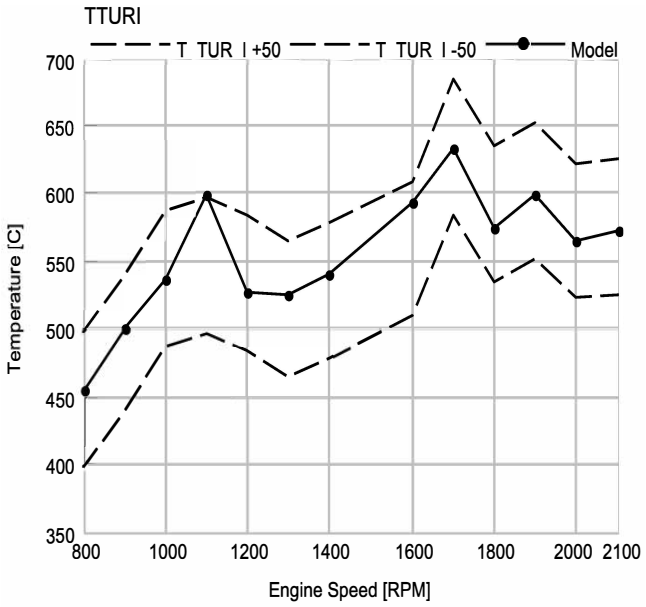

Figure 4.10. Full load correlation comparison: turbine inlet temperature

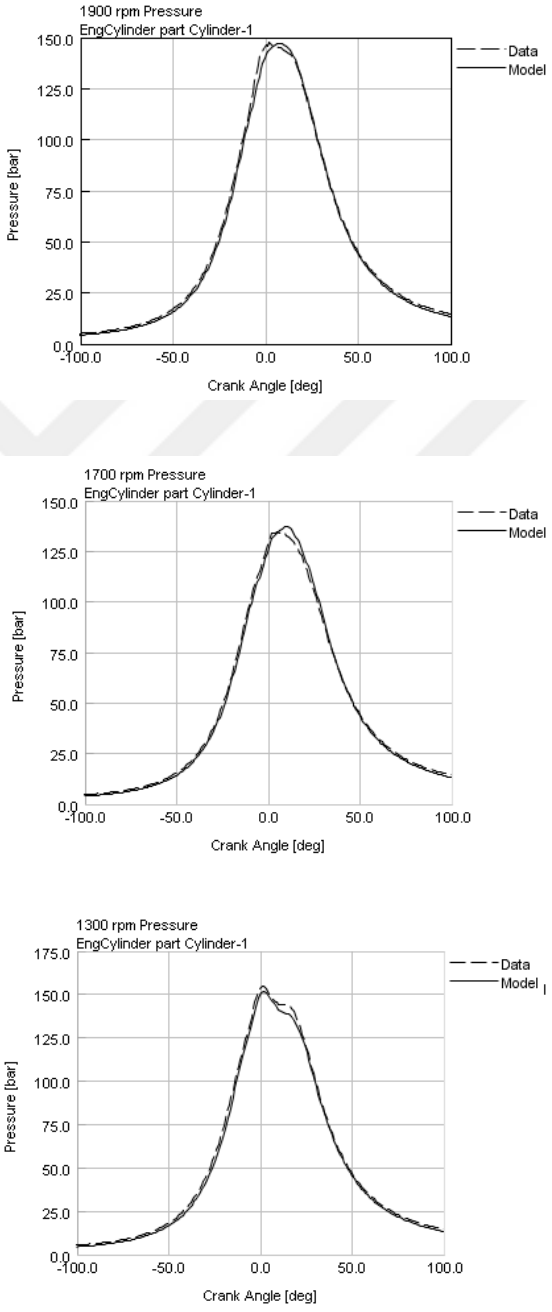

Figure 4.11. In-cylinder pressure curve comparisons at different operating points

Figure 4.12 shows NO_x emission measurements for three different fuel loops. Nondimensional contour plots are generated by dividing the measured values by the maximum NO_x measured value. HORIBA PG-250 multi-gas portable analyzer is used to gather NO_x emissions data. Technical specification of the device is showing that the measurement accuracy for NO_x emission is $\pm$ 1%. Repeatability of HORIBA device is $\pm$ 0.5% with respect to a reference point. Fuel Loop 3, which is the loop with the highest boost temperature shows the highest NO_x emissions. Maximum NO_x values are encountered near the full load range, especially in the 1200-1600 rpm range in all of these fuel loops.

4.2. NO_x Model and Calibration

In the proposed method, the NO_x emissions are calculated by using the extended Zeldovich mechanism embedded in the GT-Suite based thermodynamical model. Table 4.3 shows the reactions representing the extended Zeldovich mechanism and their rate equations. All reactions are two-way reactions and the rates shown in Table 4.3 are the forward reaction rates. Use of equilibrium constant and the forward reaction rate gives the reverse reaction rates. To tune the model NO_x emission outputs to experimental data, it is possible to employ a calibration multiplier which modifies the net rate of formation.

Table 4.3. Extended Zeldovich mechanism reactions [3]

Reaction	**Forward Reaction Rate**	**Unit**
$N_2 + O = NO + N$	$k_1 = 1.8\ 10^8 e^{-38370/T}$	$m^3 gmol^{-1} sec^{-1}$
$N + O_2 = NO + O$	$k_2 = 1.8\ 10^4 T e^{-4680/T}$	$m^3 gmol^{-1} sec^{-1}$
$N + OH = NO + H$	$k_3 = 7.1\ 10^7 T e^{-450/T}$	$m^3 gmol^{-1} sec^{-1}$

Once the model run with Fuel Loop 1 inputs, NO_x outputs of the model are compared with test data, the ratio between the model NO_x and dynamometer NO_x values is called calibration multiplier. To enhance the models NO_x emission prediction accuracy, these multipliers can be utilized via generating suitable multidimensional

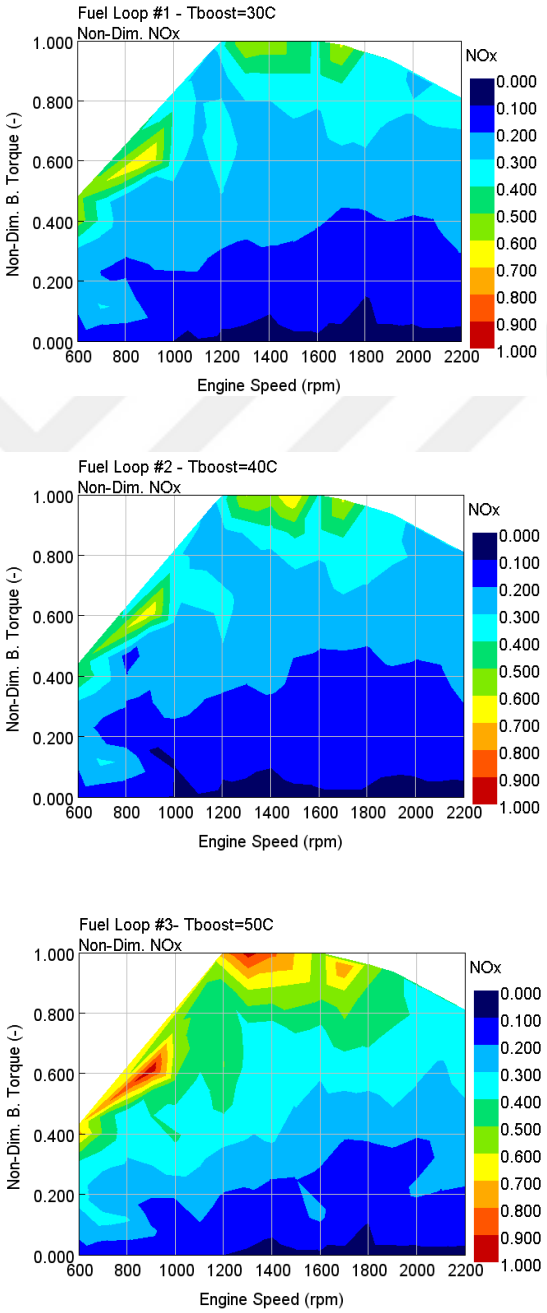

Figure 4.12. NO_x emission comparison of different fuel loops

look-up tables. The inputs of these multidimensional look-up tables are different engine performance parameters such as turbine inlet temperature, injected fuel quantity, engine speed, etc. The only output is the NO_x calibration multiplier. By utilizing from the "Multidimensional Table Look-up Using Scattered Data" object embedded into GT-Suite, it is possible to generate and use different maps providing NO_x calibration multipliers. Use of these maps enables accurate NO_x prediction with low computational resources. For example, it is possible to generate the NO_x prediction for 100 points within only 30 minutes on a PC with an i7 CPU.

In the below studies, the aim is to find out the best engine performance parameters for map generation. Hence, emission model is correlated by calculating the calibration multipliers that provide ± 2% accuracy in comparison with experimental results for each point in Fuel Loop 1.

Once the NO_x calibration multipliers generated by using Fuel Loop 1 and mapped via the use of different engine performance parameters; Fuel Loops 2 and 3 are run to see the NO_x prediction accuracy of the generated maps. These two fuel loops are not used for map generation. They are only used for measuring the prediction capability of the different maps.

So, the main steps of the correlation methodology can be summarized as listed below:

(i) Generate engine model by using 3D CAD geometry, valve lifts, discharge coefficients, etc.
(ii) Perform fuel loop correlation of engine model to test data.
(iii) Compare the model NO_x output and corresponding dynamometer data to calculate NO_x calibration multipliers for each case.
(iv) Generate maps of NO_x calibration multipliers using different engine performance parameters as inputs.
(v) Use different test data to evaluate the effectiveness of the generated maps. Compare the results of different maps regarding emission prediction accuracy.

(vi) Select the map with the highest accuracy.

It is shown in this study that, these methodological steps are valid independently of the engine volume and power. One can use the same steps with a different engine, as well.

4.3. NO_x Calibration Multiplier Maps

To enhance the NO_x prediction accuracy of the model, the selection of proper map parameters has critical importance. Various parameters such as RPM, load, EGR rate etc. are used for NO_x calibration multiplier map generation by utilizing data of Fuel Loop 1. This section includes the selection of input parameters used for the map generation and the resulting NO_x emission prediction accuracy obtained for fuel loops 2 and 3.

Independent variables such as test injection pressure, pilot and post-injection timing and quantities are not used as primary inputs since these parameters are not variables of Diesel Wiebe; the current combustion model. Air mass flow rate target (to define EGR rate), boost pressure and temperature, injected total fuel quantity, engine speed and maximum in-cylinder pressure values are the prime inputs in models including Diesel Wiebe combustion model. Utilising injection pressure, pilot and post-injection timing and quantities as direct inputs require the use of a predictive combustion tool, like DI-Pulse. However, in DI-Pulse; user needs detailed information (such as injector pulse widths, etc.) which are generally confidential for injector suppliers. In this section, the methodology is generated without any need for such kind of data. Heat release rates which are created by using Diesel Wiebe include the effect of these parameters.

Sixteen different maps are generated by the use of eleven different parameters which are engine speed (RPM), engine load (Load), EGR rate, turbine inlet temperature (TTURI), peak firing pressure (PFP), in-cylinder maximum temperature (TMax), fuel flow rate, CA50, fuel-air ratio, EGR rate and rail pressure.

To evaluate the effectiveness of different maps, two different methodologies are employed:

(i) Pie charts showing the residencies of NO_x emission prediction results are examined.
(ii) Non-dimensional Root Mean Square (nRMSE) values are calculated.

For the nRMSE calculations, below equations are used:

$$\text{Error}(\%) = 100\frac{\text{NO}_{\text{x,model}} - \text{NO}_{\text{x,test}}}{\text{NO}_{\text{x,test}}} \tag{4.1}$$

Also, non-dimensional root mean square error (nRMSE) values are calculated via Equations 4.2 and 4.3. RMSE values are non-dimensionalized to obtain proper comparison of accuracy results between different engine variants.

$$\text{RMSE (ppm)} = \sqrt{\frac{1}{n}\Sigma_{i=1}^{n}\Big(\text{NO}_{\text{x,test}} - \text{NO}_{\text{x,model}}\Big)^2} \tag{4.2}$$

$$\text{nRMSE (\%)} = 100\frac{\text{RMSE}}{\text{NO}_{\text{x,max}} - \text{NO}_{\text{x,min}}} \tag{4.3}$$

Engine speed is selected as the first parameter since it mainly represents the air flow capability, friction and pumping losses which indirectly affect the NO_x emission formation. Besides, in the literature there are many studies using engine speed parameter for NO_x emission prediction [41], [42], [43]. EGR flow is also chosen since EGR flow is one of the main parameters showing a significant trend on NO_x formation.

Hence, engine speed and the EGR flow parameters are selected as the initial input parameters used in the production of the first NO_x calibration multiplier map. Once the map is created with the outputs of fuel loop 1, fuel loops 2 and 3 are run with this

map to see the NO_x prediction capability.

Figure 4.13 shows the distribution of the points. In x-axis non-dimensional dynamometer NO_x data, in y-axis non-dimensional model NO_x values exist. Each black points seen in Figure 4.13 belongs to one of the operating points. Maximum NO_x value is used for the non-dimensionalization. The black line is a linear line representing the equation: x=y. Dashed lines are representing 10% and -10% variances with respect to the linear line. These dashed lines are used in order to obtain a clear understanding for distribution of the operating points. Calculated nRMSE is approximately 17%.

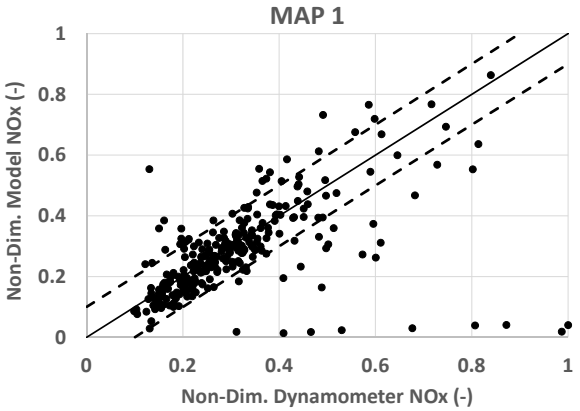

Figure 4.13. Model vs. test data comparison: MAP1= f(RPM, EGR Flow)

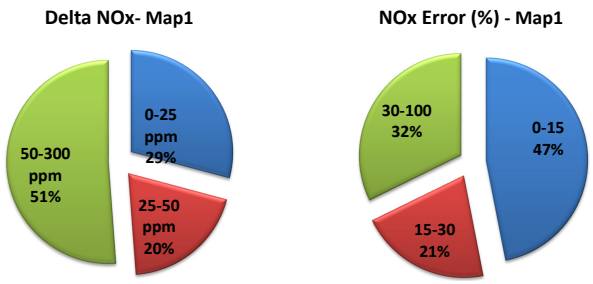

Figure 4.14. Model vs. test Data comparison in pie charts: MAP 1= f (RPM, EGR Flow)

Figure 4.14 represents the results shown in pie charts. Left hand side and right hand side graphs are showing the model and test data difference values in delta and percentage; respectively. As it is seen in the figure, 29% of total points are within 0-25

ppm delta error band, and 47% of total points are within 0-15% error band.

It seems that the EGR flow parameter does not show the expected trend for NO_x prediction. One possible reason is the lack of EGR flow measurements in dynamometer tests. Since experimentally measured EGR flow data are not available, the values are generated via the thermodynamic models. Air mass flow rate values are targeted, and EGR valve position is changed to reach the targeted air mass flow rates. So, EGR flow values calculated from the thermodynamic model may represent significant differences with respect to actual values. That may also be the explanation about the slight change in NO_x prediction of Map 9 regarding Map 8 that will be mentioned below.

In the second map, load parameter is also considered as an input parameter. Load represents the operating condition of an engine at certain engine speed. Like engine speed parameter, load is also selected as the primary input of emission based prediction neural networks in many studies [41], [44]. Because it directly represents all of the operating variables of an engine; not only injected flow, start of injection etc. but also friction and pumping losses, as well.

The distribution of the points can be viewed in Figures 4.15. nRMSE of this map is approximately 14%. As Figure 4.16 shows, 30% of total points lay between 0-25 ppm delta error band, and 49% of total points prevailed between 0-15% error band. Although the use of the engine load as an additional input gave slightly better results, the map is not still sufficiently accurate.

Since NO_x emissions are the primary function of in-cylinder temperature and combustion characteristics, it is decided to use turbine inlet temperature as one of the inputs for the map generation. The turbine inlet temperature is critical in engine combustion. It mainly depends on fuel/air equivalence ratio, injection timing and engine speed. All these parameters have significant effects on combustion. Generally, at the same operating point, higher efficiency results in lower turbine inlet temperature and higher NO_x formation.

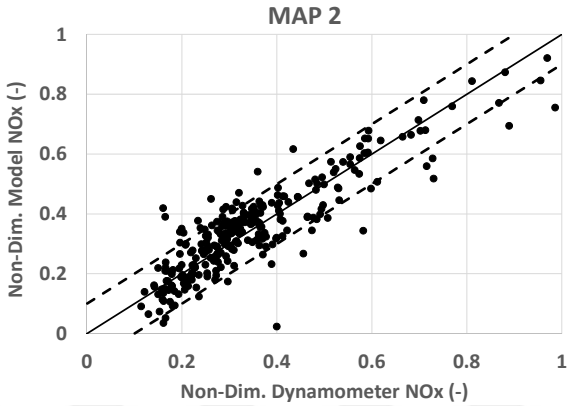

Figure 4.15. Model vs. test data comparison: MAP 2= f(RPM, Load, EGR Flow)

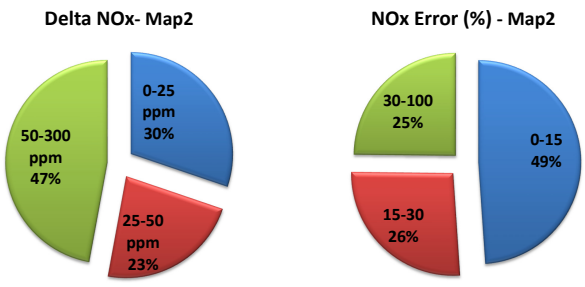

Figure 4.16. Model vs. test data comparison in pie charts: MAP 2= f (RPM, Load, EGR Flow)

On the contrary, lower combustion efficiency results in higher turbine inlet temperature and lower NO_x formation. Turbine inlet temperature, engine load, and EGR flow are parameters for the third map. Figure 4.17 shows that this map did only provide a small difference in the accuracy of the predictions, and nRMSE, which is 21%, is still too high. The distribution of the points is expressed with pie charts in Figure 4.18.

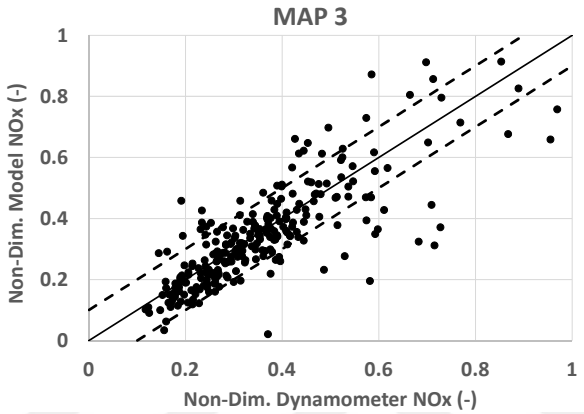

Figure 4.17. Model vs. test data comparison: MAP 3= f(TTURI, Load, EGR Flow)

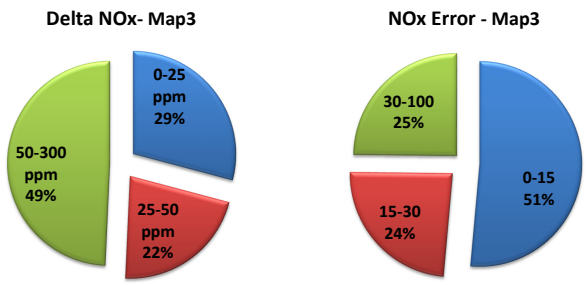

Figure 4.18. Model vs. test data comparison in pie charts: MAP 3= f (TTURI, Load, EGR Flow)

In the fourth map, maximum in-cylinder pressure, in other words, peak firing pressure (PFP) is added to the previous map. It is known that the maximum in-cylinder pressure value is an essential result of in-cylinder combustion. The maximum value of in-cylinder pressure has grand importance and effect on in-cylinder maximum temperature values and hence on NO_x emissions. Combustion at higher speed results in higher in-cylinder maximum temperature and pressure values. Higher in-cylinder

temperature values mostly result in higher NO_x formation. At the same operating point, lower maximum in-cylinder pressure values are encountered as a result of retarded combustion which means lower peak firing pressure, temperature and higher exhaust temperature. So, like in-cylinder maximum temperature, peak firing pressure values can also be selected for a better NO_x prediction.

nRMSE of the fourth map is better than the previous one: 19%. The distribution of the points is shown in Figure 4.19. As a result of the fourth map; 35% of total points lay between 0-25 ppm delta error band, and 55% of total points couched between 0-15% error bands (Figure 4.20). Hence, almost 5% enhancement is obtained on both delta and percentage differences.

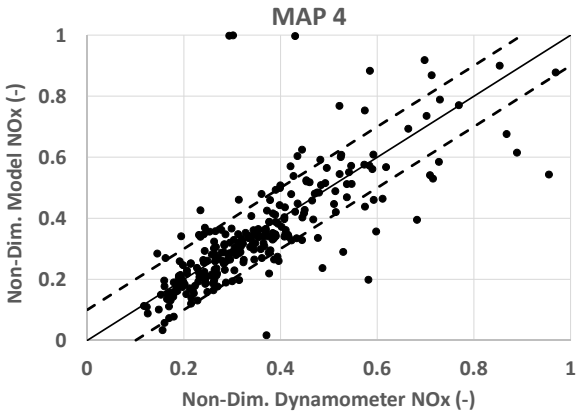

Figure 4.19. Model vs. test data comparison: MAP 4= f(TTURI, Load, EGR Flow, PFP)

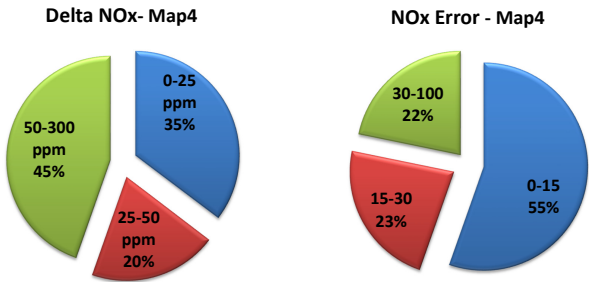

Figure 4.20. Model vs. test data comparison in pie charts: MAP 4= f (TTURI, Load, EGR Flow, PFP)

A fifth map is generated by employing turbine inlet temperature and engine load only to understand the particular impact of PFP. Accuracy is lowered for this map proving that PFP is an essential parameter for NO_x prediction. nRMSE remains almost the same: 19%. The comparison of the points can be seen in Figure 4.21. Figure 4.22 is also showing the distribution of the error in both delta and percentage forms.

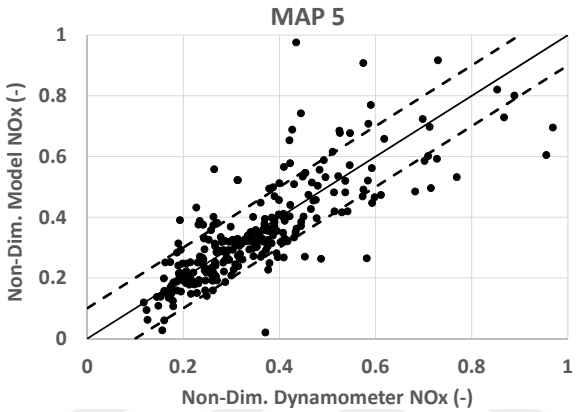

Figure 4.21. Model vs. test data comparison: MAP 5= f(TTURI, Load)

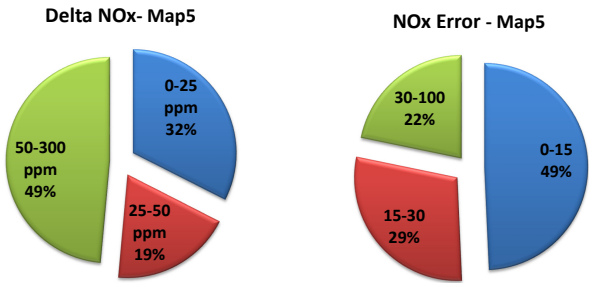

Figure 4.22. Model vs. test data comparison in pie charts: MAP 5= f (TTURI, Load)

The sixth map includes turbine inlet temperature and maximum in-cylinder temperature parameters. In this map; the effect of maximum in-cylinder temperature is investigated. It is evident that there is a strong correlation between in-cylinder maximum temperature and NO_x formation. In-cylinder maximum temperature is a significant parameter on NO_x prediction since higher in-cylinder maximum temperature values result as higher NO_x formation. Although in dynamometer tests, it is generally not possible or costly to collect in-cylinder maximum temperature values, with a correlated thermodynamic model, it is possible to calculate it and use for NO_x

emission prediction.

It is found that some NO_x calibration multipliers remain at very high values (approximately 7 to 10). As a result, these relatively high values are reducing the interpolation accuracy at the neighbour load-speed points. These high calibration multipliers, which are so-called outliers, are calculated at points that dynamometer test values are more than three times of model NO_x values. The number of these points are insignificant (approximately 1.5% of total map points), and their values are much different than their neighbouring points. Since there is no trend about the physical condition, these outliers are most probably encountered as a result of measurement errors (such as HORIBA device or measurement duration related) in the dynamometer tests. In the mapping process, these outliers are eliminated to increase accuracy.

It is essential to note that, the same investigation is performed for the previous maps as well. However, the effect of outliers was not as decisive as they are in this case. So outliers were not eliminated in the earlier maps.

Although the sixth map only includes turbine inlet temperature and maximum in-cylinder temperature values, better accuracy with respect to previous maps is obtained. nRMSE is significantly improved: 7.6%. Results can be seen in Figure 4.23. Also, Figure 4.24 shows that 33% of total points lay between 0-25 ppm delta error band, and 57% of total points lay between 0-15% error band. These results show that the in-cylinder maximum temperature has critical importance for emission prediction.

Since the main contributors of the NO_x emissions are in-cylinder temperature and pressure values, the seventh map is generated based on these two parameters and turbine inlet temperature. nRMSE slightly increases to 8.6%. The distribution of the points can be seen in Figure 4.25. As it is shown in Figure 4.26 39% of total points lay between 0-25 ppm delta error band and 60% of total points lay between 0-15% error band.

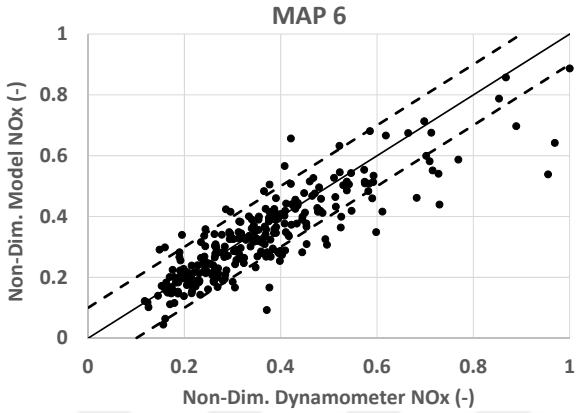

Figure 4.23. Model vs. test data comparison: MAP 6= f(TTURI, TMax) Without Outliers

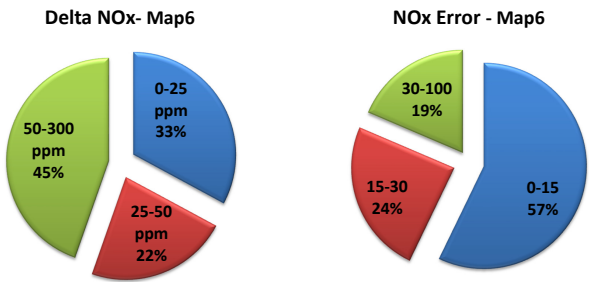

Figure 4.24. Model vs. test data comparison in pie charts: MAP 6= f (TTURI, TMax)

The load parameter is added to Map 7 parameters to generate Map 8. It is found that adding load parameter for mapping has a slight improvement on NO_x emission prediction. Accuracy is enhanced and nRMSE decreases in comparison with the previous map: 7.8%. Figure 4.27 represents the comparison between the dynamometer test data and model outputs. In Figure nRMSE slightly increases to 8.6%. The distribution of the points can be seen in Figure 4.28 error distribution can be seen.

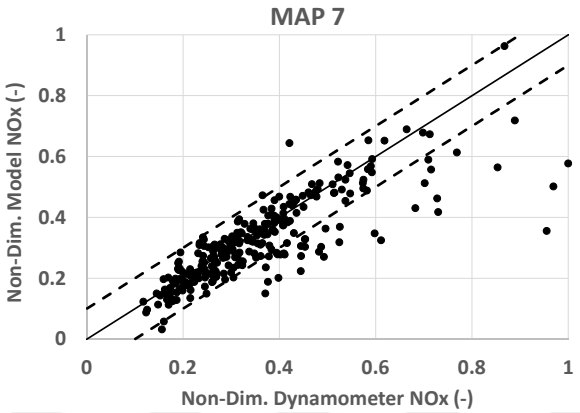

Figure 4.25. Model vs. test data comparison: MAP 7= f(TTURI, TMax, PFP)

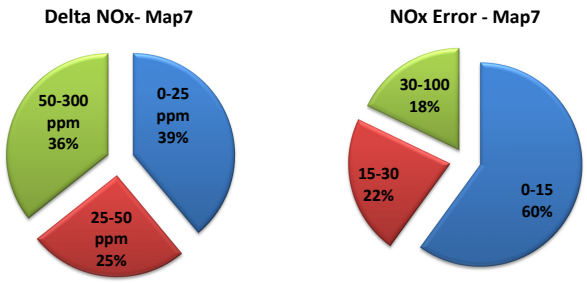

Figure 4.26. Model vs. test data comparison in pie charts: MAP 7= f (TTURI, TMax, PFP)

EGR flow parameter is added to Map 9 to enhance accuracy. However, a slight decrease in accuracy is encountered. This situation is mainly because of the non-linearity of EGR flow values and calculation errors encountered in the dynamometer test. nRMSE slightly decreases to 8.9%. The comparison can be seen in Figure 4.29. Besides, as it seen in Figure 4.30 41% of total points lay between 0-25 ppm delta error band and 62% of total points lay between 0-15% error band.

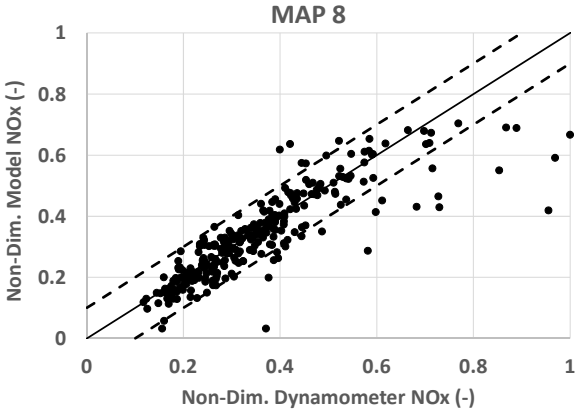

Figure 4.27. Model vs. test data comparison: MAP 8= f(TTURI, TMax, PFP, Load)

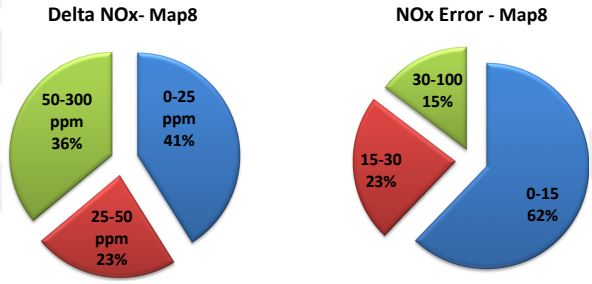

Figure 4.28. Model vs. test data comparison in pie charts: MAP 8= f (TTURI, TMax, PFP, Load)

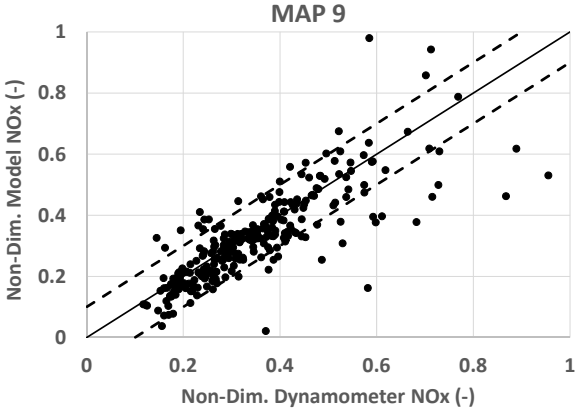

Figure 4.29. Model vs. test data comparison: MAP 9= f(TTURI, TMax, PFP, Load, EGR Flow)

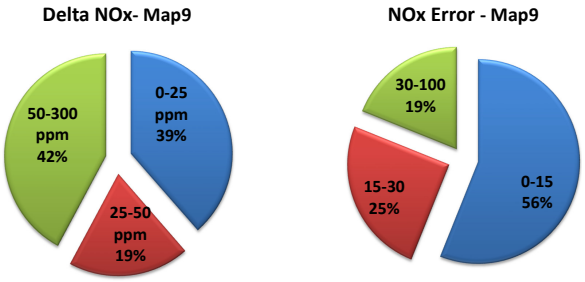

Figure 4.30. Model vs. test data comparison in pie charts: MAP 9= f (TTURI, TMax, PFP, Load, EGR Flow))

Hence, it is decided to eliminate the EGR flow from the map and introduce fuel flow rate to increase the accuracy. Similar to the load parameter, injected total fuel quantity is a direct representative of CO_2 emission. Injected total fuel quantity is also defining the air-to-fuel ratio for constant air mass flow rate, and it directly affects the combustion. As a result of higher injected fuel quantity, higher engine operating loads are obtained at a particular engine speed resulting in higher NO_x emissions.

In Figure 4.31, the correlation between test and model outputs can be examined. The regression graph shows that the model outputs seem to be in good correlation with dynamometer test results. nRMSE of this map is the best among all, which is 5.7%. Besides, as it is seen in Figure 4.32, 52% of total points lay between 0-25 ppm delta error band, and 74% of total points couched between 0-15% error band. These results are showing that these five parameters: turbine inlet temperature, peak firing pressure and temperature, engine load, and total injected fuel mass flow are the foremost parameters to be used for NO_x prediction.

Map 11 includes the effect of the CA50 parameter. CA50 is one of the critical parameters which is characterizing the combustion phasing. It is the crank angle position where 50% of the total heat release occurs. In this map, the turbine inlet temperature parameter is replaced with CA50 since it shows the combustion location and represents the premixed phase characteristics. It is found that the nRMSE is 5.8% which is similar to the Map 10 results. This result has proven that the CA50 can also

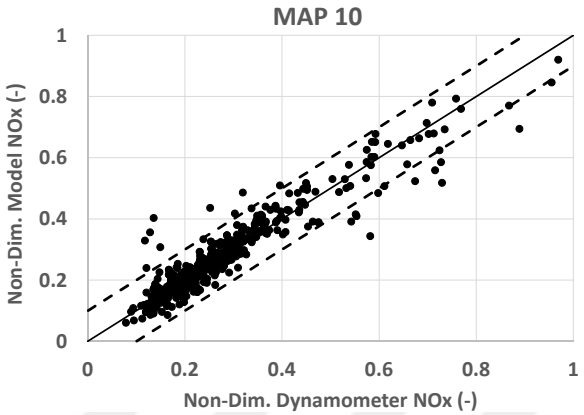

Figure 4.31. Model vs. test data comparison: MAP 10= f(TTURI, TMax, PFP, Load, Fuel Flow)

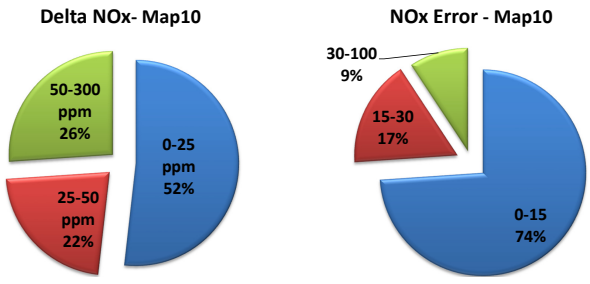

Figure 4.32. Model vs. test data comparison in pie charts: MAP 10= f (TTURI, TMax, PFP, Load, Fuel Flow))

be used for the NO_x emission prediction. Figure 4.33 shows the distribution of the points. Figure 4.34 shows that 53% of total points lay between 0-25 ppm delta error band, and 76% of total points couched between 0-15% error band.

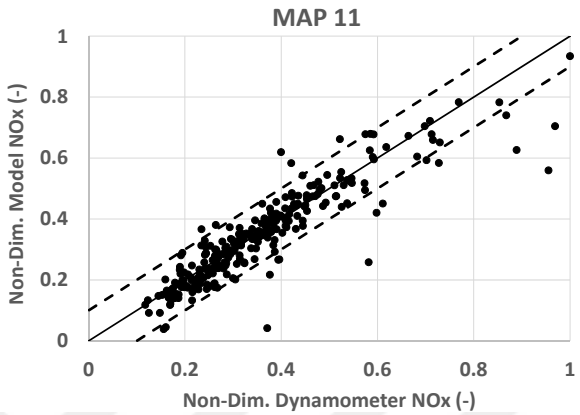

Figure 4.33. Model vs. test data comparison: MAP 11= f(CA50, TMax, PFP, Load, Fuel Flow)

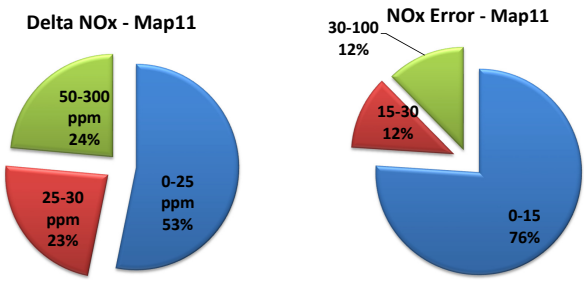

Figure 4.34. Model vs. test data comparison in pie charts: MAP 11= f (CA50, TMax, PFP, Load, Fuel Flow))

It is clear that the fuel flow parameter used in Map 10 is not a normalized parameter and may lead to some troubles when trying to generalize the model. Instead, it is replaced by the Fuel-Air equivalence ratio in Map 12, which is linked to the fuel flow but expressed in a normalized way. This state would have a clear advantage when trying to generalize the model (i.e. to use the same already calibrated model for another engine). nRMSE value of this map is 6.2%. Figure 4.35 shows the variance between model and test values. Figure 4.36 shows that 47% of total points lay between 0-25 ppm delta error band, and 70% of total points couched between 0-15% error band.

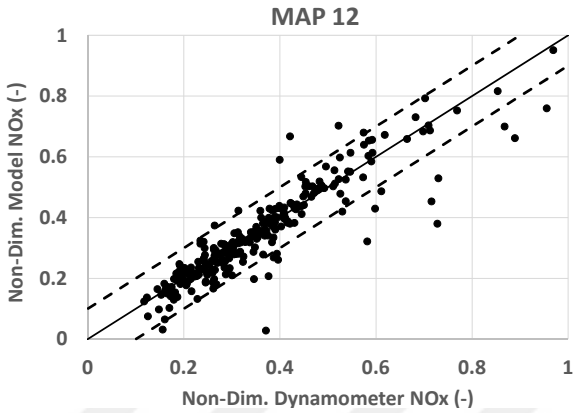

Figure 4.35. Model vs. test data comparison: MAP 12= f(TTURI, TMax, PFP, Load, Fuel-Air Ratio)

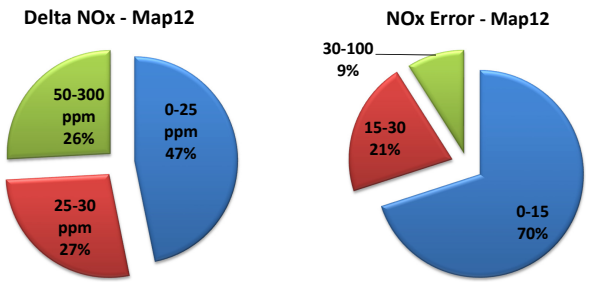

Figure 4.36. Model vs. test data comparison in pie charts: MAP 12= f (TTURI, TMax, PFP, Load, Fuel-Air Ratio))

In the previous maps, EGR flow was directly used. However, the EGR rate may be a better NO_x emission prediction parameter since, in reality, the EGR rate is the most significant parameter that can be used for NO_x control. EGR rate is calculated in the engine model via Equation 4.4:

$$\text{EGR Rate (\%)} = 100\frac{\text{EGR Flow}}{\text{EGR Flow} + \text{Air Mass Flow}} \tag{4.4}$$

Map 13 includes CA50, in-cylinder maximum temperature, load, Fuel-Air equivalence ratio and EGR rate as parameters. nRMSE value of this map is 7.2% which shows that using the model EGR rate output as a map parameter provides acceptable NO_x prediction accuracy. The result is represented in Figure 4.37. Besides as it is seen in Figure 4.38 48% of total points lay between 0-25 ppm delta error band, and 66% of total points couched between 0-15% error band.

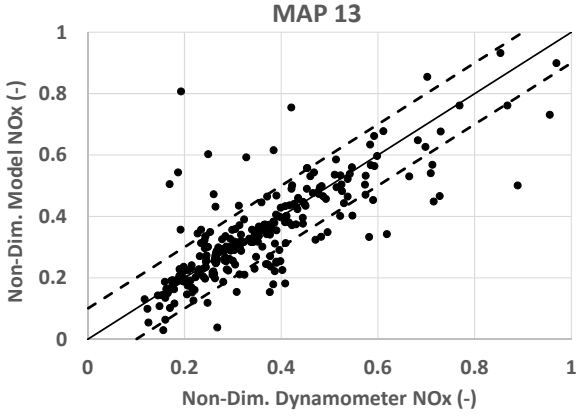

Figure 4.37. Model vs. test data comparison: MAP 13= f(CA50, TMax, EGR Rate, Load, Fuel-Air Ratio)

The last parameter taken into account in this section is the rail pressure parameter. The rail pressure is an input quantity in the engine tests. As it was mentioned previously, the current combustion model cannot use the rail pressure parameter as an input. In other words, model outputs do not change when different rail pressure values are imposed on the model. But its use as a NO_x emission prediction parameter is still possible within the scope of this methodology. To do this, the rail pressure data

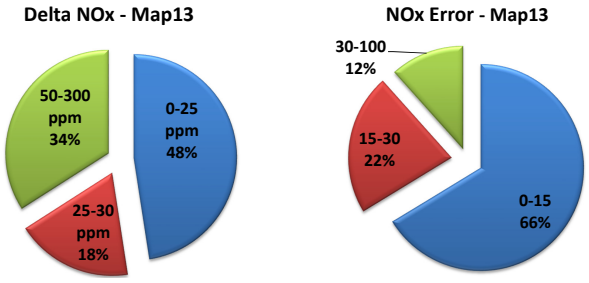

Figure 4.38. Model vs. test data comparison in pie charts: MAP 13= f (CA50, TMax, EGR Rate, Load, Fuel-Air Ratio))

collected from Fuel Loop 1 is used as a parameter in Map 14. The map also includes CA50, in-cylinder maximum temperature, load and fuel-air equivalence ratio parameters. Model is run with Fuel Loop 2 and 3 set points, also adding the rail pressure values collected from test data. nRMSE value of this map is 6.1%. This result shows the importance of the rail pressure parameter in NO_x prediction. The distribution of the points can be seen in Figure 4.39. Figure 4.40 shows that 55% of total points lay between 0-25 ppm delta error band, and 77% of total points couched between 0-15% error band.

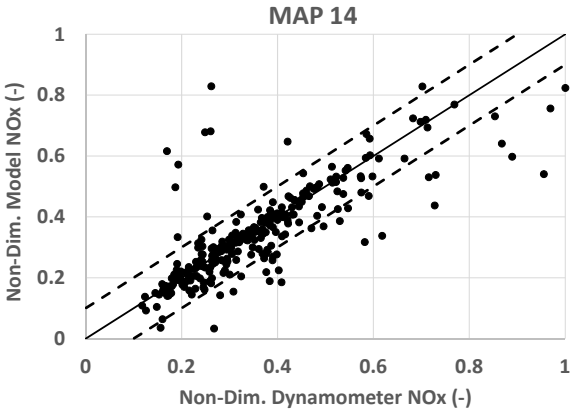

Figure 4.39. Model vs. test data comparison: MAP 14= f(CA50, TMax, Rail Pressure, Load, Fuel-Air Ratio)

In the fifteenth map; CA50, in-cylinder maximum temperature, EGR rate, rail pressure and fuel-air equivalence ratio parameters are used. nRMSE value of this map

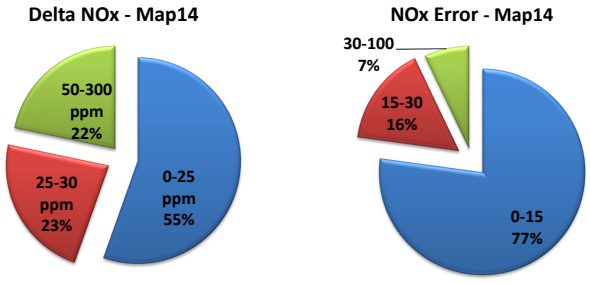

Figure 4.40. Model vs. test data comparison in pie charts: MAP 14= f (CA50, TMax, Rail Pressure, Load, Fuel-Air Ratio))

is 6.6%. The distribution of the points can be seen in Figure 4.41. Figure 4.36 shows that 42% of total points lay between 0-25 ppm delta error band, and 66% of total points couched between 0-15% error band.

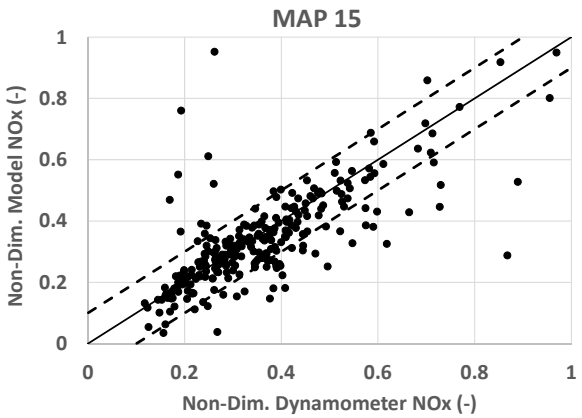

Figure 4.41. Model vs. test data comparison: MAP 15= f(CA50, TMax, EGR Rate, Rail Pressure, Fuel-Air Ratio)

In the last map; turbine inlet temperature, fuel flow, peak firing pressure and temperature parameters are used. nRMSE value of this map is 6.6%. Figure 4.43 represents the differences between dynamometer and model outputs. Figure 4.44 shows that 54% of total points lay between 0-25 ppm delta error band, and 76% of total points couched between 0-15% error band. All of the maps and their parameters are listed in Table 4.46.

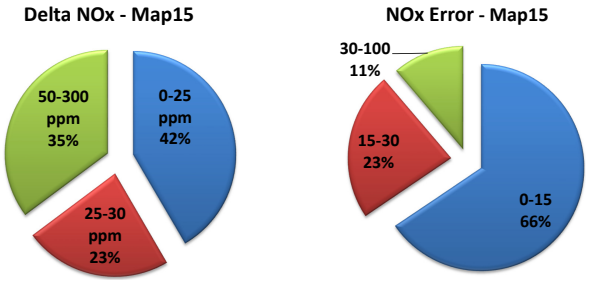

Figure 4.42. Model vs. test data comparison in pie charts: MAP 15= f (CA50, TMax, EGR Rate, Rail Pressure, Fuel-Air Ratio))

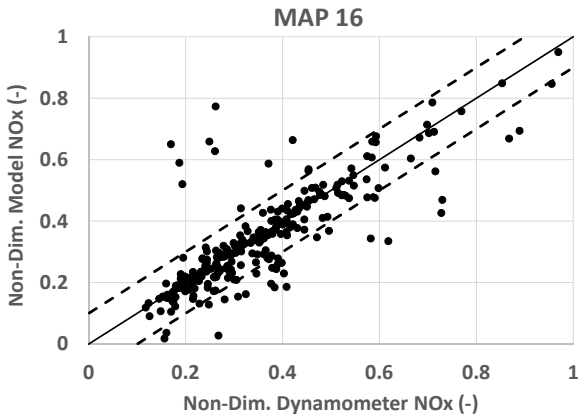

Figure 4.43. Model vs. test data comparison: MAP 16= f(TTURI, TMax, PFP, Fuel Flow)

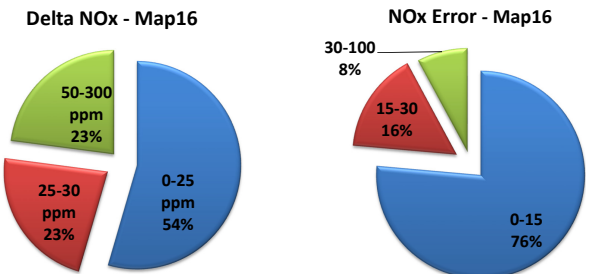

Figure 4.44. Model vs. test data comparison in pie charts: MAP 16= f (TTURI, TMax, PFP, Fuel Flow))

In Figure 4.45, accuracy values of different maps are shown. nRMSE comparison of different maps is shown in Figure 4.46. Maps 10-16 generate the best nRMSE values. This condition shows that turbine inlet temperature, maximum in-cylinder temperature, maximum in-cylinder pressure, fuel flow, CA50, fuel-air equivalence ratio, EGR rate and rail pressure parameters are the most critical emission prediction parameters. Comparison of Map 10 and Map 16 shows that load is not a crucial parameter in emission prediction. Among these parameters, it is also known that EGR rate and rail pressure are some of the essential parameters for NO_x emission control during engine calibration.

Table 4.4. 9L HD diesel engine maps and parameters

MAPS	**Parameters**	**nRMSE**
MAP 1	f(RPM, EGR Flow)	16.8%
MAP 2	f(RPM, Load, EGR Flow)	14.3%
MAP 3	f(TTURI, Load, EGR Flow)	21.3%
MAP 4	f(TTURI, Load, EGR Flow, PFP)	19.1%
MAP 5	f(TTURI, Load)	19.0%
MAP 6	f(TTURI, TMax) Without Outliers	7.6%
MAP 7	f(TTURI, TMax, PFP)	8.6%
MAP 8	f(TTURI, TMax, PFP, Load)	7.9%
MAP 9	f(TTURI, TMax, PFP, Load, EGR Flow)	8.9%
MAP 10	f(TTURI, TMax, PFP, Load, Fuel Flow)	5.6%
MAP 11	f(CA50, TMax, PFP, Load, Fuel Flow)	5.8%
MAP 12	f(TTURI, TMax, PFP, Load, Fuel-Air Ratio)	6.2%
MAP 13	f(CA50, TMax, EGR Rate, Load, Fuel-Air Ratio)	7.2%
MAP 14	f(CA50, TMax, Rail Pressure, Load, Fuel-Air Ratio)	6.1%
MAP 15	f(CA50, TMax, EGR Rate, Rail Pressure, Fuel-Air Ratio)	6.6%
MAP 16	f(TTURI, TMax, PFP, Fuel Flow)	5.4%

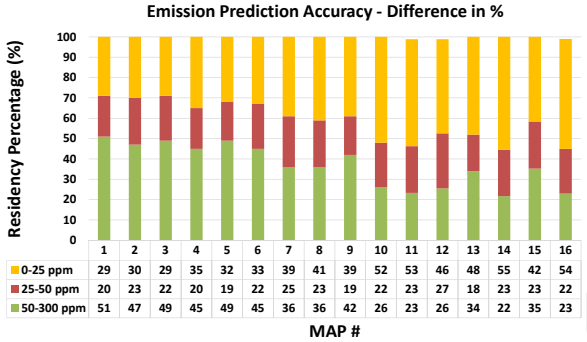

Figure 4.45. Model vs test data comparison of sixteen different maps

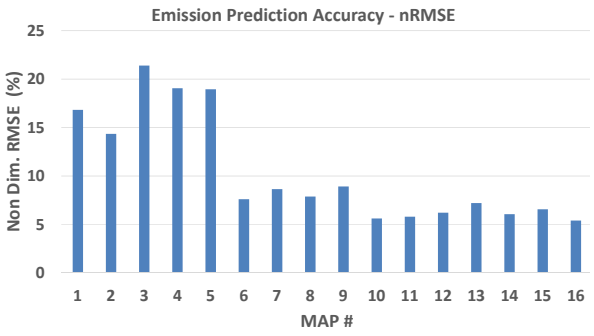

Figure 4.46. Non-dimensional RMSE values of sixteen different maps

4.4. Methodology Results In A Different Engine

For a further understanding of the effectiveness of the methodology, another heavy-duty engine is used to proceed. Important parameters for the chosen engine are as listed in Table 4.5. This table shows the main aspects of the heavy-duty diesel engine used for the methodology trial.

First of all, a thermodynamic engine model is generated in a commercial software using CAD geometry for intake, exhaust manifolds, intake and exhaust system piping, and critical inputs such as valve timings, firing order, turbocharger, charge air cooler, EGR cooler performance data.

Table 4.5. 12.7L engine specifications

Parameter	**Value**
Volume	12.7 L
Max Power	480 PS
Compression ratio	16.5:1
Bore	160 mm
Stroke	215 mm
Number of cylinders	6
Injection system	Common rail
Injection system pressure	2500 bar

Then, as it is in the 9L engine studies, fuel loop data correlation is performed. Diesel wiebe combustion model is used. Brake power, brake torque, air to fuel ratio, air mass flow and fuel mass flow values have good correlation with dynamometer test data.

The developed methodology is performed with the same steps after completing the correlation. A fuel loop data set with 173 points in total is used for this study. 33% (56 Points) are used for NO_x calibration multiplier multidimensional look-up table

generation, and the remaining 67% (117 Points) is kept for methodology examination.

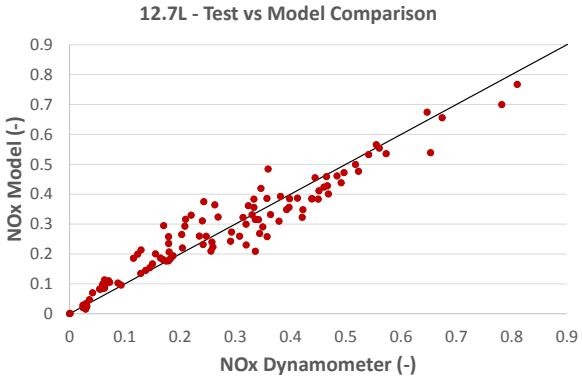

Figure 4.47. Model vs test data comparison - regression chart

Figure 4.47 illustrates that dynamometer data and model results have quite good correlation, which is even slightly better than the 9L engine comparison. Besides, non-dimensional RMSE value, in this case, is 5.1%. These results are showing that the methodology can be used for different engines with different volumes, successfully. This condition is mainly because the two engines are both representing heavy-duty diesel characteristics.

The methodological steps represented in this study apply to all heavy-duty diesel engine variants with different cylinder volume or power. As it was summarized above, by using the methodological steps developed in this study; it is possible to find out most effective parameters on feedgas NO_x formation once the thermodynamical model is created and correlated to test data.

For the case that an entirely new concept engine will be developed, NO_x prediction maps generated with similar engine properties (displacement, power, torque, etc.) may be used. But, the accuracy of the methodology most probably would be lower due to the lack of actual test data for model correlation. However, the necessary data for method application may be generated from a few 3D CFD simulations or single-cylinder engine tests at very early stages of engine development stage when an actual engine does not exist. Hence, it would be possible to direct hardware selection studies by considering

the NO_x emission outputs.

5. 12.7L HEAVY-DUTY DIESEL ENGINE STUDIES

In Chapter 4, the fast and accurate methodology development studies for emission prediction was explained. The effectiveness of the method is also examined with another heavy-duty diesel engine model: 12.7L. In this chapter, the effect of another combustion model so-called DI-Pulse is investigated.

5.1. Predictive Combustion Model: DI-Pulse

In this study, a predictive combustion model so-called DI-Pulse is used for combustion modelling. DI-Pulse is a predictive combustion model generated for modelling different injection strategies. It can be utilized for desktop calibration development studies to lower or to eliminate actual test workload.

DI-Pulse predictive combustion model mainly represents the diesel combustion phases. These phases are ignition delay, premixed combustion, diffusion controlled combustion and late combustion. These periods can be summarized as follows [45], [4]:

- Ignition Delay: It represents the difference between the start of injection and the start of combustion. It consists of two different sections which are the physical delay and chemical delay. The physical delay represents the duration in which the fuel atomization and vaporization occur. Besides, an increase in mixture temperature is encountered in this region. The chemical delay represents the duration between the initiation of chemical reaction conditions and ignition. Ignition delay is a critical parameter in diesel combustion since, higher the ignition delay, higher pressure values are encountered during the premixed combustion phase.
- Premixed Combustion: In this period rapid combustion occurs since the injected fuel is already mixed with air within the previous combustion period: ignition delay. Pressure increase mostly depends on the injected fuel quantity, spray optimization and swirl/tumble characteristics of the combustion chamber.
- Diffusion Controlled Combustion: In this period of diesel combustion; the pres-

sure and temperature values within the cylinder are already at high values. As a result, any fuel that is injected to cylinders rapidly burns. Most important control parameter at that section of diesel combustion is injected fuel quantity.

- Late Combustion: In this phase; combustion of poorly distributed fuel particles occurs.

The DI-Pulse combustion models include three different zones [45] in which the cylinder volume is divided into three different thermodynamic sections to capture the main diesel combustion phases. These sections are called; main unburnt zone, spray unburnt zone and spray burnt zone. Each zone has temperature values. The first zone includes the trapped masses at intake valve closing (IVC). The second and third zones include a mixture of fuel and gases which have been entrained during the injection event and the burnt combustion products; respectively.

DI-Pulse mainly calculates the four critical regions of combustion: entrainment, ignition delay, premixed combustion and diffusion combustion. To perform the evaluation, DI-Pulse models need energising time, rail pressure and injected quantity maps for the injector. These maps are generally gathered from suppliers. In Appendix B, detailed information about the implemention of injector maps is given.

The second step for DI-Pulse model correlation is to calculate the model parameters representing the main four sections of diesel combustion. The primary inputs of the model are, exhaust gas recirculation rate, boost pressure and temperature, injected total fuel quantity, engine speed and maximum in-cylinder pressure. Air mass flow rate depends strongly on the boost and turbine inlet pressure, and temperature values. Cylinder pressure values are the primary data for the correlation of heat release rate in the thermodynamic model.

One set fuel loop data and one set Design of Experiment (DOE) data are gathered in dynamometer tests. A fuel loop test is executed via collecting data at engine speed and load values spanning the full operation range (0% to 100%). In the fuel loop experiment data, data are collected at 193 different operating points corresponding to

Table 5.1. 12.7L HD diesel engine data sets

Data Type	Number of Points
Fuel Loop 1	193
DOE Data	940

10% intervals of engine load at different speeds.

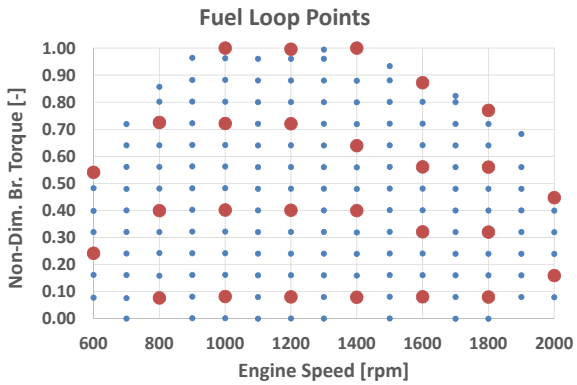

Figure 5.1. Fuel loop points

The main aim was to collect enough data covering different feed gas NO_x levels for methodology verification. Table 5.1 shows the number of operating points included by both fuel loop and DOE data sets. In each of these three experiments, data are collected at 193 different operating points corresponding to 10% intervals of engine speed and full and partial loads. Blue points in Figure 5.1 are representing the operating points used in the measurements of fuel loops. Besides; Figure 5.2 is representing the scattered DOE points. In this DOE study, rail pressure, start of injection, boost pressure and air mass flow set points are also varies at each points.

Model correlation is performed by completing the optimization via GT-Suite Advanced Optimizer, which is a module highly capable for optimization studies. Aim was to find out the best set of entrainment, ignition delay, premixed and diffusion rate parameters. 27 different operating points are selected for DI-Pulse model correlation.

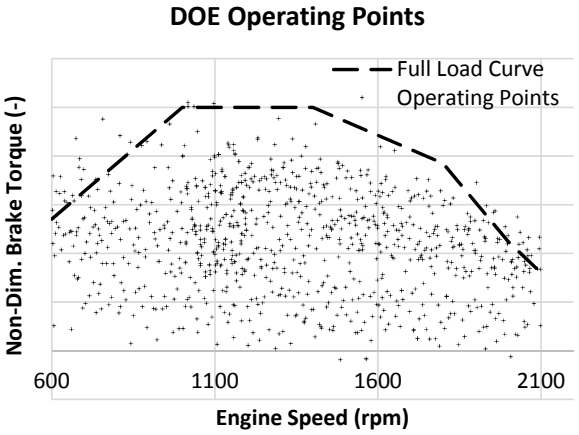

Figure 5.2. DOE points

These points are represented as red points in Figure 5.1. GT-Suite model is run in GT-Suite Advanced Optimizer to find out the optimum DI-Pulse combustion model parameters. The tool uses a non-dominated sorting genetic algorithm (NSGA-III) as the main algorithm.

NSGA-III is a Pareto optimization method which can be effectively used for solving problems having multiple objectives (three or more). This algorithm mainly utilizes a set of reference points to enhance the diversity of the Pareto points used during the optimization. Hence, it ensures that the points evenly distributed across the physical space even if there are many objectives. The current study includes 850 designs. Details of an GT-Suite optimization process is mentioned in Appendix C.

Combustion parameters, optimization range of these parameters and the optimum values are listed in table 5.2.

Fuel loop data are used for model correlation. Figures 5.3, 5.4, 5.5, 5.6, 5.7, 5.8, 5.9 and 5.10 show the full load comparison between model predictions and the test measurements. Brake torque and brake power values calculated with the model has ± 3% accuracy, BMEP and PMEP calculations are within ± 3% accuracy, temperature predictions at the intake have ± 5 ^{o}C accuracy, and predictions at the exhaust have ±

Table 5.2. 12.7L HD diesel engine DI-Pulse parameter optimization

	Optimization Range	**Optimization Results**
Entrainment	0.80-2.90	1.27420
Ignition Delay	0.10-1.90	0.38318
Premixed Comb.	0.01-2.90	0.58996
Diffusion Comb.	0.10-1.90	1.45170

50 ^{o}C accuracy. Pressure values in both compressor outlet and turbine inlet are within $\pm$ 3% accuracy range.

HORIBA PG-250 multi-gas portable analyzer is again used to gather NO_x emissions data. Technical specification of the device is showing that the measurement accuracy for NO_x emission is under $\pm$ 1% error margin.

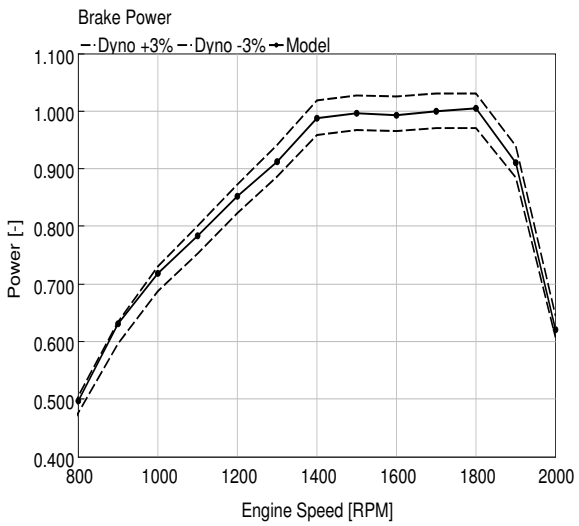

Figure 5.3. Full load correlation comparison: brake power

The main aim was to collect enough data covering different feed gas NO_x levels for methodology generation and validation. Table 4.2 shows the number of operating points included by both fuel loop and DOE data sets. Blue points in Figure 5.1 are

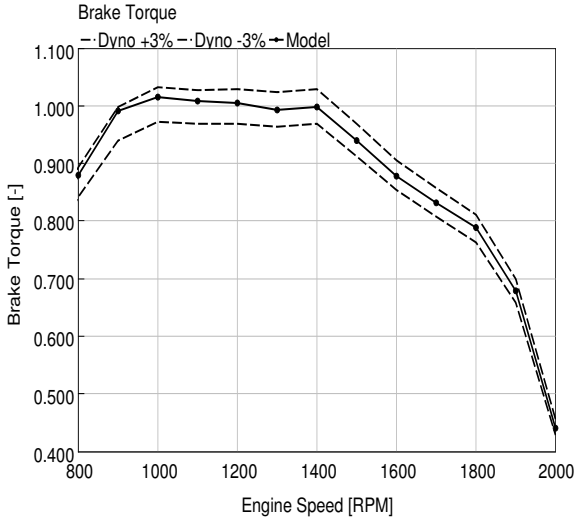

Figure 5.4. Full load correlation comparison: brake torque

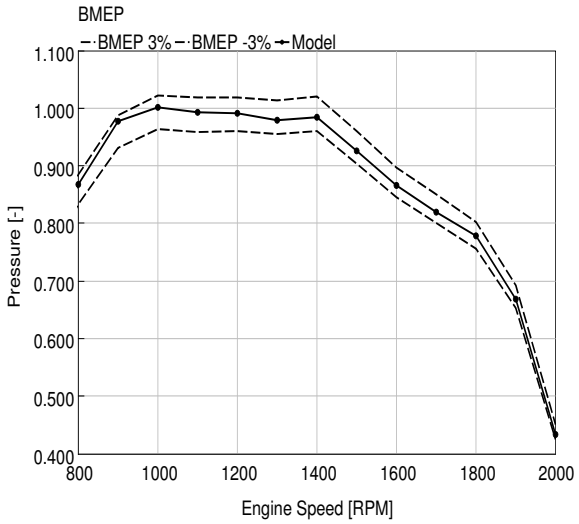

Figure 5.5. Full load correlation comparison: BMEP

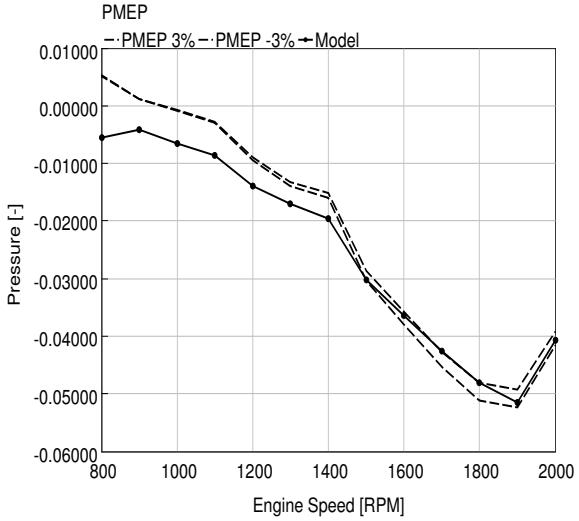

Figure 5.6. Full load correlation comparison: PMEP

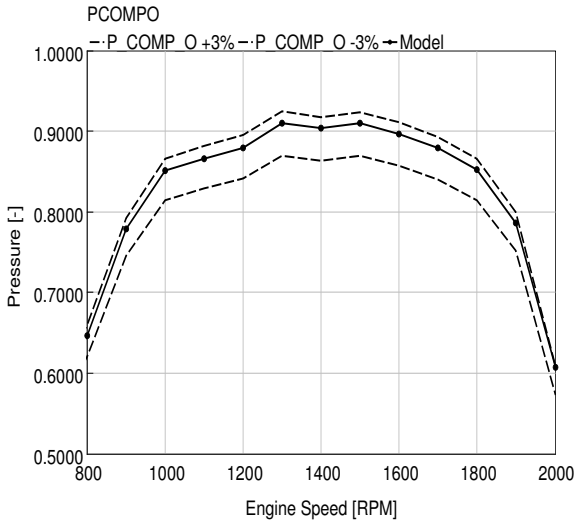

Figure 5.7. Full load correlation comparison: compressor outlet pressure

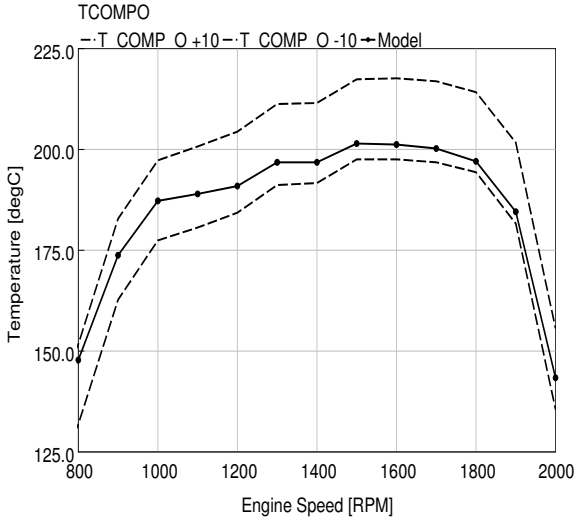

Figure 5.8. Full load correlation comparison: compressor outlet temperature

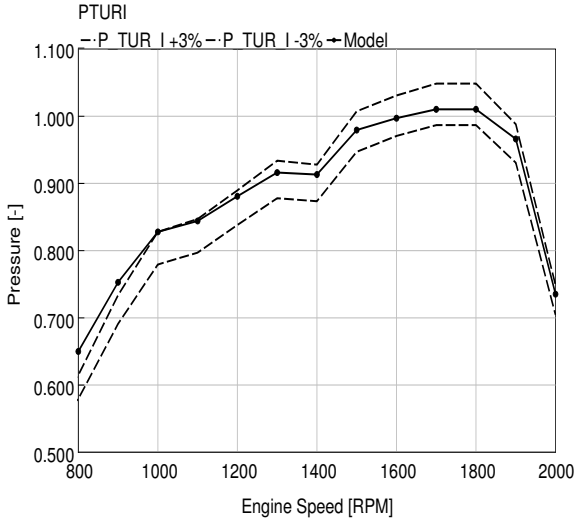

Figure 5.9. Full load correlation comparison: turbine inlet temperature

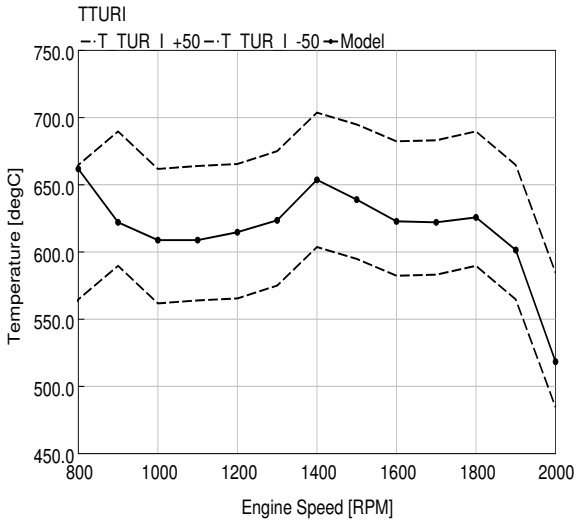

Figure 5.10. Full load correlation comparison: turbine inlet temperature

representing the operating points used in the measurements of fuel loops.

5.2. NO_x Model and Calibration

In this section of the study; extended Zeldovich Mechanism embedded in GT-Suite is used like in Section 4.2.

As the first step, half of DOE points (438 points) are separated for the model correlation. These points can be seen in Figure 5.11 with red triangles. This half of the DOE is so-called DOE Part 1 data. Once the model run with DOE Part 1 data inputs, NO_x outputs of the model are compared with test data. The ratio between the Model NO_x and dynamometer NO_x is so-called Calibration Multiplier. By utilizing from the "Multidimensional Table Look-up Using Scattered Data" object embedded into GT-Suite, it is possible to generate and use different maps providing NO_x Calibration Multipliers. The inputs of these multidimensional look-up tables are the main engine performance parameters such as boost pressure, injected fuel quantity, engine speed, etc. and the only output is NO_x Calibration Multiplier.

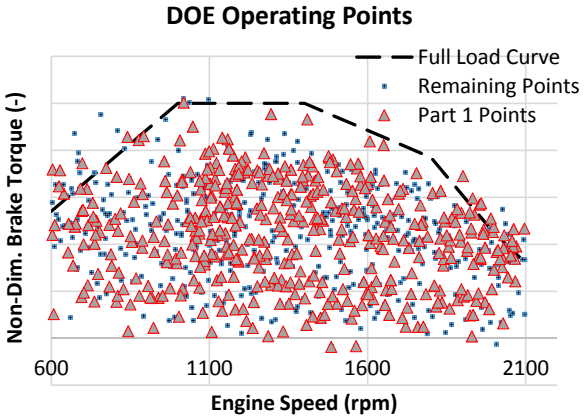

Figure 5.11. DOE part 1 points

These multipliers can be integrated to already embedded extended Zeldovich mechanism in the software for each case. Hence, it is possible to enhance model NO_x prediction accuracy. In the below-mentioned studies, the aim was to find out the best parameters to be used in NO_x calibration multiplier multidimensional look-up tables for enhanced emission prediction accuracy.

To do that, the emission model is correlated by defining the calibration multipliers that provide $\pm$ 2% accuracy with respect to experimental results for each point in DOE Part 1 data. The calibration multipliers are the main parameters which enable the use of fast NO_x prediction methodology. These maps are multidimensional look-up tables based on different parameters such as fuel quantity, EGR rate etc. as the input and NO_x calibration multiplier as the output.

Once the NO_x calibration multipliers generated via using DOE Part 1 data are transferred into different multidimensional look-up tables; remaining DOE data, so-called DOE Part 2 and fuel loop data are run to see the NO_x prediction accuracy of the generated maps. These two data sets are the ones that were not used for the map generation, so they are used for measuring the prediction capability of the different maps. Error in NO_x predictions are calculated via again Equations 4.1, 4.2 and 4.3. The main steps of the correlation methodology mentioned in Section 4.2 is directly used.

5.3. NO_x Calibration Multiplier Maps

Selection of input parameters for the map generation is critical to obtain a map with accurate NO_x prediction capability. In this study; thirteen different maps are generated by the use of ten different parameters which are crank angle at maximum pressure, rail pressure, main injection timing (SOI), calculated EGR Rate, turbine inlet temperature (TTURI), peak firing pressure (PFP), in-cylinder maximum temperature (TMax), fuel flow, rail pressure, CA50 and Fuel-Air ratio. The primary goal was to collect the NO_x prediction accuracy of different maps and find out the best engine performance parameters in NO_x prediction. In this section, the selection of input parameters used for the map generation and the resulting map predictions are explained.

Turbine inlet temperature is selected as the first parameter of Map 1. The turbine inlet temperature is one of the most critical resultants of combustion behaviour of the engine. It represents the combustion speed. Generally, at the same operating point, higher combustion efficiency results as lower turbine inlet temperature and higher NO_x formation. In contrary; lower combustion efficiency results as higher turbine inlet temperature and lower NO_x formation. Hence, turbine inlet temperature and NO_x formation have generally a good trend.

High in-cylinder pressure values are results of the in-cylinder combustion. As it is already mentioned in Section 5.3, combustion at higher speed results as higher in-cylinder maximum temperature and pressure values. Higher in-cylinder temperature mostly results as higher NO_x formation. At same operating point; lower maximum in-cylinder pressure values are encountered as combustion is retarded which means lower peak firing pressure & temperature and higher exhaust temperature. So, as in-cylinder maximum temperature; in-cylinder pressure values can also be selected for a better NO_x prediction. That's why the maximum in-cylinder pressure parameter is chosen as the second parameter of Map 1.

Besides; there is a strong correlation between in-cylinder maximum temperature and NO_x formation. In-cylinder maximum temperature is a reliable parameter on NO_x prediction since; higher in-cylinder temperature values result as higher NO_x formation. In dynamometer tests, it is generally not possible or too expensive to collect in-cylinder maximum temperature values. However, with a correlated thermodynamical model; it is possible to utilize from this output for NO_x emission prediction studies.

Last but not least; fuel flow is a direct representative of CO_2 emission. But, since injected total fuel quantity is also defining the air-to-fuel ratio for constant air mass flow rate, it directly affects the combustion. As a result of higher injected fuel quantity, higher engine operating loads are obtained at a particular engine speed resulting as higher NO_x emissions.

As a result, these four parameters: turbine inlet temperature, maximum in-cylinder pressure, maximum in-cylinder temperature and fuel flow are selected as the input parameters of the first NO_x Calibration Multiplier map. These are the same parameters with the map providing best accuracy in studies mentioned in Section 5.3.

Once the map is created with the outputs of DOE Part 1 data, model is run with this map to understand the NO_x prediction capability. Results are shown in Figure 5.12. Maximum NO_x value is used for the non-dimensionalization. The black line is a linear line representing the equation: x=y. Dashed lines are representing 10% and -10% variances with respect to the linear line. These dashed lines are used in order to obtain a clear understanding for distribution of the operating points. R^2 is 0.9046 and nRMSE is approximately 5.1%. As it was mentioned in Section 4.4, same map was used with different test data and combustion model. But the result is almost the same. This condition shows that, if the model correlation is well enough, NO_x prediction accuracy does not vary significantly as a function of used test data or combustion model. But, it is important to emphasize that use of predictive combustion models have a critical advantage: ability to use some further parameters such as pilot, main, post injection quantity & timings and rail pressure as the model input. It is possible to use these parameters as the model inputs in predictive combustion models.

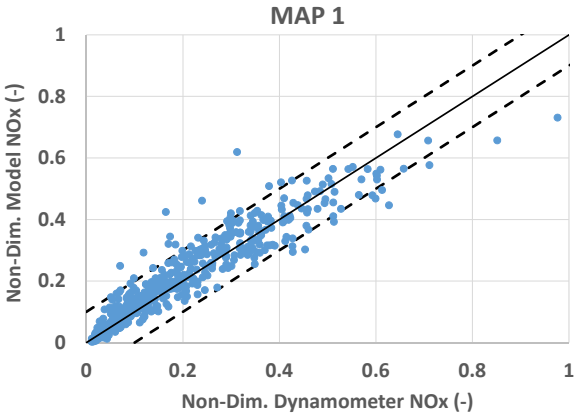

Figure 5.12. Model vs. test data comparison: MAP 1= f (TTURI, TMax, PFP, Fuel Flow Rate)

In the second map; rail pressure is also considered as an additional input parameter to enhance the accuracy. As it is known, higher injection pressure results as improved fuel atomization generating fine fuel droplets. Smaller fuel droplets evaporate at an accelerated rate with respect to bigger fuel droplets. This event mainly results in rapid fuel-air mixing and shorter injection durations. Shorter injection durations enable retarded injection and emission control [41]. All of these events have a substantial effect on NO_x and soot generation. It is known that for the same BMEP, higher rail pressure values generally result as higher in-cylinder temperature and pressure values and hence higher NO_x formation. However, as it is seen in the results; using rail pressure in combination with the other parameters did not improve the nRMSE. Results are shown in Figure 5.13. R^2 is 0.8912 and nRMSE is approximately 5.66%.

In the third map, the elimination of the rail pressure parameter follows the addition of EGR Rate parameter into the map. EGR Rate is selected for further examination since the rate of EGR Flow is one of the main parameters showing a significant trend in NO_x formation. However, since the dynamometer tests are not accomplished with a flowmeter in the EGR side to measure EGR Rates; current values are generated via the thermodynamical model. Air mass flow values are targeted, and EGR Valve position is changed to get target Air Mass Flow rates. So, EGR Rate values calculated from the thermodynamical model may represent some differences with respect to ac-

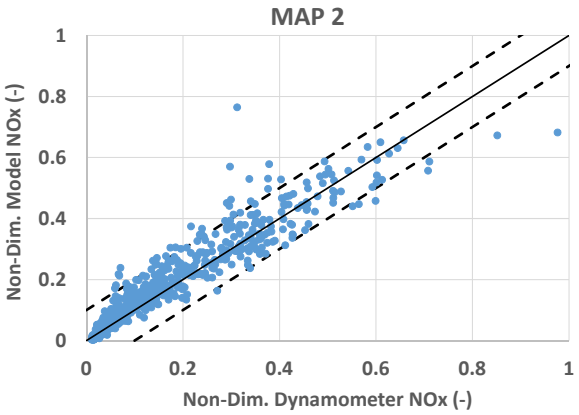

Figure 5.13. Model vs. test data comparison: MAP 2= f (TTURI, TMax, PFP, Fuel Flow Rate, Rail Pressure)

tual values. That may be the explanation about the slight change in NO_x prediction of Map 3 in comparison with Map 1. Results are shown in Figure 5.14. R^2 is 0.9194 and nRMSE is approximately 4.64%.

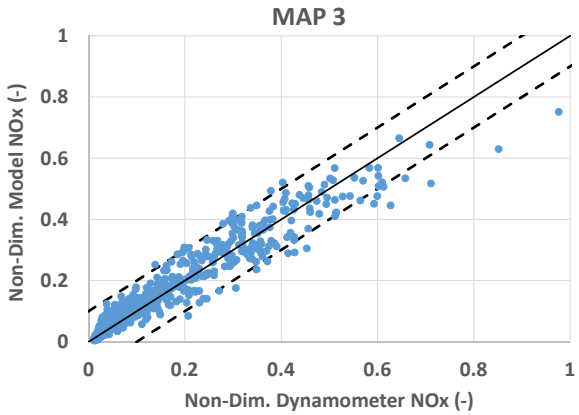

Figure 5.14. Model vs. test data comparison: MAP 3= f (TTURI, TMax, PFP, Fuel Flow Rate, EGR Rate)

In the fourth map, the effect of using another parameter: crank angle at maximum pressure is investigated. This parameter is another vital parameter having significant importance similar to in-cylinder maximum temperature and pressure values. Performing emission control via retarded or advanced fuel injection is possible. By controlling the fuel injection timing, it is possible to adjust the combustion rate to fulfill emission

regulation requirements. CA at maximum pressure is, therefore, another key parameter that would have good correlation with soot and NO_x prediction [42]. Results are shown in Figure 5.15. R^2 is 0.9016 and nRMSE is approximately 5.55%.

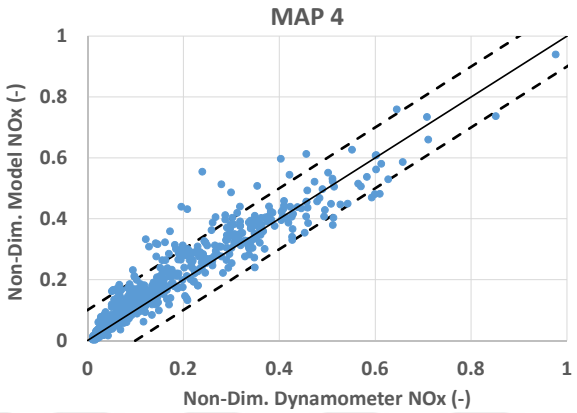

Figure 5.15. Model vs. test data comparison: MAP 4= f (TTURI, TMax, PFP, Fuel Flow Rate, CA at Maximum Pressure)

To understand the particular impact of EGR Rate in further detail, a new map is generated via using the function of the EGR Rate rather than the turbine inlet temperature parameter. So, the fifth map is created by using the parameters: EGR Rate, TMax, PFP, Fuel Flow and CA at maximum pressure. Results are shown in Figure 5.16. R^2 is 0.9397 and nRMSE is approximately 4.12%.

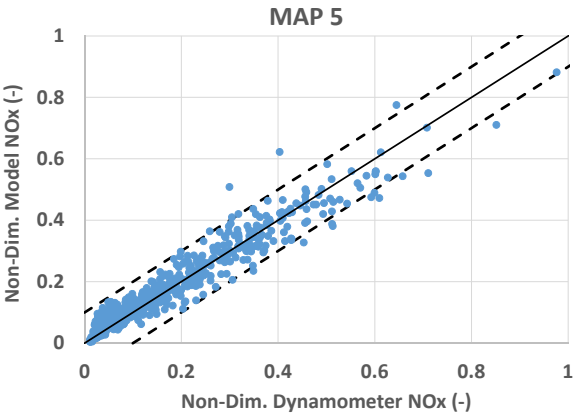

Figure 5.16. Model vs. test data comparison: MAP 5= f (EGR Rate, TMax, PFP, Fuel Flow Rate, CA at Maximum Pressure)

In the sixth map rail pressure (bar) is used rather than maximum in-cylinder pressure. It seems that the nRMSE is lower with respect to all previous maps. Results are shown in Figure 5.17. R^2 is 0.9416 and nRMSE is approximately 3.95%.

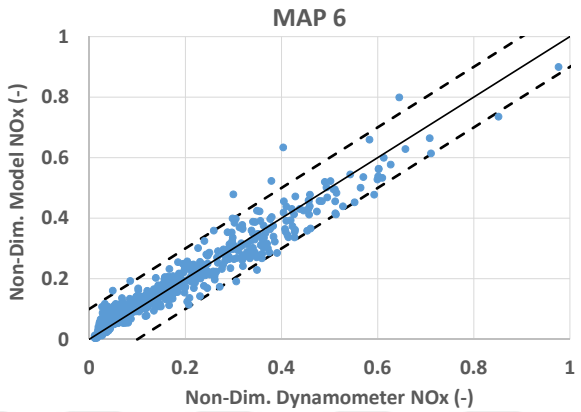

Figure 5.17. Model vs. test data comparison: MAP 6= f (EGR Rate, TMax, Rail Pressure, Fuel Flow Rate, CA at Maximum Pressure)

In the seventh map, main start of injection is used as another parameter. As it is known, start of injection is one of the critical parameters in emission control. Retarded or advanced combustion can be obtained via simply adjusting the start of injection. Besides, start of injection parameter has a direct influence on fuel burn 50 value, which represents the crank angle in which 50% of total injected fuel is consumed. Results are shown in Figure 5.18. R^2 is 0.9320 and nRMSE is approximately 4.23%.

In the eight map, EGR rate, maximum in-cylinder temperature, maximum in-cylinder pressure, rail pressure and the crank angle at maximum pressure parameters are used. Fuel flow parameter is eliminated. However, nRMSE values are worse regarding to previous results. This condition is showing the critical importance of fuel flow parameter on emission prediction studies. Figure 5.19 represents the results. R^2 is 0.8677 and nRMSE is approximately 6.47%.

In the ninth map, CA50, TMax, PFP and Rail Pressure parameters are used. In this map, the effect of the CA50 parameter is taken into account since it shows the combustion location and represents the premixed phase characteristics. Results are

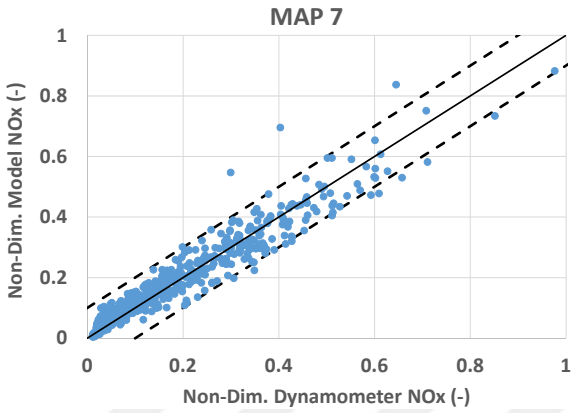

Figure 5.18. Model vs. test data comparison: MAP 7= f (EGR Rate, TMax, Main Injection Timing, Fuel Flow Rate, CA at Maximum Pressure)

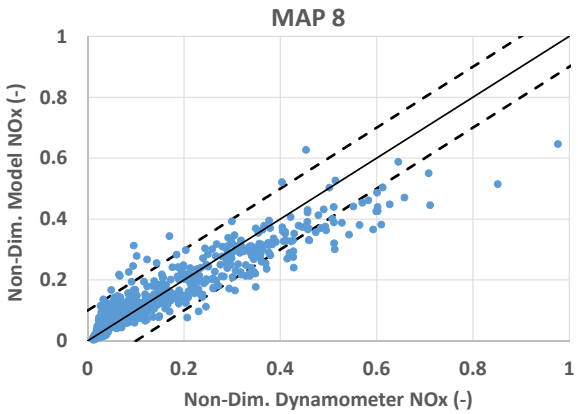

Figure 5.19. Model vs. test data comparison: MAP 8= f (EGR Rate, TMax, PFP, Rail Pressure, CA at Maximum Pressure)

shown in Figure 5.20. R^2 is 0.8936 and nRMSE is approximately 5.81%. This result has proven that the CA50 can also be used for the NO_x emission prediction.

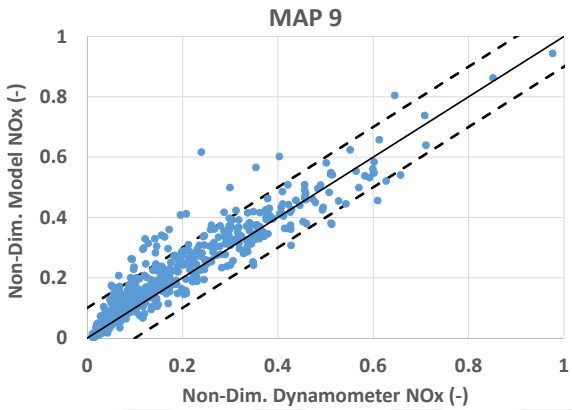

Figure 5.20. Model vs. test data comparison: MAP 9= f (CA50, TMax, PFP, Rail Pressure)

In the tenth map, TTURI, TMax, PFP and Fuel-Air Ratio parameters are used. It is evident that the fuel flow parameter used in Maps 1 to 7 is not a normalized parameter and may lead to some troubles when trying to generalize the model. Instead, it is replaced by the fuel-air equivalence ratio in Map 12, which is linked to the fuel flow but expressed in a normalized way. This status would have a clear advantage when trying to generalize the model (i.e. to use the same already calibrated model for another engine). Results are shown in Figure 5.21. R^2 is 0.9097 and nRMSE is approximately 4.89%.

In the eleventh map, CA50, TMax, EGR rate and fuel-air equivalence ratio parameters are used. Results are demonstrated in Figure 5.22. R^2 is 0.9343 and nRMSE is approximately 4.17% which a quite good accuracy value.

In the twelfth map, EGR rate parameter is replaced with rail pressure. CA50, TMax, rail pressure and Fuel-Air Ratio parameters are used in this map. Results can be seen in Figure 5.23. R^2 is 0.9150 and nRMSE is approximately 4.81%, which is showing that these parameters can also be used for emission prediction capability enhancement.

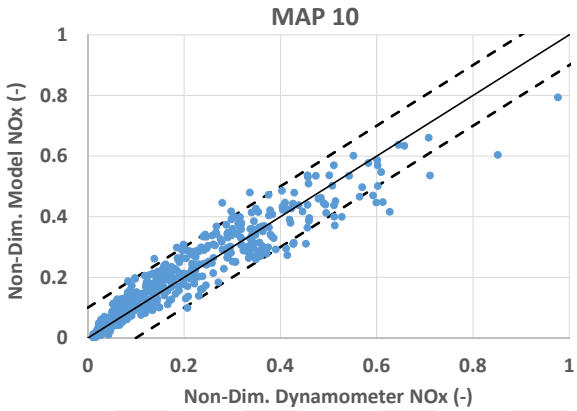

Figure 5.21. Model vs. test data comparison: MAP 10= f (TTURI, TMax, PFP, Fuel-Air Ratio)

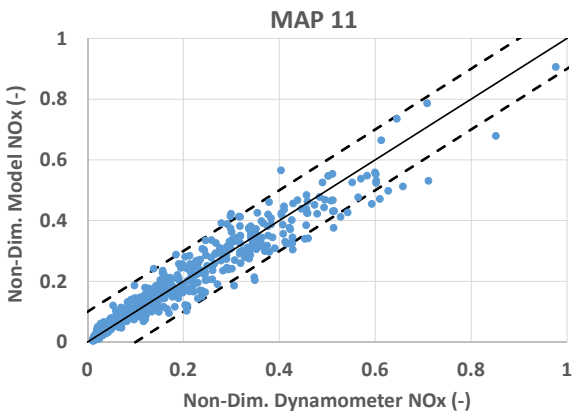

Figure 5.22. Model vs. test data comparison: MAP 11= f (CA50, TMax, EGR Rate, Fuel-Air Ratio)

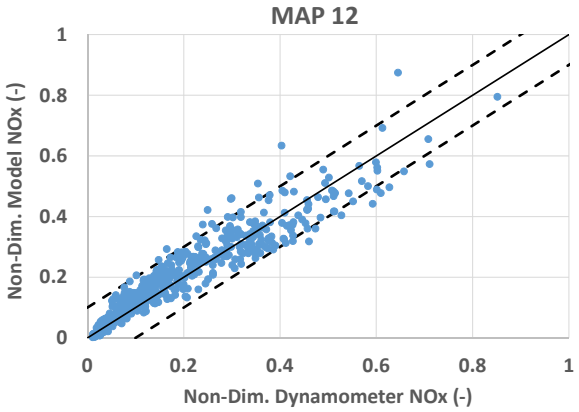

Figure 5.23. Model vs. test data comparison: MAP 12= f (CA50, TMax, Rail Pressure, Fuel-Air Ratio)

In the last map, CA50, TMax, EGR rate, TMax and rail pressure parameters are used. General trends of the model and test outputs can also be seen in Figure 5.24. As it is seen in these regression graphs, model outputs seem to be in good correlation with dynamometer outputs. R^2 is 0.9382 and nRMSE is approximately 4.06%. The accuracy of this map is the best considering all thirteen maps.

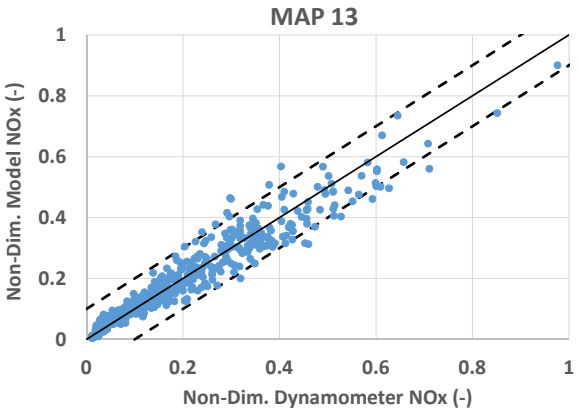

Figure 5.24. Model vs. test data comparison: MAP 13= f (CA50, TMax, EGR Rate, Rail Pressure)

All of the maps and parameters used in 12.7L HD diesel engine studies are summarized in Table 4.5. Non-dimensional RMSE comparison of these maps is shown in Figure 5.25. As it is seen in the graph, Maps 5, 6, 7, 11 and 13 have the highest NO_x

emission prediction accuracies. Turbine inlet temperature, maximum in-cylinder temperature, maximum in-cylinder pressure, load, fuel flow, CA50, Fuel-Air Ratio, EGR rate and rail pressure parameters are the most critical emission prediction parameters. Best accuracy (nRMSE of 3.95 %) is obtained via Map 6 which consists of five different parameters: EGR rate, TMax, rail pressure, fuel flow and CA at PFP.

Table 5.3. 12.7L maps and parameters

MAPS	**Parameters**	**nRMSE**
MAP 1	f(TTURI, TMax, PFP, Fuel Flow)	5.1%
MAP 2	f(TTURI, TMax, PFP, Fuel Flow, Rail Pressure)	6.0%
MAP 3	f(TTURI, TMax, PFP, Fuel Flow, EGR Rate)	4.6%
MAP 4	f(TTURI, TMax, PFP, Fuel Flow, CA at PFP)	5.6%
MAP 5	f(EGR Rate, TMax, PFP, Fuel Flow, CA at PFP)	4.1%
MAP 6	f(EGR Rate, TMax, Rail Pres., Fuel Flow, CA at PFP)	3.9%
MAP 7	f(EGR Rate, TMax, Main SOI, Fuel Flow, CA at PFP)	4.2%
MAP 8	f(EGR Rate, TMax, PFP, Rail Pres., CA at PFP)	6.5%
MAP 9	f(CA50, TMax, PFP, Fuel Flow)	5.8%
MAP 10	f(TTURI, TMax, PFP, Fuel-Air Ratio)	4.9%
MAP 11	f(CA50, TMax, EGR Rate, Fuel-Air Ratio)	4.2%
MAP 12	f(CA50, TMax, Rail Pres., Fuel-Air Ratio)	4.8%
MAP 13	f(CA50, TMax, EGR Rate, Rail Pres., Fuel-Air Ratio)	4.1%

Table 5.3 is showing that the Maps 5, 6, 7, 11, 12 and 13 are providing the lower nRMSE values. Lowest nRMSE value obtained within this section of the manuscript is 3.9% and obtained via the use of Map 6. EGR Rate, Tmax, Fuel-Air Ratio, CA @ PFP, Main SOI, Rail Pressure and CA50 are the most critical parameters.

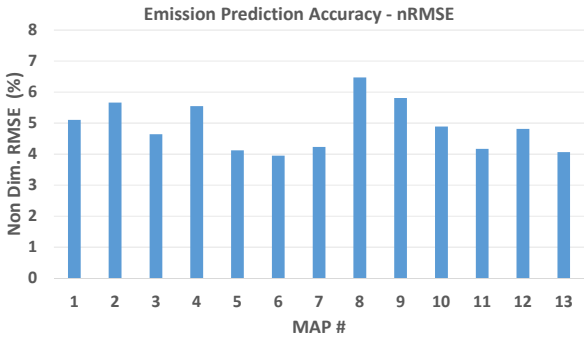

Figure 5.25. Non-dimensional RMSE values of thirteen different maps

5.4. Soot Model and Calibration

5.4.1. Hiroyasu Model

Hiroyasu *et al.* [46] developed a set of models for direct-injection diesel engines to predict, engine performance and emissions. They divided the spray into small packages to model the combustion process. The package includes many fine droplets and a small volume of air, just after the fuel injection. After the injection of the package from the nozzle, air entrainment into the package occurs, and evaporation of fuel droplets is initiated. The small package includes three different species: liquid fuel, vaporized fuel and air. Ignition occurs in the gaseous mixture just after the injection. Ignition process results with the immediate expansion of the package. Then, evaporation of the fuel droplets occurs, and fresh air entrains into the package. Mixing of vaporized fuel with both combustion products and fresh air is encountered. Spray continues to burn.

The formation rate is calculated by assuming a first-order reaction of vaporized fuel, m_s [47]:

$$\frac{dm_{sf}}{dt} = A_f m_s p^{0.5} \exp\left[\frac{-E_{sf}}{RT}\right] \tag{5.1}$$

The soot oxidation can be calculated via considering a second order reaction between soot and oxygen.

$$\frac{dm_{so}}{dt} = A_o m_s \frac{p_{O_2}}{p} p^{1.5} \exp\left(\frac{-E_{so}}{RT}\right) \tag{5.2}$$

where E_{sf}=1.25 10^4 kcal/kmol, E_{so}=1.40 10^4 kcal/kmol. Agreement between the calculated smoke and the soot measurement in the exhaust gas can be determined with the constants A_f and A_o.

The net rate of change of soot is determined by:

$$\frac{dm_s}{dt} = \frac{dm_{sf}}{dt} - \frac{dm_{so}}{dt} \tag{5.3}$$

5.4.2. Nagle and Strickland (NSC) Model

Oxidation experiments of carbon graphite in an O_2 environment over a range of partial pressure constitutes the basis of the NSC oxidation model. In the model, three reactions, rates of which depend on the surface chemistry involving less reactive B sites and more reactive A sites facilitate the carbon oxidation [48], [47]. The chemical reactions of the NSC model are:

$$\begin{aligned} A + O_2 &\leftrightarrow A + 2CO \\ B + O_2 &\leftrightarrow A + 2CO \\ A &\leftrightarrow B \end{aligned} \tag{5.4}$$

and the soot oxidation rate is given by:

$$\frac{dm_{so}}{dt} = \frac{M_C}{\rho_s d_s} m_s w \tag{5.5}$$

where ρ_s is the soot density (2.0 g/cm^3), and d_s is the soot diameter (4.5×10^{-9} m) and M_C is the carbon molecular weight (12 g/mole). Net reaction rate w in Equation 5.5 is

$$w = \left(\frac{k_A p_{O_2}}{1 + k_Z p_{O_2}} \right) x + k_B p_{O_2} (1 - x) \tag{5.6}$$

where p_{O_2} is the oxygen partial pressure in atm. The proportion, x, of A sites is given by:

$$x = \frac{p_{O_2}}{p_{O_2} + (k_T / k_B)} \tag{5.7}$$

Table 5.4 shows the rate constants used in the NSC soot oxidation model.

Table 5.4. Rate constants for NSC soot oxidation model

Parameter	**Rate Constant**	**Units**
$\mathbf{k}_A$	20 exp(-15100/T)	g-C/cm^2.s.atm
$\mathbf{k}_B$	4.46×10^{-3} exp(-7640/T)	g-C/cm^2.s.atm
$\mathbf{k}_T$	1.51×10^{5} exp(-48800/T)	g-C/cm^2.s.atm^{-1}
$\mathbf{k}_Z$	20 exp(-15100/T)	g-C/cm^2.s.atm

5.5. Soot Emission Model Calibration

In the emission model calibration about 10% (n = 90 points) of all test points shown in Figure 5.1 and Figure 5.11 are used. The test data include 940 DOE points and 193 fuel loop point. The remaining 1043 points are used to check the accuracy of the soot emission model. In the calibration process two parameters "Soot Burnup Multiplier" and "Soot Oxidation Multiplier" needs to be selected. Initial runs show that in the selection it is sufficient to cover "Soot Burnup Multiplier" range of 4 to 9 and "Soot Oxidation Multiplier" range of 4 to 8. A parameter step value of 1 is adapted for both parameters and model is run for (6x5) combinations of the parameters. The

soot emission prediction error and the root mean square error are defined as:

$$\text{Error}(\%) = 100\frac{m_{s,model} - m_{s,test}}{m_{s,test}} \tag{5.8}$$

$$\text{RMSE} = \sqrt{\frac{1}{n}\Sigma_{i=1}^{n}\Big(m_{s,test} - m_{s,model}\Big)^2} \tag{5.9}$$

$$\text{nRMSE } (\%) = 100\left(\frac{\text{RMSE}}{m_{s,max} - m_{s,min}}\right) \tag{5.10}$$

5.6. Soot Emission Model Results

Figure 5.26 and 5.27 show contour plots of nRMSE as a function of Soot Formation and Soot Burn-up multipliers both with Hiroyasu and NSC models. Error values are smaller with Hiroyasu model, and use of Hiroyasu model is more accurate in soot emission prediction related studies performed via thermodynamical models. Research conducted in [31] showed the NSC oxidation model gave higher values of peak soot concentration compared to Hiroyasu model. The underlying reason is that the oxidation rate is dependent on partial pressure of oxygen molecules which is lowered in engine like conditions. It is calculated that for Hiroyasu model the best parameter values are 8 and 7 for Soot Burn-up and Soot Formation multipliers, respectively.

Rest of the DOE data and fuel loop points are run with the chosen Soot Burn-up and Soot Formation multipliers to check the accuracy of the predictions with Hiroyasu model. Figure 5.28 shows the correlation of the model predictions with the test results. The nRMSE of the model is 7.6%. Use of the same multipliers with NSC model results nRMSE value of 15.4%.

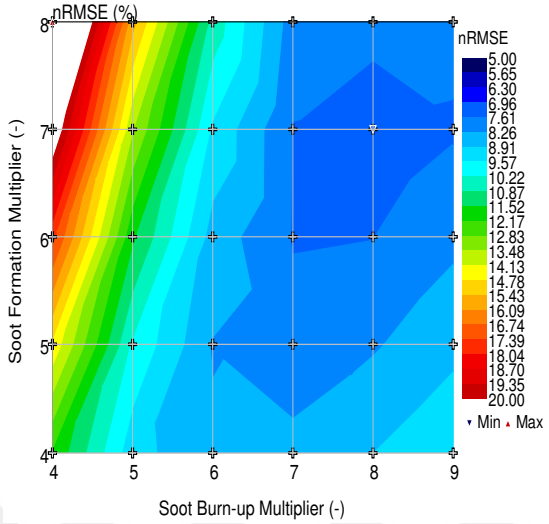

Figure 5.26. nRMSE contours as a function of soot formation and soot burn-up multipliers- Hiroyasu model

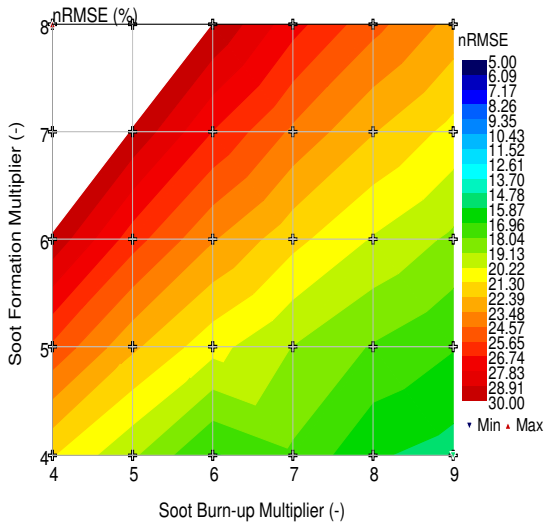

Figure 5.27. nRMSE contours as a function of soot formation and soot burn-up multipliers- NSC model

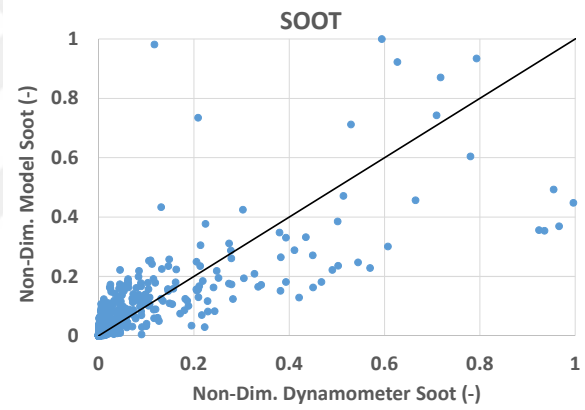

Figure 5.28. Soot: model vs test comparison

6. APPLICATION AREAS OF THE METHODOLOGY

Developed methodology can also be used for different purposes. Some these areas are summarized as below:

- Virtual calibration of engines
- Hardware selection studies
- High altitude calibration Studies
- Technology selection studies
- Coupling with calibration Tools
- Spontaneous test data diagnostics

Details of these areas are given below.

6.1. Virtual Engine Calibration

As mentioned in Chapter 1; difficulties in fulfilling the emission regulation requirements incrementally increase every year. However, there is a sharp trade-off between meeting the emission regulation requirements and satisfying the customers better fuel economy. To ensure that the products satisfy both aspects; a detailed study on the calibration parameters of the engine operating points needs to be carried on. However, obtaining the optimum set points in dynamometer is not a cost and time effective solution. OEMs generally prefer utilizing simulation environment. In this chapter, an effective way of predicting the calibration set points is represented. The developed methodology is used for calibration development in a virtual (thermodynamical model) environment. Virtual engine calibration means generating all calibration set points via virtual product, not in a real test environment.

To ensure that the problem is successfully solved for a product; engine calibration should be performed at the optimum point of NO_x vs BSFC trade-off. The main reasons are summarized below:

(i) Engine should satisfy the customer needs via providing low fuel consumption values.

(ii) Engine emissions such as NO_x, soot, CO, etc. must be within limits defined by emission regulations.

(iii) An engine that is calibrated at only minimum BSFC would most probably operate with high NO_x emissions. However, although the NO_x emissions are within the emission regulation limits, there is another critical parameter that needs to be taken into consideration: urea consumption. It is obvious that higher the feedgas (cylinder out) NO_x emissions, higher the urea consumption. To convert the extreme feedgas NO_x values, higher amounts of urea should be injected in the aftertreatment system to facilitate the SCR reactions with NO_x.

As a natural consequence of above-listed facts; detecting the optimum engine calibration points is one of the most critical engineering problems. A mostly encountered way of finding out the optimum calibration is to perform specific tests in the dynamometer environment.

In the dynamometer studies; the below steps are generally traced:

- A real driving emission or homologation cycle is selected.
- Test data is collected at that specific cycle by imposing representative engine speed and brake torque.
- Maximum fuel residency points are detected.
- DOEs are designed via changing most critical calibration parameters such as boost pressure target, air mass flow target, start of injection, etc.
- DOEs are run with approximately 60-80 points.
- DOE points that are not violating the calibration limits such as compressor outlet temperature, turbine inlet temperature, shaft speed, peak firing pressure limit are selected.
- Mathematical models are generated via using remaining DOE points.
- Optimum emission points are calculated via the mathematical models.

However, performing such kind as examinations results as very high engineering effort including engineering costs (engineer and dynamometer room allocations), test failures, consumed fuel amount, etc. In this section of the study, the use of the predictive combustion models for optimum calibration generation studies is investigated.

To understand the applicability of the methodology; optimum calibration points are collected by tracing the above-listed points. Five different operating points (cases) are selected for examination. These points are selected by examining a real driving cycle data and can be seen in Table Figure 6.1 and Figure 6.1.

Table 6.1. Desktop calibration development : optimization results

Case Number	**Engine Speed (rpm)**	**Load %**
Case 1	1000	30
Case 2	1200	10
Case 3	1200	70
Case 4	1600	45
Case 5	1800	80

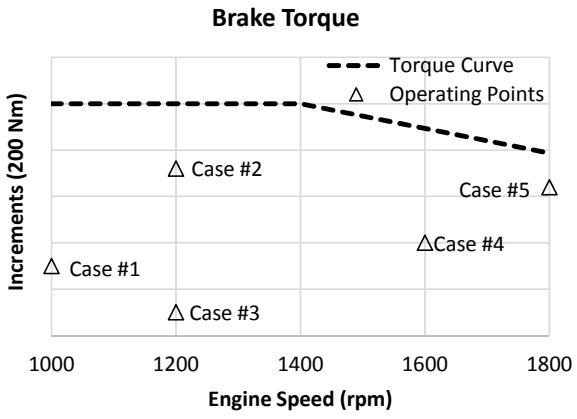

Figure 6.1. Selected operating points

In these five different points; seperate optimization studies are performed. In these optimization studies; GT-Suite Advanced Direct Optimizer tool is used. The

tool uses a non-dominated sorting genetic algorithm (NSGA-III) as the main algorithm. Details of an GT-Suite optimization process can be found in Appendix C.

In these designs in-cylinder pressure, compressor outlet temperature, turbine inlet temperature, shaft speed limitations are used as the main factors. All these limitations are obtained from suppliers as a result of durability specific concerns. DOE design parameters and optimization ranges are shown in Table 6.2.

Table 6.2. Desktop calibration development : design space

Parameter	**Range**
SOI (CA)	-20-0
Rack (-)	0.3-1.0
EGR Valve Pos. (%)	0-45

Figures 6.2, 6.3, 6.4, 6.5 and 6.6 are showing the SOI, rack position and EGR valve position values for all 850 different designs. Circles are representing the values used in each design. As it is seen in the graphs, values converge to a specific output since the optimum value is already obtained.

In these optimization studies, the primary objective is to minimize the Total Operating Cost (TOC). TOC for heavy-duty vehicles includes different items such as:

- Fuel Consumption
- Urea Consumption
- Truck Cab & trailer costs
- Driver salary
- Repair & maintanence costs
- Insurance
- Tires
- Permits,licenses and tools.
- Fuel taxes

- Driver needs: coffee, etc.

In this study, the first two items which are fuel and urea consumption values are taken into consideration. Optimization studies mainly focus on lowering these values by using the below equation:

$$\text{TOC} = \left(\frac{NOx.CF.UP}{\rho_{\text{Urea}}}\right) + \left(\frac{BSFC.FP}{\rho_{\text{Fuel}}}\right) \tag{6.1}$$

where; CF is Convertion Factor: 2.008 (2.008 unit urea is needed to convert one unit NO_x. UP and FP are Urea Price and Fuel Price, respectively. ρ_{Urea}=1.0930 g/cm^3 and ρ_{Diesel}=0.835 g/cm^3.

Figures 6.2, 6.3, 6.4, 6.5 and 6.6 are representing the main start of injection (SOI), rack position and EGR valve position. Black circles are representing the actual value of these parameter for each design numbers. Values of these parameters vary in all designs. It seems that all these values converge to a single value after approximately 500 designs.

Table 6.3 shows the optimization results of the parameters used in the design space. As it is seen in the optimization results, different SOI and rack positions are encountered in the cases. However, the EGR valve opening position is almost the same: at a fully open position. Main reasons for these conditions can be summarized as below:

- Start of injection optimization mainly searches the optimum location of BSFC. It is known that advancing the start of injection with respect to a reference point -especially at operating points near to full load-, increases the PFP. However, retarding SOI would result in lower PFP values. The optimum location of SOI mostly varies as a result of engine speed and load conditions. At full load or high

(a) Start of injection

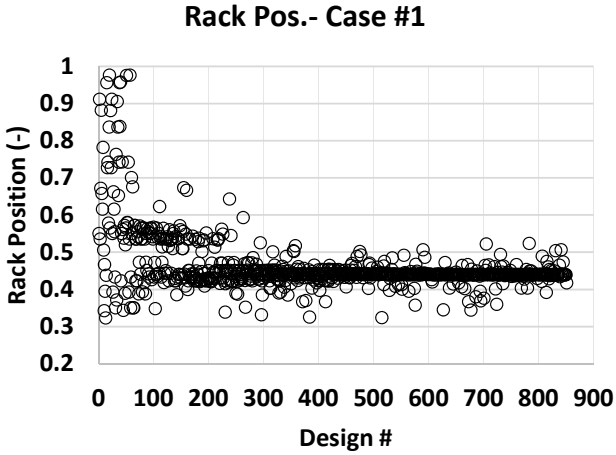

(b) Rack position

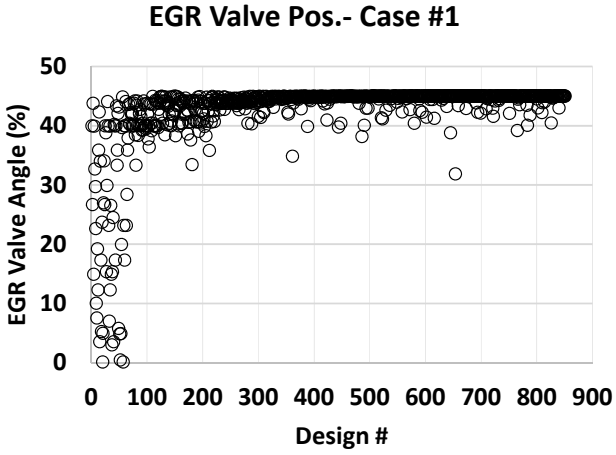

(c) EGR position

Figure 6.2. Optimization results for case 1

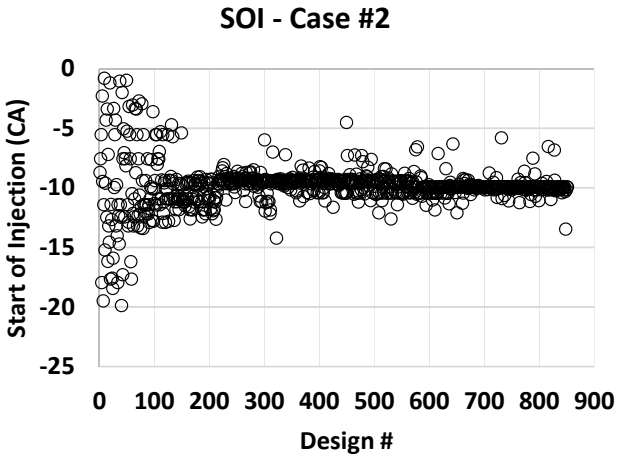

(a) Start of injection

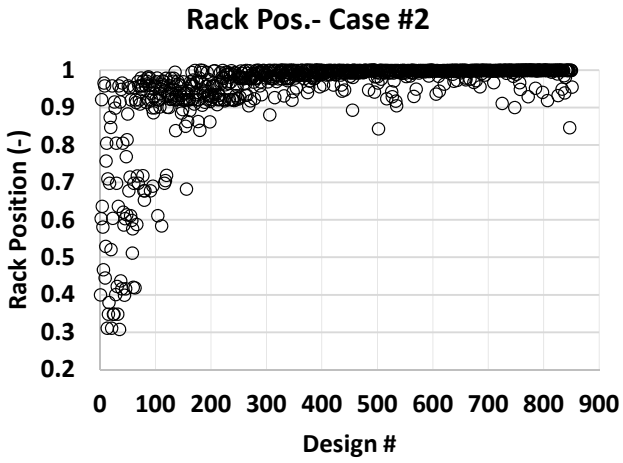

(b) Rack position

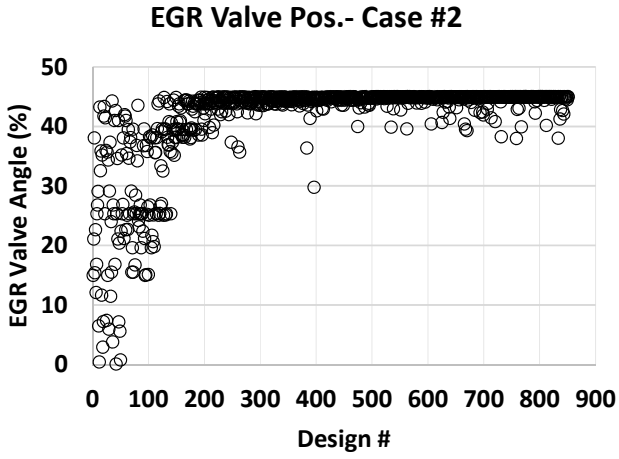

(c) EGR position

Figure 6.3. Optimization results for case 2

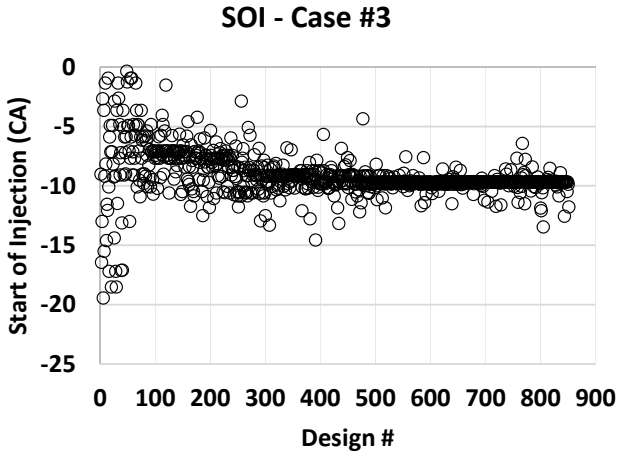

(a) Start of injection

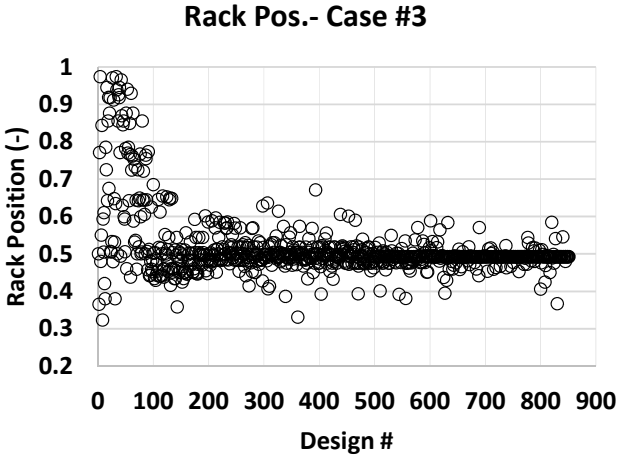

(b) Rack position

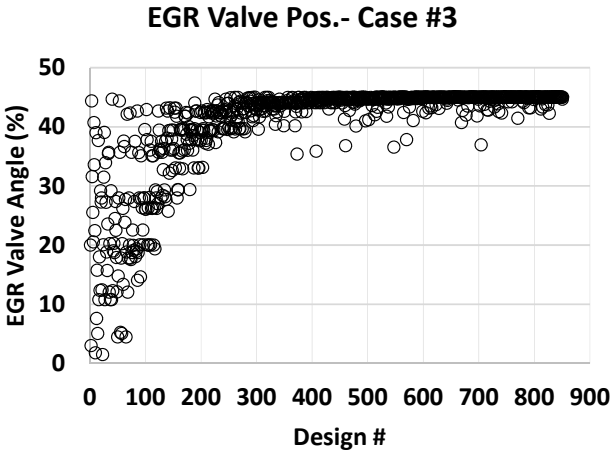

(c) EGR position

Figure 6.4. Optimization results for case 3

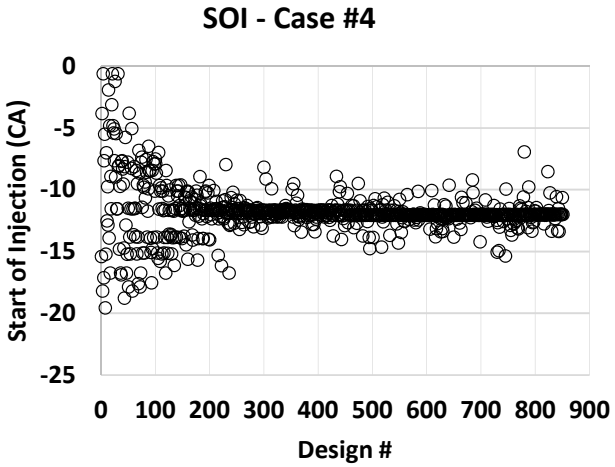

(a) Start of injection

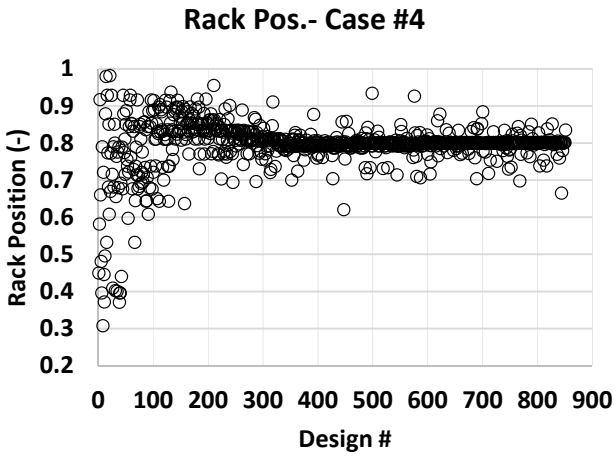

(b) Rack position

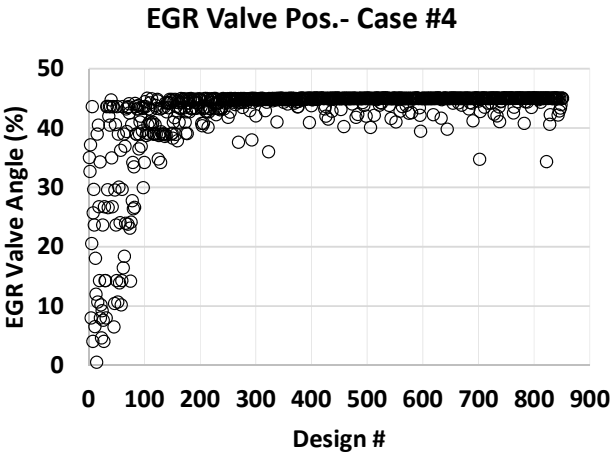

(c) EGR position

Figure 6.5. Optimization results for case 4

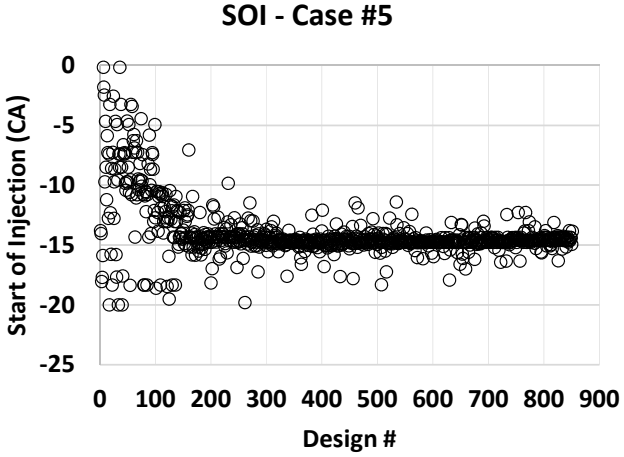

(a) Start of injection

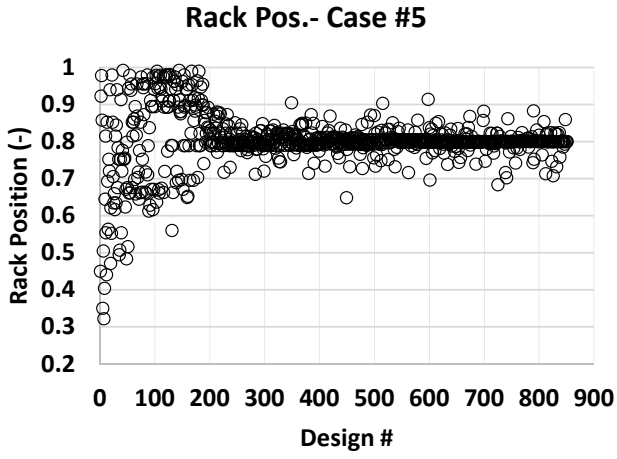

(b) Rack position

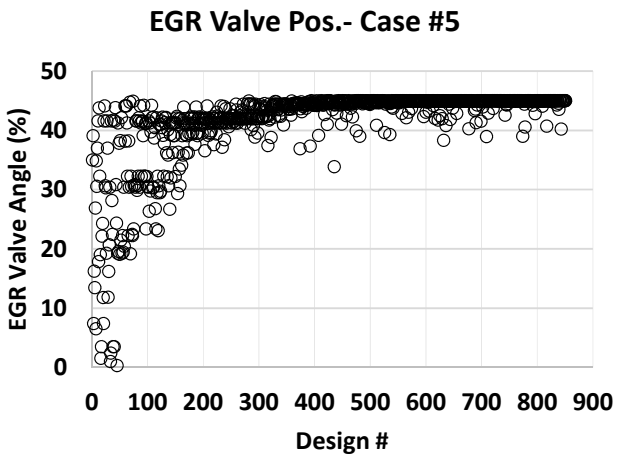

(c) EGR position

Figure 6.6. Optimization results for case 5

load, high engine speed points; advancing SOI up to PFP limitations would lower BSFC values. Figure 6.12 also proves that at higher engine speed & load points higher PFP values are the most optimum operating conditions. At lower engine speed, SOI values which make the engine operate near to the PFP limits are not desired due to lowered combustion efficiency values.

- Rack positions vary as a function of engine speed and load conditions. In very low load conditions such as Case 2, maximum rack position (1.0) is needed to lower boost pressure values and hence pumping losses as it viewed in Figure 6.11. In other cases, rack position locates at the optimum of the trade-off for increasing the boost pressure and lowering the pumping losses.
- In each of the cases EGR valve position is at the limitation: 45 % since lowering the TOC needs lower NO_x emissions. Optimizations are trying to maximize the EGR rate to reduce NO_x emissions.

Table 6.3. Desktop calibration development : optimization results

Case #	**Model SOI (CA)**	**Model Rack (-)**	**Model EGR Valve Pos. (%)**
Case 1	-5.0	0.44	45
Case 2	-10.1	0.99	45
Case 3	-9.67	0.49	45
Case 4	-12.0	0.79	45
Case 5	-14.35	0.86	45

Figures 6.7, 6.8 are representing the TOC results of different cases concerning design number. It is important to note that the TOC is non-dimensionalized with the maximum value of all cases.

Figures 6.9, 6.10 and 6.11 are representing the most critical comparisons between test and model results since these three parameters are generating the basis of calibration at a specific operating point. In other words, to perform a test at a particular point, an engineer needs to clarify the boost pressure target, air mass flow target and

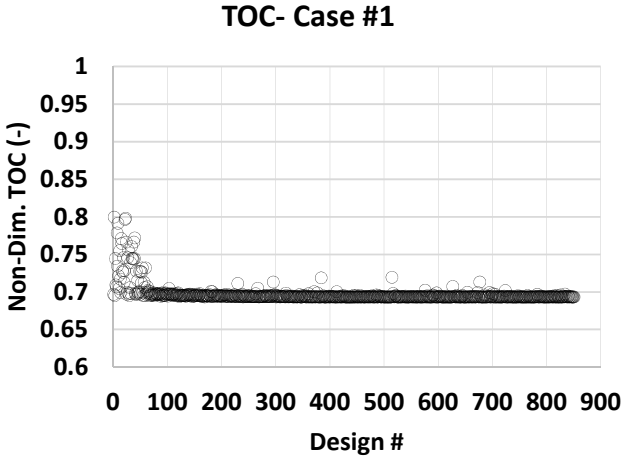

(a) Case 1

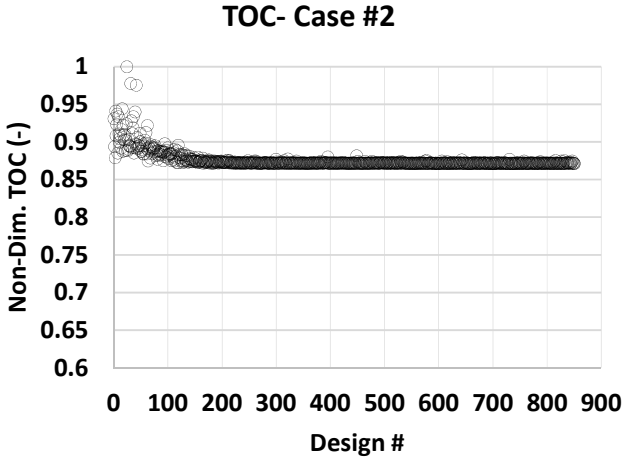

(b) Case 2

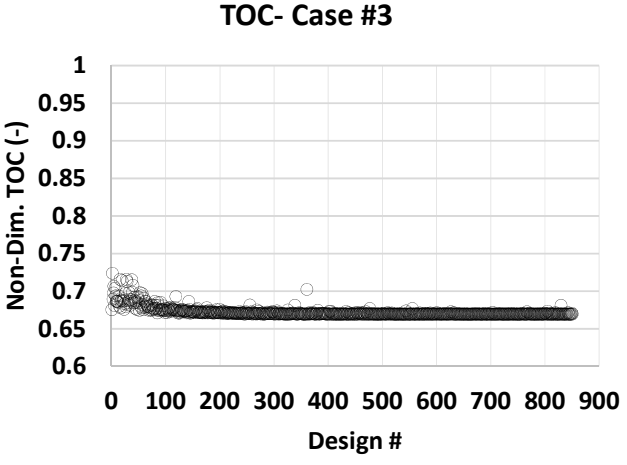

(c) Case 3

Figure 6.7. Non-dim. TOC optimization results: cases 1-2-3

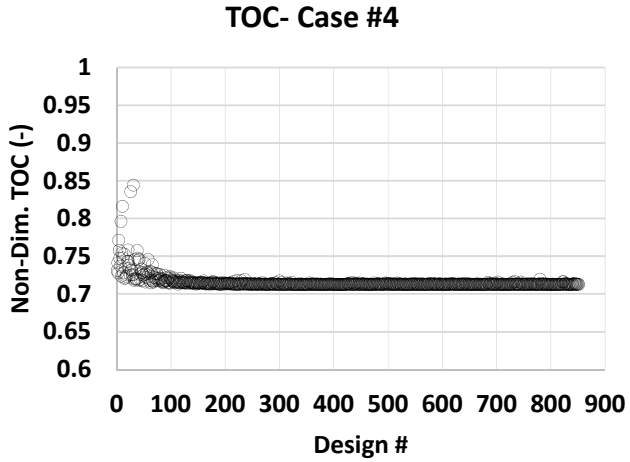

(a) Case 4

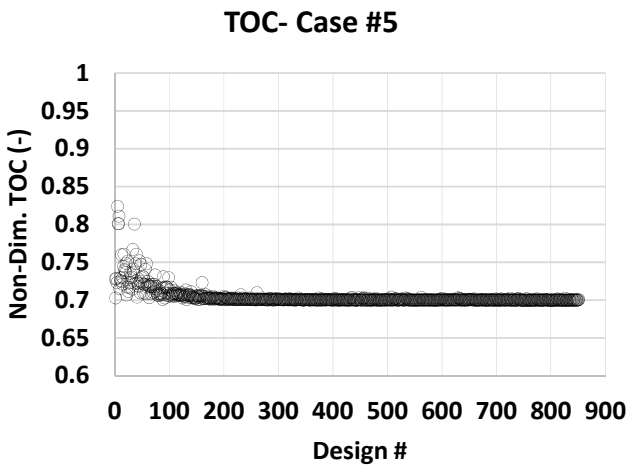

(b) Case 5

Figure 6.8. Non-dim. TOC optimization results: cases 4-5

start of injection values. These graphs are showing that analytical methods can be used for rapid and accurate detection of these three parameters. These three figures are showing that the predictive model results are in excellent correlation with test data. Main SOI values are predicted in ± 2 CA error margin, air mass flow target is predicted witin ± 500 mg/stroke error margin and boost pressure target is predicted within ± 0.4 bar error margin.

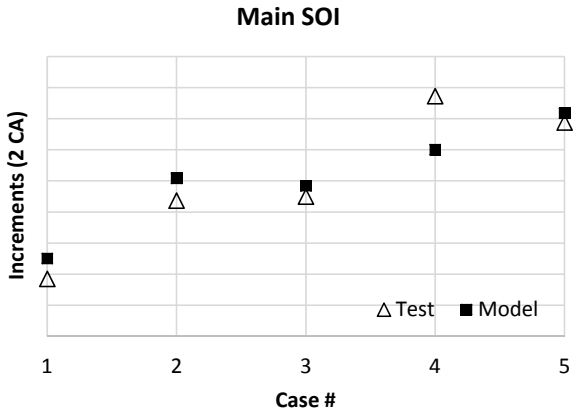

Figure 6.9. Start of injection comparison: test vs model

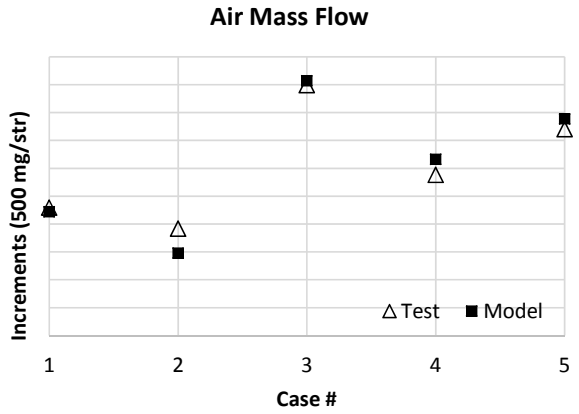

Figure 6.10. Air mass flow comparison: test vs model

Figure 6.12 shows the correlation between the test and model peak firing pressure values are good.

Besides; Figures 6.13, 6.15, 6.14 and 6.16 are proving that the results obtained via analytical optimization are in good correlation with the test reciprocals. PFP values

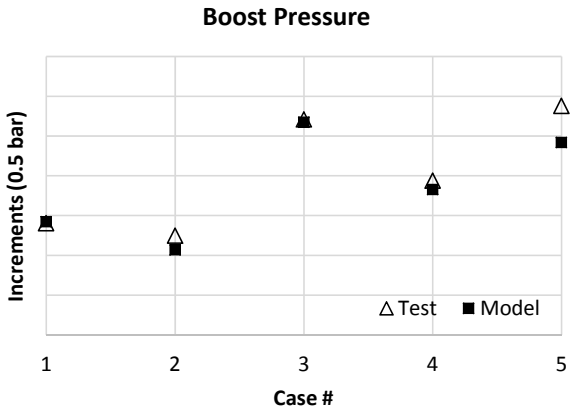

Figure 6.11. Boost pressure comparison: test vs model

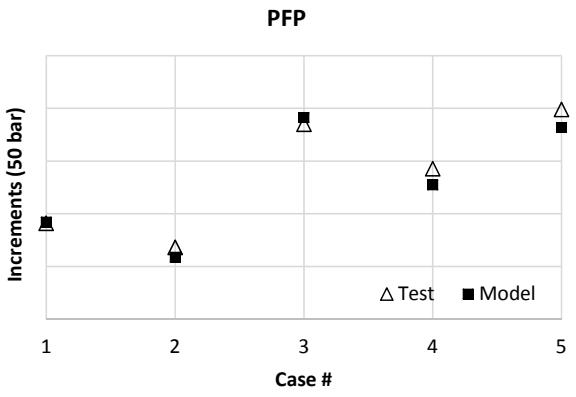

Figure 6.12. Peak firing pressure comparison: test vs model

obtained at the end of optimization are within ± 9 bar error margin. Turbocharger shaft speed values are within ± 15 krpm error margin. Turbine inlet temperature, compressor outlet temperature adn turbine outlet temperature results of the optimizations are within ± 20, ± 10 °C and ± 30 °C error margins, respectively.

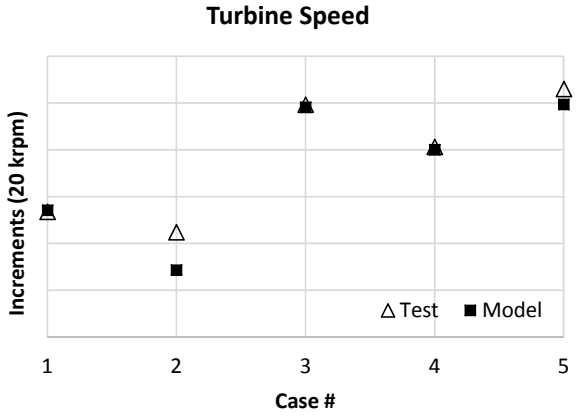

Figure 6.13. Turbocharger shaftspeed comparison: test vs model

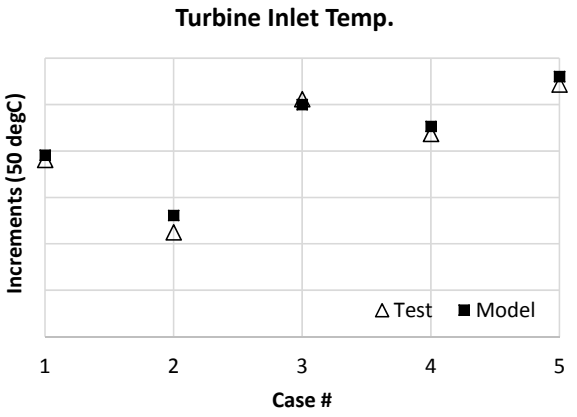

Figure 6.14. Turbine inlet temperature comparison: test vs model

Figure 6.17 represents that the NO_x outputs obtained via desktop calibration are very similar to the test results. Results are within the error margin of ± 2 g/kWh.

Last but not least; BSFC comparison of the methodology results with test data is investigated. As it is seen in 6.18, both results are in perfect correlation. Results are within the error margin of ± 5 g/kWh.

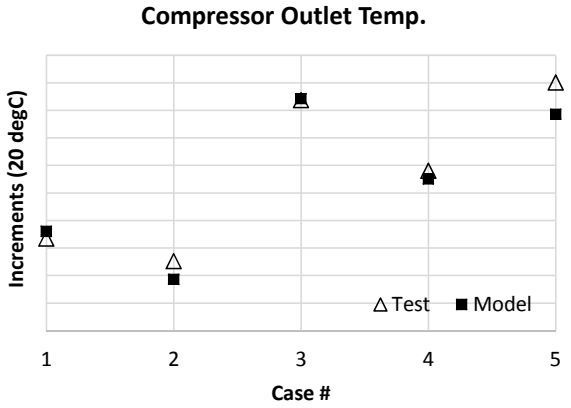

Figure 6.15. Compressor outlet temperature comparison: test vs model

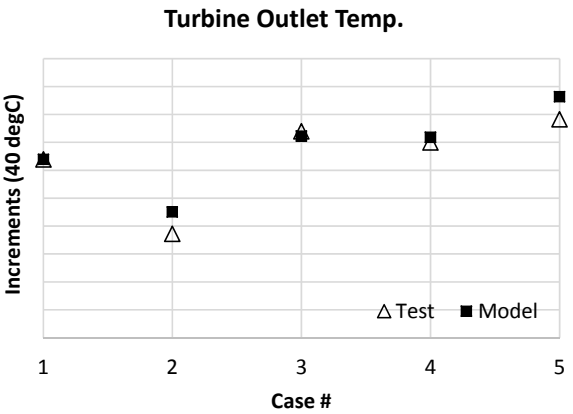

Figure 6.16. Turbine outlet temperature comparison: test vs model

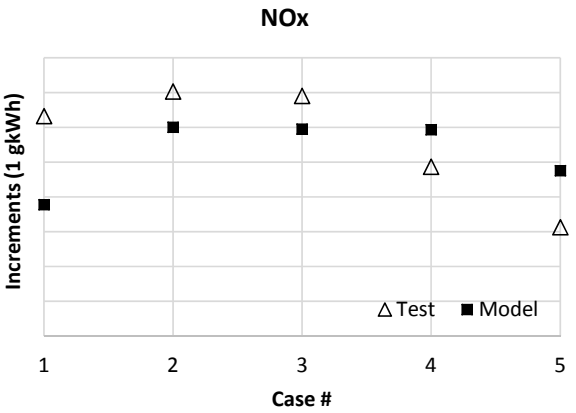

Figure 6.17. NO_x emission comparison: test vs model

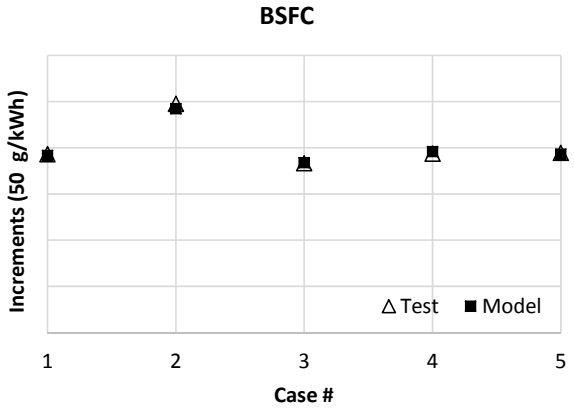

Figure 6.18. Brake specific fuel consumption comparison: test vs model

These outputs are showing that predictive combustion models can successfully be used for performing virtual calibration. After considering the above-listed results, it would be appropriate to say that; by using the developed methodology, it is easy to eliminate the risks of test failures; dynamometer room/test engineer allocation problems and consumed fuel costs, etc. Furthermore, since it is possible to perform DOE with a higher set of points with respect to test studies; optimum points can be rapidly and accurately detected.

6.2. Hardware Selection Studies

One of the challenging problems in automotive is to select the correct components for the first time within the project scope and boundaries. Many elements such as turbocharger, injector, charge air cooler, EGR cooler must be selected at the early stages of engine development in which there is no actual engine to test. For the case that the selected component does not fit to the project targets such as fuel economy, acoustics, emissions, etc.; then a new hardware selection is needed which mostly ends with delay in project timings. A first-time true hardware selection process can only be obtained if accurately predicted emission outputs with the selected hardware are taken into consideration. However, via the developed methodology; component selection can be performed at the early engine development stages of the project without encountering any problems.

For example, turbocharger matching studies can be completed by using this methodology. Selection can be performed by a detailed investigation of BSFC vs NO_x trade-off curves for different turbochargers. Figures 6.19, 6.20 and 6.21 are showing the main trends generated with 12.7L HD diesel engine at single engine speed point: 1400 rpm by varying air mass flow set points and hence EGR Rate. It is important to note that, all of the variables shown in these figures are non-dimensionalized via using the maximum value at that specific engine speed.

As it is seen in Figure 6.19, BSFC decreases by the increased EGR rate values. This is a normal condition since increasing the EGR rate can only be obtained by multiplying the difference between turbine inlet pressure and boost pressure; which means higher pumping losses. Besides, higher EGR rates would result as lower combustion efficiency and hence higher BSFC values. Figure 6.20 shows the variance of NO_x emissions as a function of the EGR rate. Increase in EGR rate results as lower NO_x emissions, as expected. 6.21 simply represents the trade-off between BSFC vs NO_x. These lines can be increased by applying the same steps with different turbochargers. Hence, it would be easy to see which turbocharger enables better optimum point.

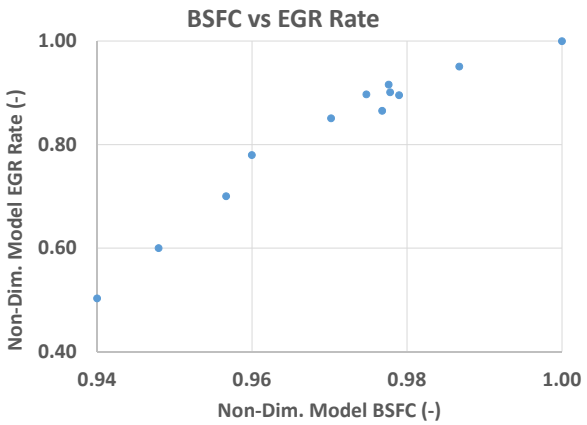

Figure 6.19. BSFC vs EGR rate

It is possible to select the maximum fuel residency points and perform the same sweeps to obtain a proper comparison between different turbochargers. It is obvious that selection of turbocharger would be much easier and accurate with respect to

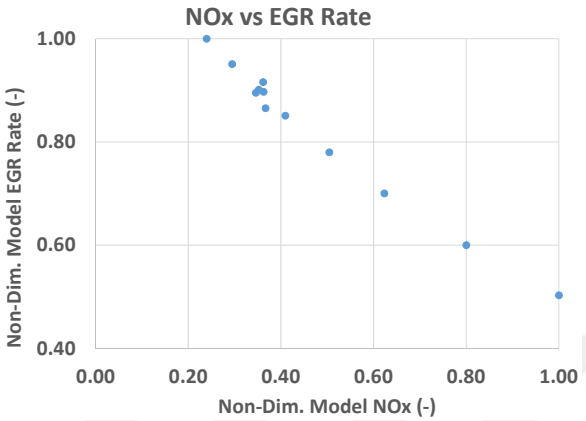

Figure 6.20. NO_x vs EGR rate

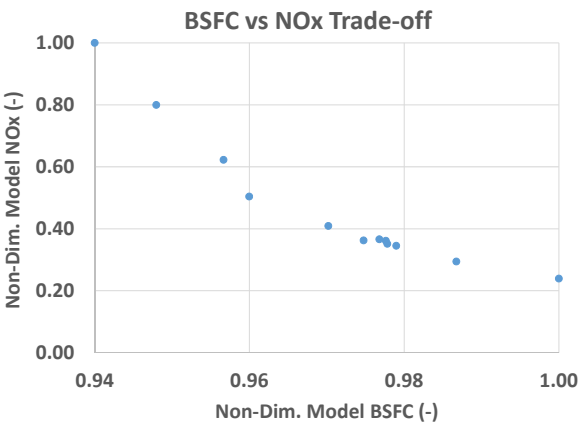

Figure 6.21. BSFC vs NO_x

conventional methods which only include the BSFC aspect, not also the emissions.

6.3. High Altitude Calibration Studies

High altitude performance and calibration of an engine is a problematic condition due to several reasons:

- Higher the altitude, lower the ambient pressure and temperature values. It is too complex and expensive to perform high altitude tests in dynamometer environment. So, high altitude tests need real high altitude conditions to collect data (Figure 6.22).
- High altitude tests can only be accomplished at limited time zones of the year to perform the tests at desired temperature range.
- Actual vehicle tests can easily end with failure due to vehicle, sensor or engineer based errors.
- A high altitude test generally lasts for three weeks.

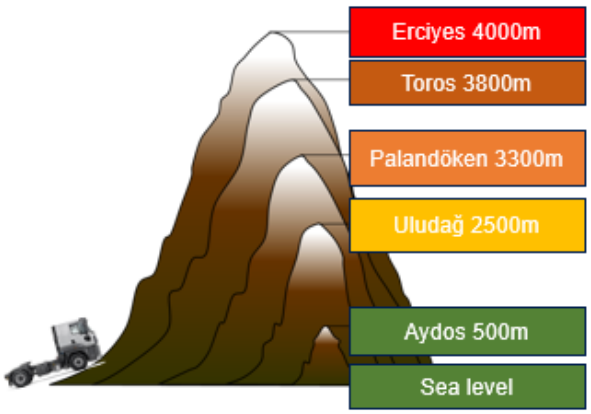

Figure 6.22. High altitude conditions

It is also possible to use the methodology for virtual calibration at high altitude conditions. Before the trip, it is possible to perform a detailed DOE by varying main calibration parameters such as SOI, air mass flow set point, boost pressure set point, injected fuel quantity and rail pressure. Hence, it would be possible to find out the most effective calibration set points at high altitude pressure and temperature conditions.

6.4. Technology Selection Studies

As it is mentioned in section 6.1, it is possible to find out the best engine performance parameters and calibration set points which can be used in minimizing the TOC output. As a natural result of this capability, the methodology can also be used for evaluation of different technologies such as variable valve timing, variable compression ratio, miller cycle, electronic controlled turbocharger, belt started generator; etc.

6.5. Coupling With Calibration Tools

The methodology outputs can be used to generate mathematical regression models via using ASCMO or Matlab based codes. Hence, it would be possible to model all design space that can be used for further examinations. Besides, it is possible to couple these models with Hardware in the Loop (HIL) systems (Figure 6.23) to perform real time simulations.

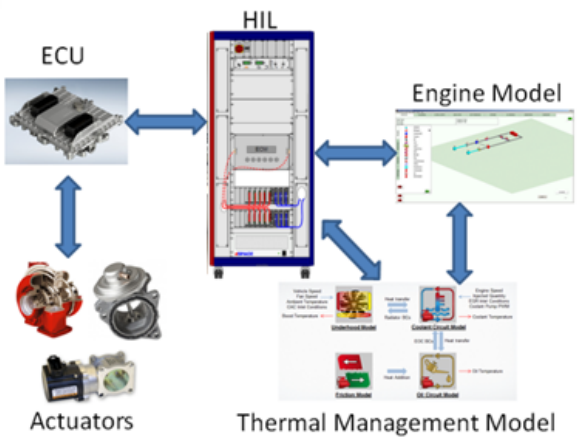

Figure 6.23. HIL and model integration

6.6. Test Data Diagnostics

These models can also be used for test data diagnostics; during the test or just after the test. Via performing simultaneous simulations with the same set points, it is possible to directly diagnose if the test data is ok or not. Hence, one can easily

detect any test specific problems such as peak firing pressure sensor errors, pressure, temperature sensor related errors, leakages in pipings or surge in a compressor.

Figure 6.24. Test data diagnostics via thermodynamical models

7. SUMMARY AND CONCLUSIONS

Nowadays, more and more stringent emission regulations are encountered in whole regions of the world. As a natural result, engine performance development studies mostly focus on emission reduction. Nitrogen oxide, soot, CO and UHC emissions are the most critical diesel engine emissions. As a result, there are many studies in literature focusing on emission prediction. Undoubtedly, the development of accurate and robust emission prediction methodologies is a must especially for the early stage of engine performance development studies. Engine component selection, accurate, specific fuel consumption prediction and defining the correct EGR strategy (low and mid-high) can only be achieved via accurate and fast NO_x emission prediction. However, the current emission prediction methodologies such as; 3D combustion, stochastic reactor, semi-empirical, phenomenological models and neural networks need either an excessive amount of data or simulation duration which means high license costs.

In this study; a fast, agile and accurate methodology for NO_x emission prediction that can be used at all stages of engine development is developed.

In Chapter 4, a 9 L 380 PS heavy-duty diesel engine model is generated and correlated with fuel loop data which includes whole engine speed range with 10% load increments. Diesel wiebe combustion model is preferred. Extended Zeldovich mechanism is used in GT-Suite for NO_x emission calculation. NO_x emission output correlation to test data is completed via using NO_x calibration multiplier maps. Most critical maps & parameters with high NO_x emission prediction accuracy are investigated. Sixteen different maps are generated, and model NO_x prediction results are compared with two separate fuel loop data. Lowest nRMSE value obtained in 9L HD diesel engine studies is 5.7%.

Results show that peak firing pressure and in-cylinder maximum temperature are the most critical parameters for NO_x emission prediction. Turbine inlet temperature, fuel flow, CA50, EGR rate and fuel-air equivalence ratio are the other important

parameters that can be used in NO_x calibration multiplier map generation.

Furthermore, to understand the robustness of the developed methodology; another heavy-duty engine data are also used. In the Chapter 5; a 12.7 L heavy-duty diesel engine model is created, and model correlation is performed via using a fuel loop and a DOE test data. As the main difference from the previous section, a predictive combustion model, so-called DI-Pulse is used. DI-Pulse enables the use of critical calibration parameters such as pilot, main, post injection timing & quantities and rail pressure. Same methodological steps are accomplished, and 13 different maps are created. turbine inlet temperature, maximum in-cylinder temperature, maximum in-cylinder pressure, load, fuel flow, CA50, F/A equivalence ratio, EGR rate and rail pressure parameters are detected as the most critical emission prediction parameters.

Best accuracy is obtained via the use of five of these parameters which are; CA50, TMax, EGR rate, rail pressure and F/A equivalence Ratio. In the 12.7 L diesel engine study lowest nRMSE value between dynamometer and model NO_x outputs is 3.96%. These accuracy results are showing that the developed methodology is competitive with the other NO_x emission prediction modelling strategies mentioned previously in the Chapter 2.

It is evident that, fulfilling the emission regulation requirements incrementally increase every year. To ensure that the products meet both the regulative obligations and customer needs; a detailed study on the virtual calibration of the engine operating points is completed. In Chapter 6.1, virtual calibration generation study is performed via a 12.7L heavy-duty diesel engine model in which the developed methodology is used. Five different operating points are selected for the evaluation. Optimization simulations are run in all of these five points, and the results are compared with test data. It is proven that the model and test outputs are in good correlation which means that the developed methodology can be successfully used for virtual calibration development. Undoubtedly; the need for actual tests will significantly reduce via virtual calibration.

As it is mentioned in Chapter 6; the developed methodology can be used for many further complex studies. Hardware selection, high altitude calibration, technology selection, calibration tool couplings and spontaneous test data diagnostics are some of the possible areas in which utilizing from the developed methodology is feasible.

Hence, this study has shown that; if the minimum data requirement is satisfied via dynamometer tests, global optimization can be done in the simulation environment without any further tests. Furthermore, since thermodynamical models are physically based, the demonstrated methodology can be used at the very early stages of engine development in which no actual engine or test data exist. Undoubtedly, this will provide both a cheaper and faster solution for global optimization and component selection studies.

Last but not least, traditional emission prediction methodologies require significantly high simulation duration (almost 3-4 days per operating point on a typical workstation PC). However, this methodology enables accurate NO_x prediction with very low CPU time. For example, it is possible to generate the NO_x prediction for 100 points in 30 minutes. Using a single cylinder thermodynamical model rather than a detailed model (six-cylinders) may even further decrease the required computational effort. Taking the points that are mentioned above into consideration, it is possible to state that the methodology presented in this thesis document can be used as a fast and reliable tool for NO_x prediction at any phase of engine development.

As the future study, soot and CO prediction accuracies can be developed further by also comparing with different test data. Besides, for NOx prediction accuracy improvement; effect of varying DI-Pulse predictive combustion model parameters with respect to engine operating points can also be investigated.

REFERENCES

1. ICCT, "Recommendations for the Proposed Heavy-Duty Vehicle CO2 Standards in the EU", *International Council of Clean Transportation, Position Brief*, 2018.

2. ICCT, "The European Commission's Proposed CO2 Standards for Heavy-Duty Vehicles", *International Council of Clean Transportation, Position Brief*, 2018.

3. Gamma-Technologies-LLc, "GT-Power Manual", *GT-Suite*, 2017.

4. Heywood, J. B., *Internal Combustion Engine Fundamentals*, McGraw-Hill, Inc, 1988.

5. Huck, F., "Predictive Combustion on Diesel Engine for Heat Rejection Determination", *PSA, GT-Suite Conference*, 2014.

6. Rodríguez, F., "Fuel Consumption Simulation of HDVs in the EU: Comparisons and Limitations", *International Council of Clean Transportation, White Paper*, 2018.

7. Zhang, Q., A. Pennycott, R. Burke and S. Akehurst, "Predicting the Nitrogen Oxides Emissions of a Diesel Engine using Neural Networks", *SAE Technical Paper, 10.4271/2015-01-1626, 2015*, Vol. 26, pp. 214–224, 1983.

8. Ricardo, "Ricardo Wave Manual", *Ricardo Wave*, 2012.

9. Shi, X., X. Qiao and J. Ni, "Study on the combustion and emission characteristics of a diesel engine with multi-injection modes based on experimental investigation and computational fluid dynamics modelling", *Proceedings of the Institution of Mechanical Engineers Part D Journal of Automobile Engineering*, Vol. 224, pp. 1161–1176, 2010.

10. Almeida, F., P. Zoldak, M. Pimenta and P. Lacava, "Directional Emissions Predictions of NOx and Soot of a Diesel ICE via Numerical Simulation", *SAE Technical Paper, 10.4271/2015-01-2880*, 2015.

11. Kim, H., B. Ryu and C. Lee, "Modelling for investigation of combustion and emission characteristics in a high speed direct injection diesel engine with light duty under various operating conditions", *Proc., IMechE PartD: J. Automobile Engineering*, Vol. 222, pp. 2159–2170, 2008.

12. Bhave, A., M. Kraft, L. Montorsi and F. Mauss, "Modelling a Dual-Fuelled Multi-Cylinder HCCI Engine Using a PDF Based Engine Cycle Simulator", *SAE International, 10.4271/2004-01-0561*, 2004.

13. Smallbone, J., A. Bhave, A. R. Coble, S. Mosbach, M. Kraft and R. McDavid, "Identifying optimal operating points in terms of engineering constraints and regulated emissions in modern diesel engines", *SAE Technical Paper, 10.4271/2011-01-1388*, 2011.

14. Maurya, R. K. and P. Mishra, "Parametric investigation on combustion and emissions characteristics of a dual fuel (natural gas port injection and diesel pilot injection) engine using 0-D SRM and 3D CFD approach", *Fuel*, Vol. 210, pp. 900–913, 2017.

15. Jochim, B., M. Korkmaz and H. Pitsch, "Scalar dissipation rate based multi-zone model for early-injected and conventional diesel engine combustion", *Combustion and Flame*, Vol. 175, pp. 138–154, 2017.

16. Wang, H., R. D. Reitz, M. Yao, B. Yang, Q. J. b and L. Qiub, "Development of an n-heptane-n-butanol-PAH mechanism and its application for combustion and soot prediction", *Combustion and Flame*, Vol. 160, pp. 504–519, 2013.

17. Paul, C., S. F. Fernandez, D. C. Haworth, S. Roy and M. F. Modest, "A detailed modeling study of radiative heat transfer in a heavy-duty diesel engine", *Combus-*

tion and Flame, Vol. 200, pp. 325–341, 2019.

18. Aubagnac-Karkar, D., J.-B. Michel, O. Colin, P. E. Vervisch-Kljakic and N. Darabiha, "Sectional soot model coupled to tabulated chemistry for Diesel RANS simulations", *Combustion and Flame*, Vol. 162, pp. 3081–3099, 2015.

19. Duvvuri, P. P., S. Sukumaran, R. K. Shrivastava and S. Sreedhara, "Modeling soot particle size distribution in diesel engines", *Fuel*, Vol. 243, pp. 70–78, 2019.

20. Rajkumar, S., S. Bakshi and P. Mehta, "Multizone Phenomenological Modeling of Combustion and Emissions for Multiple-Injection Common Rail Direct Injection Diesel Engines", *Journal of Engineering for Gas Turbines and Power*, Vol. 138, pp. 122805–122813, 2016.

21. Rakopoulos, C. D., D. C. Rakopoulos, G. C. Mavropoulos and G. M. Kosmadakis, "Investigating the EGR rate and temperature impact on diesel engine combustion and emissions under various injection timings and loads by comprehensive two-zone modeling", *Energy*, Vol. 157, pp. 990–1014, 2018.

22. Provataris, S. A., N. S. Savva, T. D. Chountalas and D. T. Hountalas, "Prediction of NOx emissions for high speed DI Diesel engines using a semiempirical, two-zone model", *Energy Conversion and Management*, Vol. 153, pp. 659–670, 2017.

23. Abbe, C., R. Nzengwa, R. Danwe, Z. Ayissi and M. Obonou, "A study on the 0D phenomenological model for diesel engine simulation: application to combustion of Neem methyl esther biodiesel", *Energy Conversion and Management*, Vol. 89, pp. 568–576, 2015.

24. Finesso, R., G. Hardy, C. Maino, O. Marello and E. Spessa, "A New Control-Oriented Semi-Empirical Approach to Predict Engine-Out NOx Emissions in a Euro VI 3.0 L Diesel Engine", *Energies*, Vol. 10, p. 1978, 2017.

25. Finesso, R., S. d'Ambrosio, L. Fu, A. Mittica and E. Spessa, "A control-oriented

real-time semi-empirical model for the prediction of NOx emissions in diesel engines", *Applied Energy*, Vol. 130, pp. 265–279, 2014.

26. Pennycott, A., C. Brace, R. Burke and S. Akehurst, "An empirical model for the carbon dioxide emissions of a diesel engine", *Proc IMechE Part D:J Automobile Engineering*, Vol. 226, pp. 1507–1513, 2012.

27. Traver, M. L., R. J. Atkinson and C. M. Atkinson, "Neural Network-Based Diesel Engine Emissions Prediction Using In-Cylinder Combustion Pressure", *SAE Technical Paper, 10.4271/1999-01-1532*, 1999.

28. Brahma, I., M. Sharp and T. Frazier, "Empirical Modeling of Transient Emissions and Transient Response for Transient Optimization", *SAE Technical Paper, 10.4271/2009-01-1508*, Vol. 2, pp. 1433–1443, 2009.

29. Liu, Z. and S. Fei, "Emissions Prediction of CNG/Diesel Dual Fuel Engine Based on RBF Neural Network", *SAE Technical Paper, 10.4271/2004-01-0646*, 2004.

30. Zhang, Q., A. Pennycott, R. Burke, S. Akehurst and C. Brace, "Predicting the Nitrogen Oxides Emissions of a Diesel Engine Using Neural Networks", *SAE Technical Paper, 10.4271/2015-01-1626*, 2015.

31. Shailaja, M. and A. S. R. Raju, "Neural Network—Based Diesel Engine Emissions Prediction for Variable Injection Timing, Injection Pressure, Compression Ratio and Load Conditions", *Emerging Trends in Electrical, Communicationsand Information Technologies, Lecture Notes in Electrical Engineering*, Vol. 394, pp. 109–122, 2016.

32. Domínguez-Saez, A., G. A. Ratta and C. C. Barrios, "Prediction of exhaust emission in transient conditions of a diesel engine fueled with animal fat using Artificial Neural Network and Symbolic Regression", *Energy*, Vol. 149, pp. 675–683, 2018.

33. Niu, X., C. Yang, H. Wanga and Y. Wanga, "Investigation of ANN and SVM

based on limited samples for performance and emissions prediction of a CRDI-assisted marine diesel engine", *Applied Thermal Engineering*, Vol. 111, pp. 1353–1364, 2017.

34. Bhowmik, S., A. P. b, R. Panua, S. K. Ghosh and D. Debroy, "Performance-exhaust emission prediction of diesosenol fueled diesel engine: An ANN coupled MORSM based optimization", *Energy*, Vol. 153, pp. 212–222, 2018.

35. Nikzadfara, K. and A. H. Shamekhib, "Investigating a new model-based calibration procedure for optimizing the emissions and performance of a turbocharged diesel engine", *Fuel*, Vol. 242, pp. 455–469, 2019.

36. Lotfan, S., R. A. Ghiasi, M. Fallah and M. Sadeghi, "ANN-based modeling and reducing dual-fuel engine's challenging emissions by multi-objective evolutionary algorithm NSGA-II", *Applied Energy*, Vol. 175, pp. 91–99, 2016.

37. Burke, R., W. Baumann, S. Akehurst and C. Brace, "Dynamic Modelling of Diesel Engine Emissions using the parametric Volterra Series", *Proc., IMechE PartD: J. Automobile Engineering, 10.1177/0954407013503629*, Vol. 228, pp. 164–169, 2010.

38. Bernard, G., M. Scaife, A. Bhave, D. Ooi and J. Dizy, "Application of the SRM Engine Suite over the Entire Load-Speed Operation of a U.S. EPA Tier 4 Capable IC Engine", *SAE Technical Paper, doi:10.4271/2016-01-0571*, 2016.

39. Özbek, F., *Turbo Matching Study in 4-Cylinder Diesel Engine*, M.Sc. Thesis, İ.T.Ü., 2013.

40. Gamma-Technologies-LLC., "GT-Suite Engine Performance Tutorials", *GT-Suite*, 2017.

41. Obodeh, O. and C. Ajuwa, "valuation of Artificial Neural Network Performance in Predicting Diesel Engine Nox Emissions", *European Journal of Scientific Research, ISSN 1450-216X*, Vol. 33, pp. 642–653, 2009.

42. E.Tosun, T. Ozgur, C. Ozgur, M. Ozcanli, H. Serin and K. Aydin, "Comparative analysis of various modelling techniques for emission prediction of diesel engine fueled by diesel fuel with nanoparticle additives", *Research Journal of Applied Sciences, European Mechanical Science 2017*, Vol. 1, 2017.

43. Kokkulunk, G., E. Akdogan and V. Ayhan, "Prediction of emissions and exhaust temperature for direct injection diesel engine with emulsified fuel using ANN", *Turkish Journal of Electrical Engineering Computer Sciences*, Vol. 21, pp. 2141–2152, 2013.

44. Wang, M., J.Zhang, S. Zhang and Q. Ma, "Prediction emission of an marine two stroke diesel engine based on modeling of radial basis function neural networks", *Second WRI Global Congress on Intelligent Systems*, Vol. 3, pp. 184–188, 2011.

45. Venkateshmohan, V. and M. Kumar, *Predictive Diesel Combustion Using DI-Pulse in GT-Power*, M.Sc. Thesis, Chalmers University of Technology, Sweden, 2015.

46. Hiroyasu, H., T. Kadota and M. Arai, "Development and Use of a Spray Combustion Modeling to Predict Diesel Engine Efficiency and Pollutant Emissions", *Bulletin of the JSME*, Vol. 26, pp. 214–224, 1983.

47. Sabau, A. and O. Emil, "Soot Modeling in Diesel Engine", *Proceedings of the 3rd International Conference on Environmental and Geological Science and Engineering*, pp. 123–131, 2008.

48. Nagle, J. and R. Strickland-Constable, "Oxidation of Carbon between 1000-2000C", *Fifth Carbon Conference, Pergamon, Oxford*, Vol. 1, pp. 154–164, 1962.

49. Deb, K. and H. Jain, "An Evolutionary Many-Objective Optimization Algorithm Using Reference-Point-Based Nondominated Sorting Approach, Part I: Solving Problems With Box Constraints", *IEEE Transactions on Evolutionary Computation*, Vol. 18, pp. 577–601, 2014.

APPENDIX A: DI-PULSE CO PREDICTIONS

Carbon monoxide (CO) is a bland, odourless and toxic air pollutant. It is mainly a result of the incomplete combustion of carbon-containing fuels. Partially burned fuel is the leading resource for carbon monoxide. Carbon monoxide occurs mostly if there is not enough oxygen exist during the combustion process. Oxygen-starved conditions will result in incomplete combustion. Since the combustion takes place in an oxygen-starved environment, carbon atoms may create a bond with only one oxygen atom rather than two which is required for CO2 generation.

If the air/fuel ratio values are lower than the stoichiometric ratio, lack of oxygen will be encountered in the combustion zone. Some special operating conditions such as warm-up, cold operation or regeneration may result with higher CO emission generation. Besides, high fuel pressure or leaky injectors are some other possible reasons for high CO concentrations.

There are two crucial phenomena [4] which decide on both CO and HC concentration during the combustion process. These are; overleaning and undermixing.

- Overleaning / Overmixing: A distribution in the fuel-air equivalence ratio across the fuel sprays develops just after the injected fuel advances into the cylinder. In that period, there is an increase in the amount of fuel that is mixed leaner than the lean combustion limit. The equivalence ratio distribution in the fuel spray at the time of ignition can be seen in Figure A.1. Ignition occurs in the slightly lean region of stoichiometric region of the spray core (especially in swirling flow) since the fuel has spent the most time within combustible limits. Lean burn means the burning of fuel with an excess of air in an internal combustion engine. The magnitude of the unburned HC from these overlean regions will depend on the amount of fuel injected during the ignition delay, the mixing rate with air during this period, and the extent to which prevailing cylinder conditions are conducive to autoignition.

- Undermixing: If the fuel leaves the injector nozzle at a low velocity or excess fuel enters the cylinder under overfueling conditions; slow or under mixing with air can be identified. This condition also has a significant impact on CO and HC emissions.

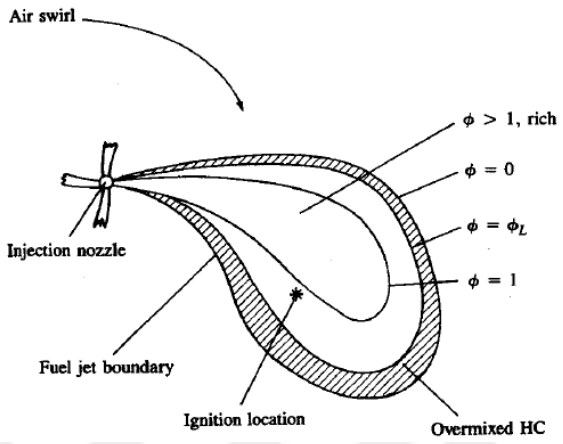

Figure A.1. Schematic of diesel engine fuel spray showing equivalence ratio (ϕ) contours at the of ignition [4]

In summary, there are two major causes of HC emissions in diesel engines under normal operating conditions:

- Fuel mixed to leaner than the lean combustion limit during the delay period;
- Undermixing of fuel which leaves the fuel injector nozzle at low velocity, late in the combustion process.

DI-Pulse states that CO emissions can be mainly attributed to partial oxidation of unburned hydrocarbons. Overmixing primarily occurs for lower load operating points where the ignition delay can be quite large (especially for early pilot injections). For these conditions, 'Overmixing Rate Multiplier' parameter can be used to tune the amount of unburned HC emissions from overmixing. At ignition, this overmixed fuel is set aside and one of the following can occur:

- The fuel can be re-entrained by another injection pulse

- The fuel can be partially oxidized to CO, H_2, H_2O, etc.
- The fuel can exit the cylinder at EVO contributing to HC emissions

Besides; 'Partial Oxidation Rate Multiplier' parameter can also be used to control how much overmixed fuel is partially oxidized to CO.

As a results, it is expected that increasing the 'Overmixing Rate Multiplier' will lead to increased HC emissions, primarily at low loads. Increasing the 'Partial Oxidation Rate Multiplier' will reduce the HC emissions and increase the CO emissions.

In order to understand the CO emission prediction capability of the model, DOE points are run with different Partial Oxidation Rate Multiplier and Overmixing Rate Multiplier values. The range of these parameters are summarized in Table A.1.

Table A.1. CO model constants optimization

Parameter	**DOE Range**	**DOE Results**
Partial Oxidation Rate Multi.	1-5	5
Overmixing Rate Multi.	1-5	5

Results are shown in Figure A.2 as the contour plot of nRMSE values. It is detected that the maximum accuracy that can be obtained via correlated DI-Pulse model is about 15.81%.

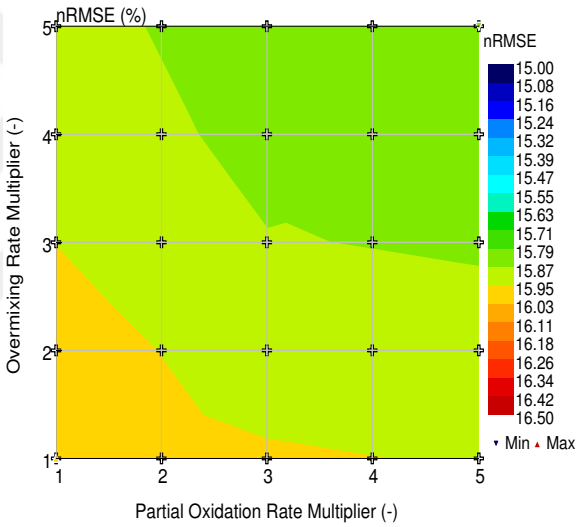

Figure A.2. CO Model: nRMSE contours as a function of partial oxidation rate and overmixing rate multipliers

APPENDIX B: INJECTOR MAP IMPLEMENTATION IN DI-PULSE

Predictive combustion models require some further data to initiate the simulations. These can be listed as:

- Specification the injected fuel such as density, the heat of vaporization, absolute entropy at 25 C, thermal conductivity etc.
- Injected fuel temperature
- Nozzle hole diameter
- Number of holes per nozzle
- Nozzle discharge coefficient
- Pilot injection mass and timing
- Main injection mass and timing
- Post-injection mass and timing
- Injection rate map

All of the above-listed items can be obtained from dynamometer data, but injection rate maps. These maps include data with very high confidentiality. That's why it is hard to acquire these maps from the suppliers.

These injection rate maps are three-dimensional maps including injection mass flow rate (g/sec) as a function of rail pressure (bar) and energizing time (microseconds). Figure B.1 represents different injection mass flow rate patterns as a function of energizing time and rail pressure [5].

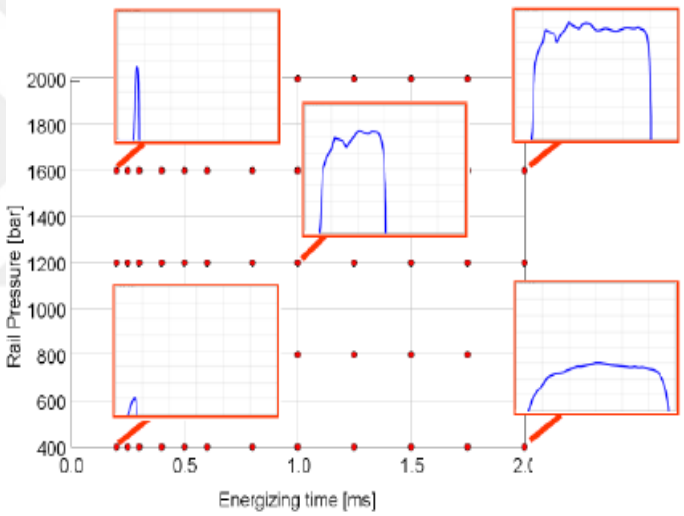

Figure B.1. Representative injection maps [5]

APPENDIX C: ADVANCED OPTIMIZER TOOL IN GT-SUITE

There is still a huge need for multi-objective optimization especially in automotive studies. NSGA-III is the successor to the well-known genetic algorithm NSGA-II and is optimized for multi-objective Pareto optimization. The algorithm is created in the open-source, Java-based environment. The main variance between these two algorithms is that NSGA-III utilizes from a set of reference points to maintain the diversity of the Pareto points during the search. Hence, although the objective number is very large, it would be possible to obtain very even distribution of Pareto points within the all objective space [49].

This genetic algorithm is generally recommended for problems including three or more factors; for multi-modal or non-linear problems. The most critical inputs of the algorithm are population size and the number of generations. The optimizer runs a total number of designs calculated by multiplication of these two parameters. The optimizer stops only if all of the designs are run in a simulation environment.

In order to initiate an optimization study in GT-Suite; below steps must be traced:

- Number of objectives must be selected. If there is only one objective to achieve, the user can select "Single Objective". If there is more than one objective than it is important to select "Multi-objective (Pareto)".
- Case handling must be selected. It is both possible to optimize each case independently or via case sweeps.
- Objective must be selected. For example, minimizing BSFC is an objective. BSFC must be selected as the objective parameter.
- Population size and number of generations must be selected.
- Factor that will be used to fulfill the optimization must be selected. For example,

the start of injection, rack position and EGR valve position are the main variables that were used in TOC optimization study. Upper and lower limits must be defined. Optimization space will be created within this range.

- Constraints must be defined. For example, if an optimization study is performed without taking the main calibration limits such as turbine inlet temperature, compressor outlet temperature, shaft speed, peak firing pressure, air-to-fuel ratio; then the optimum solution may violate one of these limitations.